Chair of Mechanics

Master's Thesis

Finite element investigation of packing rings

Dipl.-Ing. Marcel Ruetz, BSc

February 2023

MONTANUNIVERSITÄT LEOBEN
www.unileoben.ac.at

EIDESSTATTLICHE ERKLÄRUNG

Ich erkläre an Eides statt, dass ich diese Arbeit selbständig verfasst, andere als die angegebenen Quellen und Hilfsmittel nicht benutzt, und mich auch sonst keiner unerlaubten Hilfsmittel bedient habe.

Ich erkläre, dass ich die Richtlinien des Senats der Montanuniversität Leoben zu "Gute wissenschaftliche Praxis" gelesen, verstanden und befolgt habe.

Weiters erkläre ich, dass die elektronische und gedruckte Version der eingereichten wissenschaftlichen Abschlussarbeit formal und inhaltlich identisch sind.

Datum 20.02.2023

Unterschrift Verfasser/in
Marcel Ruetz

Acknowledgement

I hereby want to thank my supervisors Univ.-Prof. Dipl.-Ing. Dr.mont. Thomas Antretter, chair of Mechanics, University of Leoben as well as Dipl.-Ing. Dr.mont. Andreas Kaufmann of HOERBIGER Wien GmbH. I would also like to thank Mag. Markus Orthaber and Dipl.-Ing. Wolfgang Flachberger for making their cluster access available.

Abstract

This Master thesis is the result of a cooperative project between the Chair of Mechanics at the University of Leoben and HOERBIGER Wien GmbH. The aim of this thesis is to investigate the mechanical behaviour of polymer-based packing rings in industrial reciprocating piston compressors by means of the finite element (FE) method. Polymers show some specific features in their mechanical behaviour, among others that they tend to creep already at room temperature.

The FE model is generated automatically using a Python script. To validate the modelling assumptions of the FE model, the FE results are compared with the analytical solution from plate theory (Kirchhoff and Mindlin-Reissner) under the assumption of linear-elastic material behaviour. The comparison with the analytical solution shows that the deformations due to shear stress outweigh the deformations due to bending.

The parameters of a viscoelastic/viscoplastic material model are calibrated from the material data provided by HOERBIGER Wien GmbH. The material model takes into account the time dependence of the mechanical material behaviour as well as the temperature and load dependence.

Furthermore, the influence of the different system parameters (time, pressure difference, temperature, friction, and pressure gap width) on the creep behaviour of the packing ring is investigated. The influence of the geometry parameters is also studied. The results show that temperature, pressure difference and pressure gap width have the strongest impact on the creep behaviour. The results also show that the axial ring thickness is the only relevant geometrical parameter.

Using the FE analysis and the calibrated material model, the behaviour of the packing ring is simulated over the operating time. With this simulation data, an interpolation function for the displacement depending on pressure and pressure gap width is proposed. Using this interpolation function and a defined deformation limit value, the permissible pressure gap widths are determined.

With the help of automatically generated three-dimensional FE models, the influence of pressure balancing elements (pressure balancing bores) on the creep behaviour of the material is investigated. In a parameter study, the diameter and position of the pressure balancing bores are varied. Furthermore, the influence of asymmetry of the pressure gap on the creep behaviour of the material is investigated.

Zusammenfassung

Die vorliegende Masterarbeit ist das Ergebnis einer Kooperation des Lehrstuhls für Mechanik der Montanuniversität Leoben und der HOERBIGER Wien GmbH. Ziel dieser Arbeit ist die Untersuchung des mechanischen Verhaltens von kunststoffbasierten Packungsringen in industriellen Kolbenkompressoren mit Hilfe der Finite Elemente (FE) Methode. Polymere weisen einige Besonderheiten in ihrem mechanischen Verhalten auf, unter anderem dass sie bereits bei Raumtemperatur zum Kriechen neigen.

Das FE-Modell wird automatisiert mithilfe eines Python Skriptes generiert. Zur Validierung der Modellierungsannahmen des FE Modells werden die FE-Ergebnisse unter Voraussetzung von linear-elastischem Materialverhaltens mit der analytischen Lösung der Plattentheorie verglichen (Kirchhoff und Mindlin-Reissner). Der Vergleich mit der analytischen Lösung zeigt, dass die Verformungen zufolge der Schubbeanspruchung gegenüber den Verformungen zufolge der Biegung überwiegt.

Aus den von HOERBIGER Wien GmbH. zur Verfügung gestellten Materialdaten werden die Parameter eines viskoelastisch/viskoplastischen Materialmodells kalibriert. Das Materialmodell berücksichtigt neben der Zeitabhängigkeit des mechanischen Materialverhaltens auch die Temperatur- sowie die Lastabhängigkeit.

Weiters wird der Einfluss der unterschiedlichen Systemparameter (Zeit, Druckdifferenz, Temperatur, Reibung, und Druckspaltweite) sowie der Geometrieparameter auf das Kriechverhalten des Packungsringes untersucht. Die Ergebnisse zeigen, dass Temperatur, Druckdifferenz und Druckspaltweite das Kriechverhalten am stärksten beeinflussen. Die Ergebnisse zeigen auch, dass die axiale Ringdicke der einzig relevante Geometrieparameter ist.

Mithilfe der Finite Elemente Methode und dem kalibrierten Materialmodell wird das Verhalten des Packungsringes über die Betriebsdauer simuliert. Mit diesen Simulationsdaten wird die Verschiebung als Interpolationsfunktion von Druck und Druckspaltweite bestimmt. Mithilfe der Interpolationsfunktion und eines definierten Verformungsgrenzwertes werden die zulässigen Druckspaltweiten bestimmt.

Mithilfe von automatisiert generierten dreidimensionalen FE Modellen wird der Einfluss von Druckausgleichselementen (Druckausgleichsbohrungen) auf das Kriechverhalten des Materials untersucht. In einer Parameterstudie werden die Durchmesser und deren Positionen variiert. Weiters wird der Einfluss von Asymmetrie des Druckspaltes auf das Kriechverhalten des Materials untersucht.

Personal motivation

After completing my first Master's thesis on the topic of "FE-based design of cylinder rings of reciprocating piston compressors", I became highly motivated to dig deeper into the simulation of plastic components of compressors and to thus deepen my knowledge. The focus in my second Master's thesis is no longer on the analysis of a classical fatigue problem as in the first Master's thesis, but on a creep problem. Consequently, the packing rings are to be dimensioned for maximum displacement values rather than a critical stress value.

Material data

Material data required for the calculations were not provided in this Master's thesis at the request of the company partner.

Franz-Josef-Str. 18/III, 8700 Leoben
mechanik@unileoben.ac.at

Chair of Mechanics

Contents

Franz-Josef-Str. 18/III, 8700 Leoben
mechanik@unileoben.ac.at
Chair of Mechanics

Chapter 1

Introduction

1.1 Nomenclature

In this section, all symbols which can be found in further chapters and sections of this thesis, are listed in the order they appear.

1.1.1 Thermodynamic essentials of piston compressors

p...pressure [Pa]
V...volume [m^3]
T...temperature [K]
S...entropy [J/K]
V_c...compression volume [m^3]
V_h...stroke volume [m^3]
κ...isentropic exponent [-]
W...volume change work [J]

1.1.2 Continuum mechanics of large strains

$\underline{u}$...displacement vector [m]
$\underline{r}$...position vector for a material point in current configuration [m]
$\underline{R}$...position vector for a material point in reference configuration [m]
$\underline{\underline{F}}$...deformation gradient [-]
$\underline{\underline{I}}$...identity matrix [-]
$\underline{\underline{R}}$...rotational tensor [-]
$\underline{\underline{U}}$...right stretch tensor [-]
$\underline{\underline{V}}$...left stretch tensor [-]
$\underline{\underline{C}}^R$...right Cauchy-Green tensor [-]
$\underline{\underline{C}}^L$...left Cauchy-Green tensor [-]
$\underline{\underline{E}}^*$...Green-Lagrange strain tensor [-]
$\underline{\underline{\sigma}}$...Cauchy stress tensor [MPa]
$\underline{\sigma}_n$...Stress vector [MPa]
$\underline{\underline{P}}$...first Piola-Kirchhoff stress tensor [MPa]
$\underline{F}$...external force vector [N]
k...volume force density in the current configuration [N/m^3]
ρ...mass density in the current configuration [kg/m^3]
$\underline{\ddot{u}}$...acceleration vector in the current configuration [m/s^2]
ρ_o...mass density in the reference configuration [kg/m^3]
$\underline{\ddot{U}}$...acceleration vector in the reference configuration [m/s^2]
K...volume force density in the reference configuration [N/m^3]

1.1.3 Material models for thermoplastic polymers

σ_{ij}... Cauchy stress tensor [MPa]
ε_{kl}...linearised strain tensor [-]
E_{ijkl}... elasticity tensor [MPa]
α_{kl}...thermal expansion tensor [1/K]
$\Delta T(\underline{r},t)$...change in temperature field [K]
Y_S...yield surface [-]
J_2...second invariant of the stress deviator [MPa^2]
I_1...first invariant of the stress tensor [MPa]
α, d...material parameters of the Drucker-Prager model
σ_y...yield stress [MPa]
A, B, C...parameters of the Johnson-Cook model
ε_{pl}...plastic strain [-]
n...hardening exponent [-]
$\dot{\varepsilon}_{pl}$...plastic strain rate [1/s]
$\dot{\varepsilon}_0$...reference strain rate [1/s]
Θ...temperature coefficient [-]
T_G...transition temperature [K]
T...temperature [K]
T_m...melting temperature
$\dot{\varepsilon}$...strain rate [1/s]
A, m, n...material parameters of the Norton Bailey law
σ... stress [MPa]
t...time [s]
K...bulk modulus [MPa]
$\dot{\varepsilon}^{(vol)}$...volumetric strain rate [1/s]
δ_{ij}...Kronecker delta [-]
G...shear modulus [MPa]
$\dot{\varepsilon}_{ij}^{(dev)}$...deviatoric strain rate tensor [1/s]
τ...relaxation time [s]

1.1.4 Plate theory according to Kirchhoff

w...bending displacement [mm]
Δ...Laplace operator [1/m^2]
q_0...surface load [MPa]
K...plate stiffness []
p...surface pressure [MPa]
r...radius [mm]
$C_1 ... C_4$...integration constants

1.1.5 Criterion for maximum pressure gap

a_{stat}...static degree of utilisation [-]
σ_{Vmax}...maximum equivalent stress [MPa]
u_max...maximum displacement [mm]
$\dot{\varepsilon}^{pl}$...equivalent plastic strain rate [1/s]
$\dot{\varepsilon}_{ij}^{pl}$...plastic strain rate tensor [1/s]
ε^{pl}...plastic equivalent strain [-]

1.1.6 Dimensioning of the pressure gap

$u(\Delta p, g)$...displacement into the pressure gap after $\Delta t = 28.8 \cdot 10^6$s [mm]
Δp...pressure difference [bar]
g...pressure gap width [mm]
C_1, m, n...parameters of the interpolation function
$K_0 K_1, K_2, m, n, \alpha, \beta$...parameters of the interpolation function

Franz-Josef-Str. 18/III, 8700 Leoben
mechanik@unileoben.ac.at
Chair of Mechanics

1.2 Compressors

Compressed gas is needed in many applications, whether in technical or private use. The compressed gas is produced by compressors. Their main task is to compress a gaseous medium according to the laws of thermodynamics. Rotary compressors are designed for large volume flows but small pressure differences, while piston compressors are designed for large pressure differences but smaller volume flows [19].

1.2.1 Piston compressors

Piston compressors are used in a wide range of applications. Smaller designs of piston compressors are used in the private sector whereas for industrial applications larger designs are commonly encountered, e.g. to ensure the supply of compressed gas. Figure 1.1 shows the basic structure of a piston compressor. Its most important components are the piston, the piston rod, the cylinder rings and the rider rings. The working space is defined by the cylinder and the piston. [19]

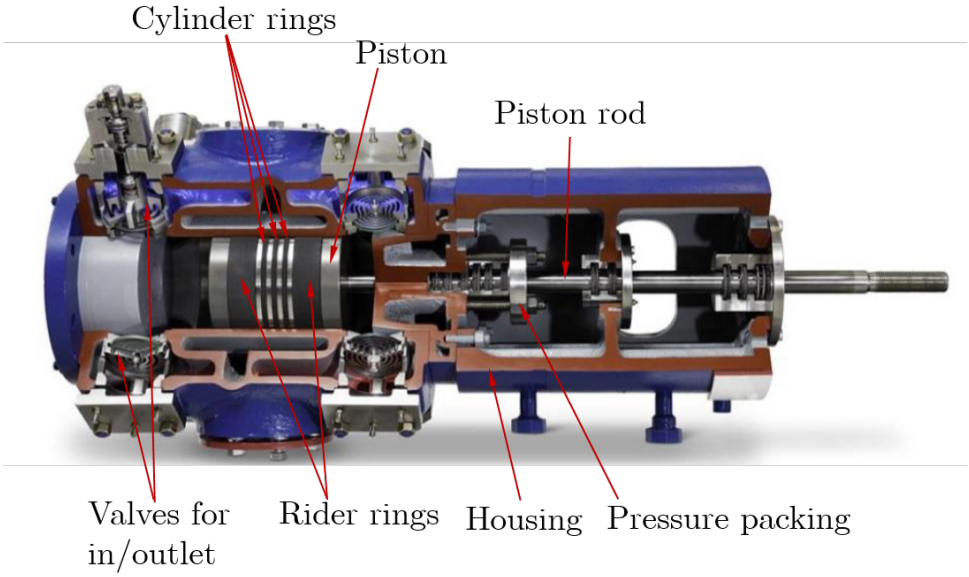

Figure 1.1: Double acting piston compressor [19]

During a working cycle, the following steps take place in the working chamber.
1) Gas intake (Suction stroke):
Here the piston moves towards the bottom dead centre. This creates a low pressure in the working chamber, which leads to gas being sucked in. Then the inlet valve closes.
2) Compressing the gas:
The piston moves in the direction of top dead centre. The sucked gas is compressed. This leads not only to an increase in pressure but also to an increase in temperature.
3) Pushing out the compressed gas:
Before reaching top dead centre, the exhaust valve is opened. The compressed gas is pushed out of the working chamber by the piston.
4.) Re-expansion:
This creates a low pressure in the working chamber.

1.2.2 Thermodynamic essentials of a piston compressor

The individual working steps of the reciprocating compressor are idealised by using the changes of states from classical thermodynamics. Figure 1.2 shows the idealised cycle of a piston compressor, where V_H is the displacement of the compressor and V_C is the compression volume.

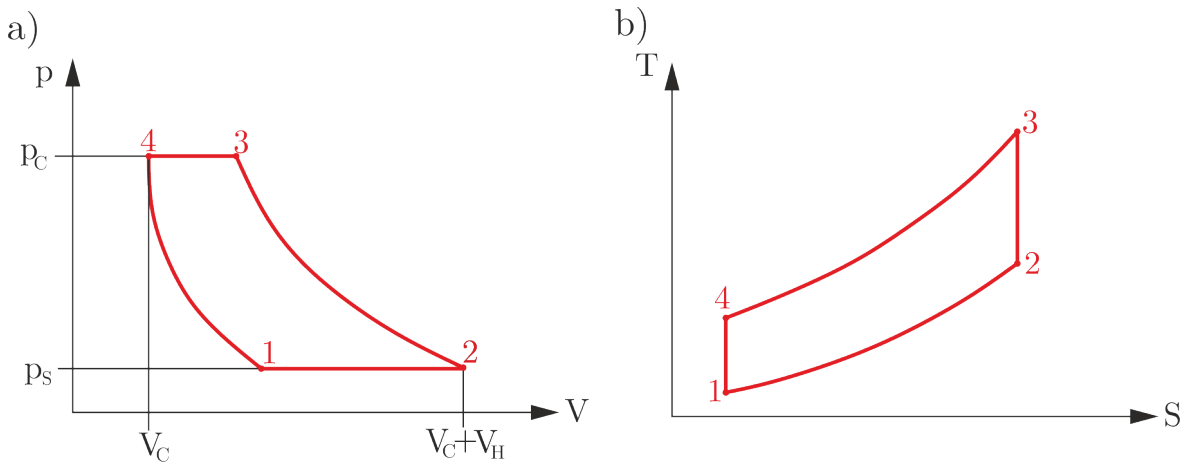

Figure 1.2: Idealised thermodynamic cycle for a piston compressor, a.) p-V-diagram, b.) T-S-diagram

The intake of fresh gas is idealised by an isobaric process. Here, the volume of the working chamber increases due to the movement of the piston in the direction of bottom dead centre $(1 \rightarrow 2)$. The ejection process from the work chamber is also modelled as an isobaric process $(3 \rightarrow 4)$. For the isobaric change of state applies:

$$\frac{V}{T} = \text{const.} \tag{1.1}$$

where p is the pressure in the system and V is the volume of the system. This is followed by an isentropic compression of the sucked air $(2 \rightarrow 3)$. The re-expansion stroke is also modelled as an isentropic change of state$(4 \rightarrow 1)$. For the isentropic change of state applies:

$$pV^{\kappa} = \text{const.} \tag{1.2}$$

where κ is the isentropic exponent. The total work done during a cycle is defined as follows.

$$W = \oint p \mathrm{d}V \tag{1.3}$$

In contrast to combustion engines, more work is consumed by the system than is delivered, since mechanical work needs to be added to the system in order to take the working medium to a higher pressure level.

1.2.3 Kinematics of double acting piston compressors

In piston compressors, motion is transmitted from the crankshaft using a thrust crank mechanism. The kinematics of the crank mechanism follows from the geometric configuration. A schematic sketch of the crank mechanism of the double-acting piston compressor is shown in Figure 1.3.

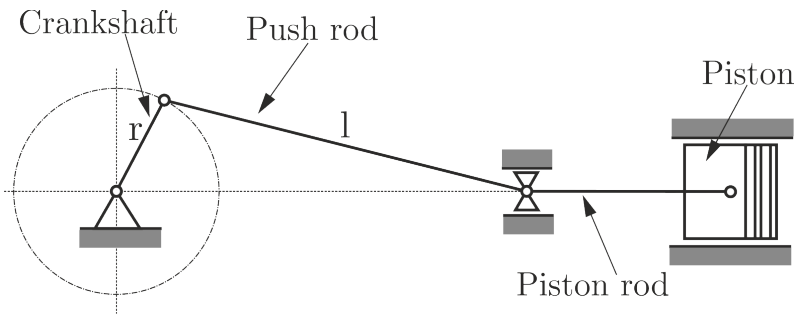

Figure 1.3: Schematic of the crank mechanism of a double-acting compressor

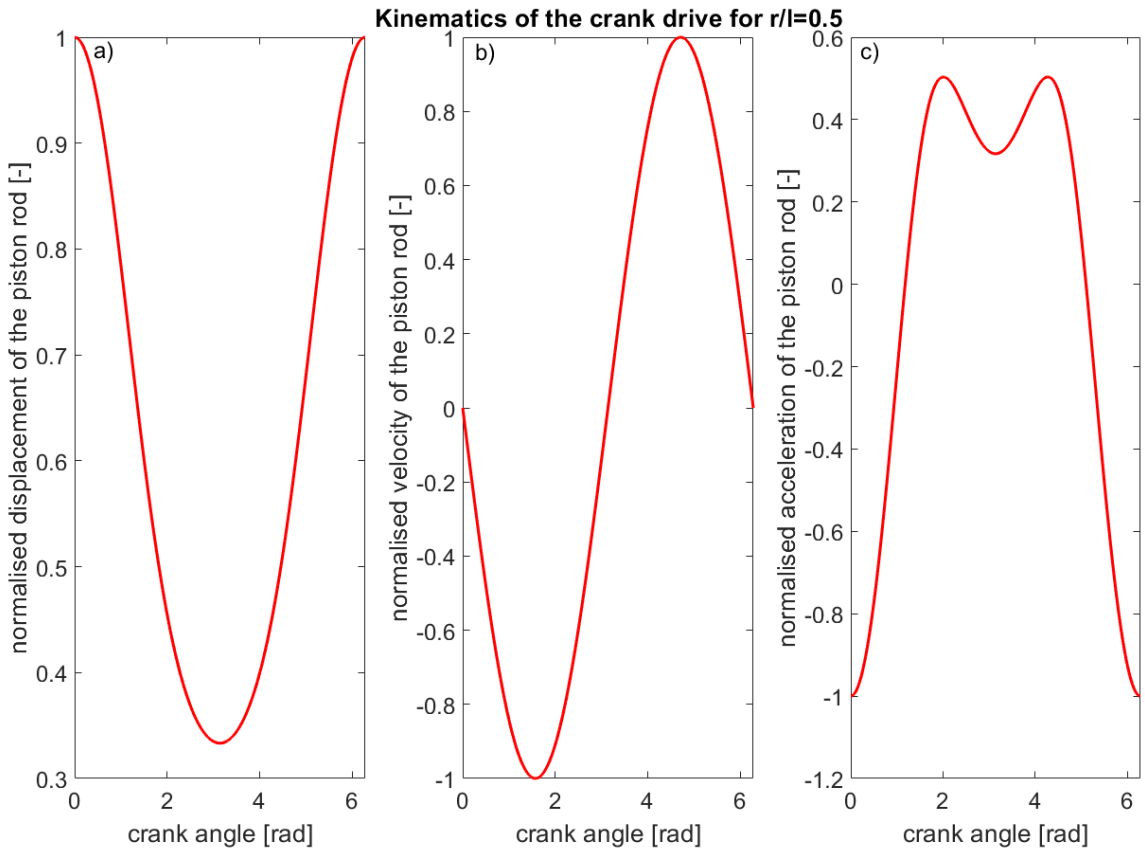

Figure 1.4: Kinematics of the crank drive for $\frac{r}{l} = 0.5$. a) Normalised displacement of the piston, b) Normalised velocity of the piston, c) Normalised acceleration of the piston rod.

Franz-Josef-Str. 18/III, 8700 Leoben
mechanik@unileoben.ac.at
Chair of Mechanics

Figure 1.4 shows the normalised curves of the piston rod movement, as well as the speed of the piston rod and the acceleration for the given ratio of the crank length to the push rod length. The shape of the piston rod movement always corresponds to a sine or cosine function, independent of the specific r/l ratio. The normalised course of the acceleration function changes significantly depending on the specific r/l ratio. This was a brief overview of the design and operation of compressors. More detailed information regarding compressors can be found in [**?**].

1.2.4 Packing rings

This Master's thesis focuses on the packing rings. The packing rings have the task of sealing the crank end side against atmospheric pressure. This is important for effective operation of the compressor. The packing rings are loaded by bending as well as shear due to the pressure difference at the gap and by compression due to the compressive stress. If the load is high enough, the material creeps into the gap between piston rod and packing housing. Furthermore, there is a tribological load at the packing ring-piston rod contact. This is characterised by a contact pressure and a relative movement of the components. This leads to material abrasion and wear in general. Figure 1.5 shows the different packing rings manufactured by HOERBIGER Wien GmbH.

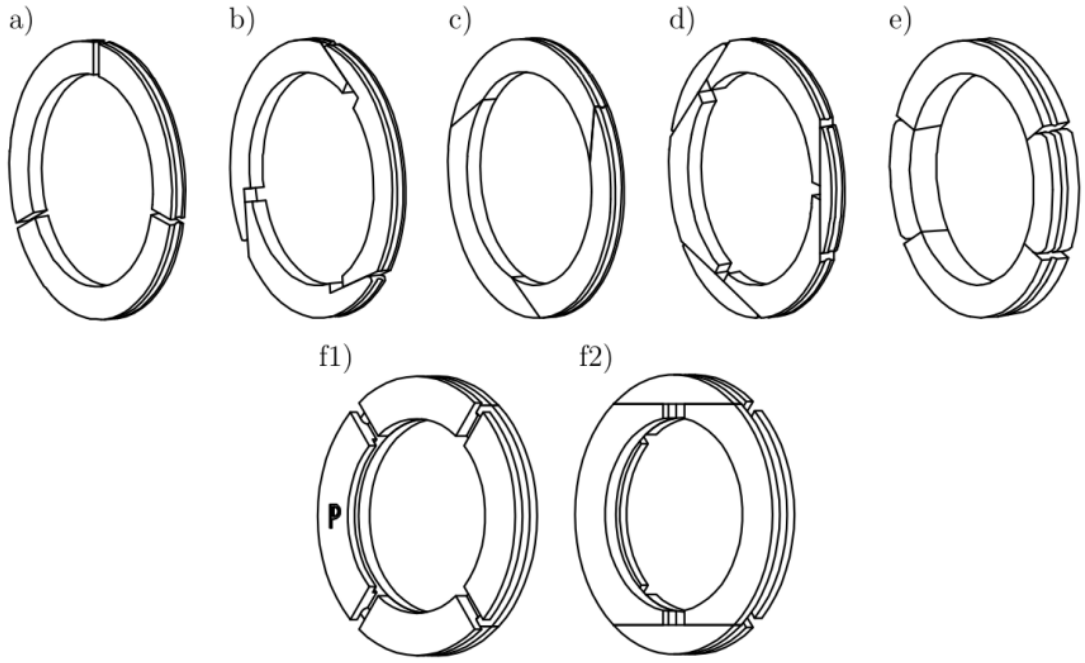

Figure 1.5: Typical designs of packing rings [8]
a) 3 piece radial cut ring, b) 3 piece tangential cut ring with wear stop, c) 3 piece tangential to rod cut ring without wear stop, d) 6 piece tangential cut ring ("bridge"), e) 4 piece ring design, f) balanced cap design (BCD) ring (f1 shows the pressure side, f2 the sealing side)

Figure 1.6 shows a sectional view of the pressure packing.

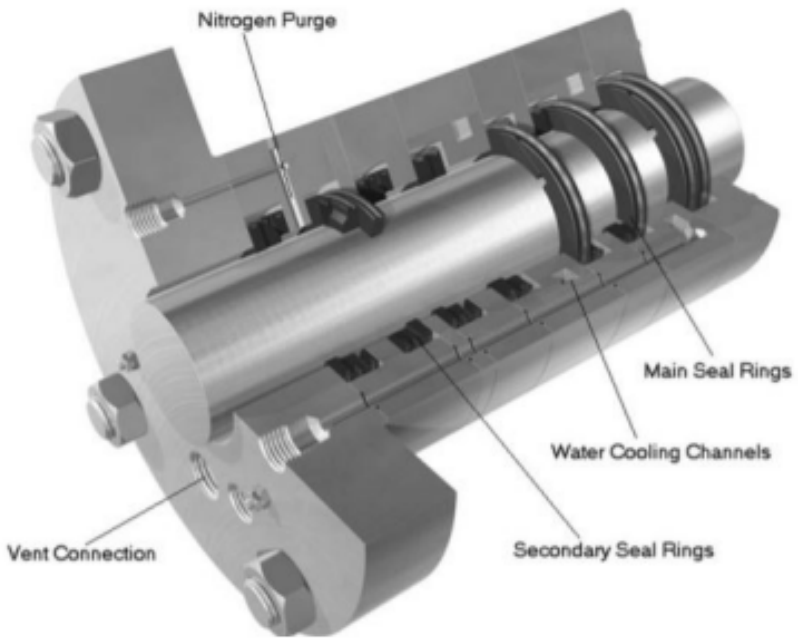

Figure 1.6: Cut view through a pressure packing [18]

1.3 State of the art packing rings

Although packing rings have already been used in machines for a long time, the design is still strongly reliant on experimental data and empirically determined formulas. The reason for this is the complex local stress state inside the ring, which is not analytically describable, as well as the complex material behaviour. However, the use of powerful computers in combination with the use of numerical methods such as the finite element analysis (FEA) allow detailed predictions about the behaviour of the packing rings in operation.

Scientific works that have already dealt with packing rings. Kaufmann [11], [12] deals in detail with the wear of the packing rings. Humpel [10] investigated the influence of material, processing and test parameters on the leakage of polymer-based sealing materials for reciprocating piston compressors. Radcliffe [18] deals with materials for the use of packing rings in compressors. [22] investigated the temperature distribution in packing rings of reciprocating compressors. In [23], the pressure distribution and the heating due to friction in packing rings are investigated. Although there are many other scientific papers dealing with the tribological properties of the packing rings, the material of the packing rings and the temperature development within the packing rings, there are hardly any papers dealing with the design of the pressure gap.

The central research questions of this Master's thesis are the determination of the maximum possible pressure gap width as well as the determination of the influence of pressure balancing elements. Furthermore, the influence of the geometry parameters as well as other system parameters are investigated in more detail.

Chapter 2

Theoretical Fundamentals

2.1 Continuum mechanics of large deformations

2.1.1 Large strain theory

Large strains and displacements occur during the creep of the packing ring in operation time. Thus, regardless of the material behaviour, the linearised strain-displacement relationships are no longer valid. It should be noted, that for these strain and displacement levels the large strain theory should be used. Many authors, like Bergstroem [6] recommend the large strain theory for strain magnitudes larger than 1%.

Lagrangian and Eulerian description

When considering the kinematics of the continuum, a distinction is made between two modes of description. With the description after Lagrange the temporal change of the material properties of a defined material point is considered. The reference configuration is considered as the configuration at time $t = 0$. This approach is common in solid mechanics.

In the description according to Euler the current configuration is considered as the reference configuration. The Eulerian description method is common in fluid mechanics.

Figure 2.1 shows a deformable continuum in the reference and current configurations. The reference configuration is at time t =0 and the current configuration at time $t > 0$s. The reference configuration represents the undeformed continuum, whereas the current configuration represents the deformed continuum.

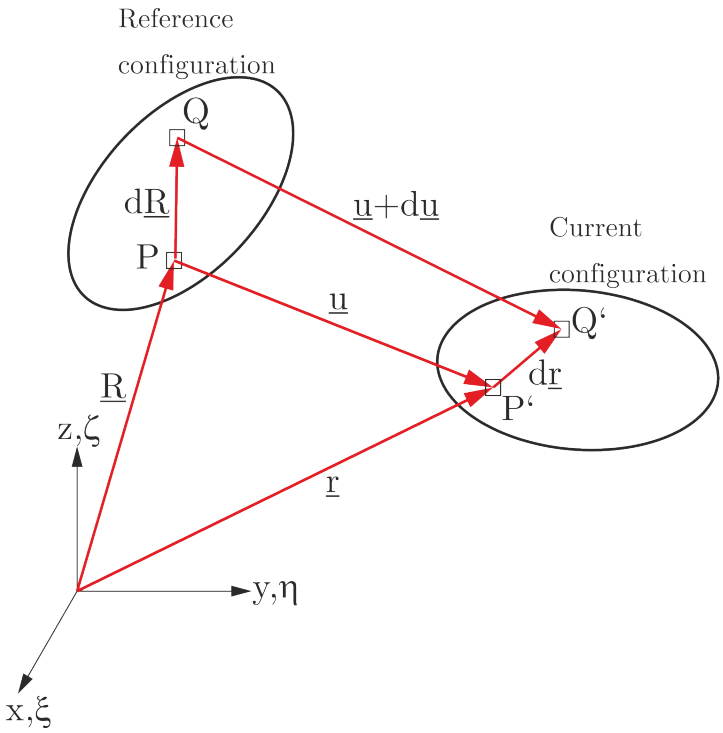

Figure 2.1: Kinematics of a solid continuum in the reference coordinate system and the current coordinate system

Deformation gradient

The displacement vector for the current configuration is calculated according to equation 2.1

$$\underline{u} = \underline{r}(\underline{R}) - \underline{R} \tag{2.1}$$

where $\underline{u}$ is the displacement vector, $\underline{r}(\underline{R}) = [x, y, z]$ is the position vector of the considered material point in the current configuration (deformed position) and $\underline{R} = [\xi, \eta, \zeta]$ is the position vector of the considered material point in the reference configuration (initial position). The formation of the partial derivatives after the reference configuration provides the deformation gradient $\underline{\underline{F}}$.

$$\underline{\underline{F}} = \nabla \underline{r} = \begin{bmatrix} \frac{\partial x}{\partial \xi} & \frac{\partial x}{\partial \eta} & \frac{\partial x}{\partial \zeta} \\ \frac{\partial y}{\partial \xi} & \frac{\partial y}{\partial \eta} & \frac{\partial y}{\partial \zeta} \\ \frac{\partial z}{\partial \xi} & \frac{\partial z}{\partial \eta} & \frac{\partial z}{\partial \zeta} \end{bmatrix} \tag{2.2}$$

The deformation gradient is an important quantity in continuum mechanics for assessing the deformation of the continuum.The deformation gradient does not necessarily have to be symmetrical. It allows the transformation from the reference configuration to the current configuration, as equation 2.3 shows.

$$\mathrm{d}\underline{r} = \underline{\underline{F}} \mathrm{d}\underline{R} \tag{2.3}$$

The deformation gradient therefore corresponds to the Jacobian matrix. For the reverse transformation from the current configuration to the reference configuration, the inverse of the deformation gradient must be applied.

$$\mathrm{d}\underline{R} = \underline{\underline{F}}^{-1} \mathrm{d}\underline{r} \tag{2.4}$$

According to the rules of matrix calculus, the following must also apply

$$\underline{\underline{F}}\ \underline{\underline{F}}^{-1} = \underline{\underline{I}} \tag{2.5}$$

where $\underline{\underline{I}}$ is the identity matrix.The determinant of the deformation gradient is a measure of the volume change during a transformation. In the case that $\underline{\underline{F}}$ is not a function of position, the deformation is homogeneous. If the deformation depends on the position (i.e. $\underline{\underline{F}}(\underline{R})$), it is inhomogeneous. In the case that $\det(\underline{\underline{F}}) = 1$ the deformation is isochoric, i.e. it occurs under constant volume. Any large deformation can be decomposed into a rotational and an stretch component(see equation 2.6).

$$\underline{\underline{F}} = \underline{\underline{R}}\ \underline{\underline{U}} \tag{2.6}$$

where $\underline{\underline{R}}$ is the rotational tensor and $\underline{\underline{U}}$ is the right stretch tensor. $\underline{\underline{U}}$ is positively defined and is symmetric, $\underline{\underline{R}}$ is volume-preserving and orthogonal. Alternatively, the deformation gradient can also be decompoesed according to equation 2.7, where

$$\underline{\underline{F}} = \underline{\underline{V}}\ \underline{\underline{R}} \tag{2.7}$$

$\underline{\underline{V}}$ is the left stretch tensor. Just like the right stretch tensor this tensor is symmetric. For the definition of a strain tensor either the right or the left stretch tensor, respectively, is relevant. The rotation tensor, by contrast, does not contribute to a straining of the material. In fact, it cancels out when formulating the right or the left Cauchy-Green tensor, respectively [6].

$$\underline{\underline{C}}^R = \underline{\underline{F}}^T \underline{\underline{F}} \tag{2.8}$$

where $\underline{\underline{C}}^R$ is the right Cauchy-Green tensor. Considering the orthogonality of the rotation tensor $(\underline{\underline{R}}^T \underline{\underline{R}})$ it is very simple to show with equation 2.7 that,

$$\underline{\underline{C}}^R = \underline{\underline{U}}^T \underline{\underline{U}} = \underline{\underline{U}}^2 \tag{2.9}$$

By analogy, the left Cauchy-Green [6] tensor follows.

$$\underline{\underline{C}}^L = \underline{\underline{F}}\,\underline{\underline{F}}^T \tag{2.10}$$

where $\underline{\underline{C}}^L$ is the left Cauchy-Green tensor. Again considering the orthogonality of the rotation tensor $(\underline{\underline{R}}\,\underline{\underline{R}}^T)$ and equation 2.7 yields

$$\underline{\underline{C}}^L = \underline{\underline{V}}\,\underline{\underline{V}}^T = \underline{\underline{V}}^2 \tag{2.11}$$

Strain tensors

Numerous strain tensors exist in the literature. In the Lagrangian approach, the strain tensors are typically formed with the right stretch tensor whereas in the Eulerian approach they are formed with the left stretch tensor. In the context of this Master's thesis, only the Green-Lagrange strain tensor is presented because FE programmes typically use this definition. It is defined as follows.

$$\underline{\underline{E}}^* = \frac{1}{2}\left[\underline{\underline{U}}^2 - \underline{\underline{I}}\right] \tag{2.12}$$

The strain tensor entries are directly calculated from the deformation gradient using equation 2.8 and equation 2.11.

$$\underline{\underline{E}}^* = \frac{1}{2}\left[\underline{\underline{F}}^T \underline{\underline{F}} - \underline{\underline{I}}\right] \tag{2.13}$$

For reasons of clarity the index notation is now used.

$$E^*_{kl} = \frac{1}{2}\left[\frac{\partial r_j}{\partial R_k}\frac{\partial r_j}{\partial R_l} - \delta_{kl}\right] \tag{2.14}$$

where δ_{kl} is the Kronecker delta, which represents the unit tensor.

$$\delta_{kl} = \begin{cases} 1, & \text{if } k = l \\ 0, & \text{if } k \neq l \end{cases} \tag{2.15}$$

Considering equation 2.1 and the tensor calculation rules, the expression for describing the entries of the strain tensor using the displacements follows

$$E^*_{kl} = \frac{1}{2}\left(\frac{\partial u_k}{\partial Rl} + \frac{\partial u_l}{\partial R_k} + \frac{\partial u_m}{\partial R_k}\frac{\partial u_m}{\partial R_l}\right) \tag{2.16}$$

2.1.2 Stress state

Stresses are induced in the material as a result of external loads. The stress state in each point of the material is characterised by the stress tensor. Like the displacement state, the stress state can be formulated both in the reference configuration and in the current configuration.

Stress state in the current configuration

The stress state in the current configuration is characterised by the symmetric second order Cauchy stress tensor. The symmetry results from the moment equilibrium for an infinitesimal volume element leading to the well-known duality of the shear stresses.

$$\underline{\underline{\sigma}} = \begin{bmatrix} \sigma_x & \tau_{xy} & \tau_{xz} \\ \tau_{yx} & \sigma_y & \tau_{yz} \\ \tau_{zx} & \tau_{zy} & \sigma_z \end{bmatrix} \tag{2.17}$$

Cauchy's law (equation 2.18) describes the relationship between the stress tensor $\underline{\underline{\sigma}}$ and the traction vector $\underline{\sigma}_n$ acting on an arbitrary section plane characterised by the normal vector $\underline{n}$.

$$\underline{\sigma}_n = \underline{\underline{\sigma}}\,\underline{n} \tag{2.18}$$

Stress state in the reference configuration

Analogous to strains, the stresses can also be described in the reference configuration. The corresponding tensor $\underline{\underline{P}}$ is called the first Piola Kirchhoff stress tensor. As with the strain state, a relationship between the stress formulation in the reference configuration and the current configuration is established via the deformation gradient (equation 2.19).

$$\underline{\underline{P}} = \det\left(\underline{\underline{F}}\right) \underline{\underline{\sigma}}\,\underline{\underline{F}}^{-T} \tag{2.19}$$

2.1.3 Conservation of linear momentum

The force is defined as the time derivative of the continuum's linear momentum $\underline{F} = \frac{d\underline{p}}{dt}$. For a generally loaded deformable body, the force vector $\underline{F}$ consists of the sum of the external loads and the volume force.

$$\underline{F} = \oint_A \underline{\sigma}_n \mathrm{d}A + \int_V \underline{k} \mathrm{d}V \tag{2.20}$$

where, $\underline{\sigma}_n$ is the traction vector, $\underline{n}$ is the normal vector characterising the surface and $\underline{k}$ is the volume force density. Using Cauchy's law (equation 2.18), the following expression 2.21 follows

$$\underline{F} = \oint_A \underline{\underline{\sigma}}\,\underline{n} \mathrm{d}A + \int_V \underline{k} \mathrm{d}V \tag{2.21}$$

Using the divergence theorem 2.22, surface integrals allow themselves to be converted into volume integrals. The divergence theorem is defined as follows, where $\underline{\underline{q}}$ is a tensorial quantity.

$$\oint_A \underline{\underline{q}}\,\underline{n} dA = \int_V \underline{\nabla} \cdot \underline{\underline{q}} dV \tag{2.22}$$

As a consequence of the divergence theorem only external forces are affecting the motion of the centre-of-mass. Applied to equation 2.23, conservation of linear momentum as an integral equation provides

$$\underline{F} = \int_V \underline{\nabla} \cdot \underline{\underline{\sigma}} \mathrm{d}V + \int_V \underline{k} \mathrm{d}V \tag{2.23}$$

Using Newton's second law yields

$$\int_V \rho \underline{\ddot{u}} \mathrm{d}V = \int_V \underline{\nabla} \cdot \underline{\underline{\sigma}} \mathrm{d}V + \int_V \underline{k} \mathrm{d}V \tag{2.24}$$

where ρ is the mass density in the current configuration and $\underline{\ddot{u}}$ is the acceleration of a mass point. Differentiating with respect to the volume delivers

$$\rho \underline{\ddot{u}} = \underline{\nabla} \cdot \underline{\underline{\sigma}} + \underline{k} \tag{2.25}$$

By analogy, the conservation of linear momentum can be derived in the reference configuration as

$$\rho_0 \underline{\ddot{U}} = \underline{\nabla} \cdot \underline{\underline{P}} + \underline{K} \tag{2.26}$$

where, ρ_0 is the density in the reference configuration and $\underline{K}$ is the volume force density in the reference configuration.

2.2 Material models for thermoplastic polymers

The real deformation behaviour of polymer materials includes a spontaneous elastic, a time-dependent viscoelastic and a time-dependent viscoplastic component, depending on the existing stress state and the load level. A large number of material models exist in the literature. Some of these material models are well suited for describing the behaviour of polymeric materials. The choice of a suitable material model depends on the loading rate and the magnitude of the loading. According to table 2.1, the following material models are recommended.

Table 2.1: Material models for thermoplastic materials according to Strommel [20]

Time period of loading	load profile	Material model
$t < 1$s	shock, monotoneously rising	elastic-plastic, viscoelastic
1s$<t<$1h, "short therm"	constant, monotonously rising	elastic, elastic-plastic
1h $< t$, "long term"	constant, monotonously rising	elastic, viscoelastic, creep
periodic	cyclic, osciliating	viscoelastic

2.2.1 Elasticity

A purely elastic constitutive law is in principle not well suited to describe the mechanical behaviour of polymers, because the time dependence of the material properties is not taken into account. However, it already allows first estimations of the influence of various parameters, e.g. the influence of the load or geometry parameters on the maximum stresses and displacements. The elastic material law is generally described by the generalized Hooke's law

$$\sigma_{ij} = C_{ijkl}\left(\varepsilon_{kl} - \alpha_{kl}\Delta T\right) \tag{2.27}$$

where σ_{ij} is the stress tensor, C_{ijkl} is the fourth-order elasticity tensor, ε_{kl} is the strain tensor, α_{ij} is the thermal expansion tensor and ΔT represents the difference of the temperature field inside the continuum relative to a reference temperature. The entries of the elasticity tensor do not necessarily have to be constant in space and time.

2.2.2 J_2 plasticity

Under load, ductile materials initially behave elastically. If the load is increased further, the yield condition is reached at some point. From this point on, the material is plastically deformed. When the yield strength of the material is reached, hardening effects occur. If the material is unloaded a permanent deformation occurs. According to Mises, the yield condition is reached when the second invariant of the stress deviator J_2 reaches a critical value. Besides the Mises yield condition, other yield conditions exist (Tresca, Drucker-Prager and Mohr-Colomb). These flow conditions describe a surface in the stress space. In the case of the Mises criterion, it is a cylinder along the hydrostatic axis. Elastic material behaviour is present for all states within the yield surface Y_S. Yielding begins when the yield surface is reached [2].

$$dY_S = \frac{\partial Y_S}{\partial \sigma_{ij}} : d\sigma_{ij} + \frac{\partial Y_S}{\partial \varepsilon_{ij}} : d\varepsilon_{ij} \tag{2.28}$$

Isotropic hardening is characterised by the fact that the yield surface expands uniformly in the stress space. The origin of the yield surface remains unchanged and the yield function therefore remains isotropic even after the onset of plastic deformation [15]. Figure 2.2 a) shows the uniform expansion of the yield surface in principal stress space during isotropic hardening. The dashed curve shows the yield surface in the initial state. The solid curve shows the yield surface after exceeding the yield strength. Isotropic hardening is appropriate for predicting the polymer material's answer to monotonic loads.

Kinematic hardening is characterised by a pure translational movement of the yield surface in the stress space. This translation causes the originally isotropic yield surface to become anisotropic [15]. Figure 2.2 b) shows the translation in principal stress space of the yield surface during kinematic hardening. For cyclic loads the kinematic hardening plasticity model is recommended for polymer based materials. Like other plasticity models this model underestimates the magnitude of the recovery during the unloading phase. Kinematic hardening plasticity yields for some polymers results that are not as accurate as the results of isotropic hardening plasticity [6].

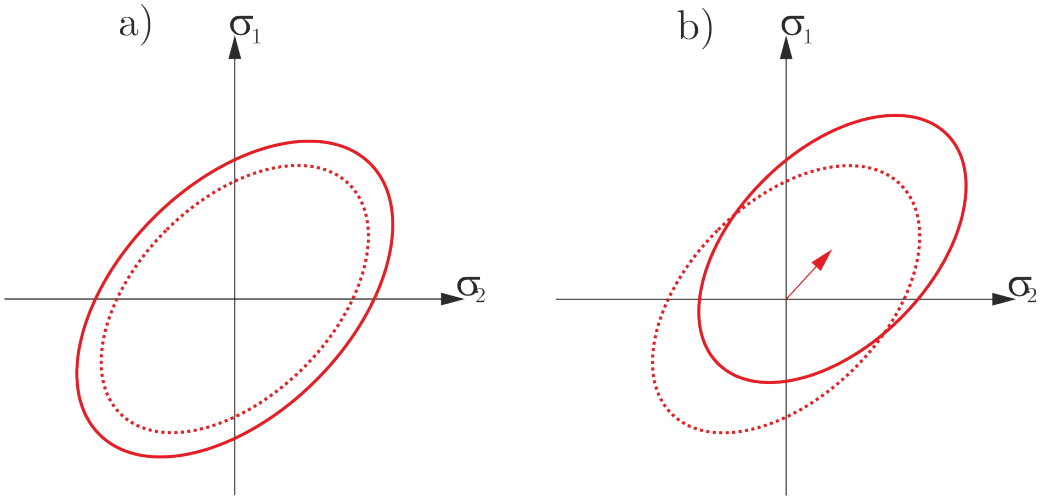

Figure 2.2: Hardening effects, Yield surface in the plane stress space for a) isotropic hardening, b) kinematic hardening.

2.2.3 Drucker-Prager plasticity

Polymeric materials exhibit a tension-compression asymmetry of the yield strength. The Drucker-Prager criterion takes into account that the compressive yield strength is higher than the tensile yield strength. Figure 2.3 shows the yield surface of the conical Drucker-Prager criterion. Figure 2.3 shows that the material begins to yield at higher stress levels in the compressive stress range than in the tensile range. The hydrostatic pressure is plotted on the abscissa axis. The flow criterion is shown along the hydrostatic axis. This representation is chosen because the Drucker-Prager criterion describes the dependence of the yield strength on the hydrostatic stress component. The yield stress is plotted on the ordinate axis.

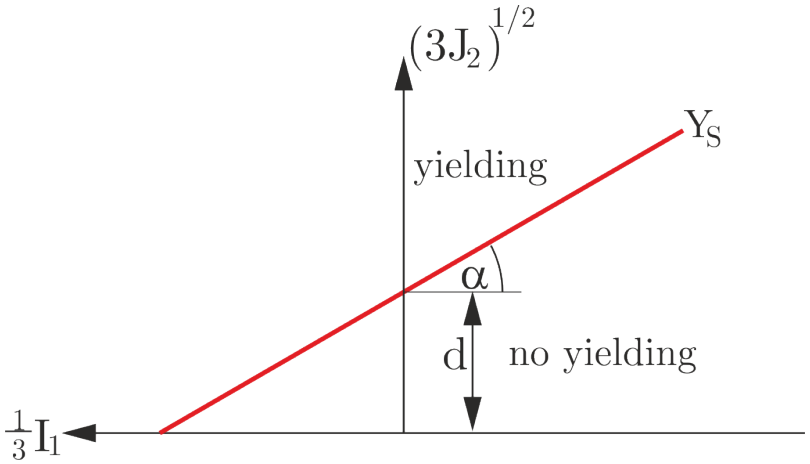

Figure 2.3: Yield surface of the Drucker-Prager criterion in the conical form

The yield surface Y_S is described by the following equation 2.29, where

$$Y_S = \sqrt{3J_2} - \frac{1}{3} I_1 \tan(\alpha) - d = 0 \tag{2.29}$$

J_2 is the second invariant of the deviatoric stress state, I_1 is the first invariant of the stress state. α and d are the material parameters of the Drucker-Prager model. In Abaqus, the Drucker-Prager criterion has the ability to be coupled with a creep law, allowing viscoplastic material behaviour to be modelled. More detailed information is available in e.g. [1].

Although the Drucker-Prager criterion describes the influence of the hydrostatic pressure on the yield strength of a material, it is possible to calibrate the parameters of the model using experimental data from one-dimensional tests. The hydrostatic pressure is calculated from the uniaxial stress state.

2.2.4 Johnson-Cook plasticity

For some materials the yield strength might depend on strain rates. For metals this influence is typically low, except for very high strain rates and at elevated temperatures. For polymeric materials, the strain rate dependency already occurs at low strain rates. The Johnson Cook model provides a description of the hardening and strain rate dependence of the yield strength of the material (see equation 2.31) [6].

$$\sigma_y = \left[A + B\varepsilon_{pl}^n\right]\left[1 + C\ln\left(\frac{\dot{\varepsilon}_{pl}}{\dot{\varepsilon}_0}\right)\right] \tag{2.30}$$

where, A, B and C are the parameters of the Johnson-Cook model, ε_{pl} is the equivalent plastic strain, n is the hardening exponent, $\dot{\varepsilon}_{pl}$ is the plastic strain rate and $\dot{\varepsilon}_0$ is the reference strain rate. The first term of this equation describes the hardening of the material with increasing plastic deformation fraction. The second term describes the influence of the strain rate on the yield stress of the material.

The Johnson-Cook model also allows to consider the influence of temperature on the yield strength of the material.

$$\sigma_y = \left[A + B\varepsilon_{pl}^n\right]\left[1 + C\ln\left(\frac{\dot{\varepsilon}_{pl}}{\dot{\varepsilon}_0}\right)\right](1 - \Theta) \tag{2.31}$$

where Θ is the temperature coefficient.

$$\Theta = \begin{cases} 0, & \text{if } T < T_g \\ \frac{T - T_G}{T_m - T_G}, & \text{if } T_G \leq T \leq T_m \\ 1 & \text{if } T_m < T \end{cases} \tag{2.32}$$

where T is the temperature, T_G is the transition temperature and T_m is the melting temperature. The transition temperature is the temperature at which the yield strength starts to drop. Below the transition temperature, the yield stress according to equation 2.31 and equation 2.32 is independent of temperature. When the melting temperature is reached, the yield stress of the material drops to $\sigma_y = 0$, so that deviatoric stress components are no longer transmitted.

2.2.5 Creep models

Creep models describe the time-dependent material behaviour of materials. In contrast to the viscoelastic material model, creep laws also allow the description of the material behaviour when the yield strength is exceeded (viscoplasticity). Creep models allow a good approximation of the material behaviour under load. However, they fail in the description of the unloading process. For this reason, they are not suitable for cyclic loads. Usually, the Norton-Bailey approach is used, where the creep rate is formulated as a power law 2.33.

$$\dot{\varepsilon} = A\sigma^m t^n \tag{2.33}$$

where, $\dot{\varepsilon}$ is the creep strain rate, A, m and n are material parameters. σ is the mechanical stress and t is the time. Integrating over time gives the creep strain as a function of time.

$$\varepsilon = \frac{A}{n+1}\sigma^m t^{n+1} \tag{2.34}$$

The determination scheme of material parameters is shown in Figure 2.4. The creep parameters are calibrated by means of experimentally determined creep curves, i.e. creep strain versus time. In a double logarithmic representation these date can well be approximated by straight lines whose slopes as well as intercepts can be determined via regression.

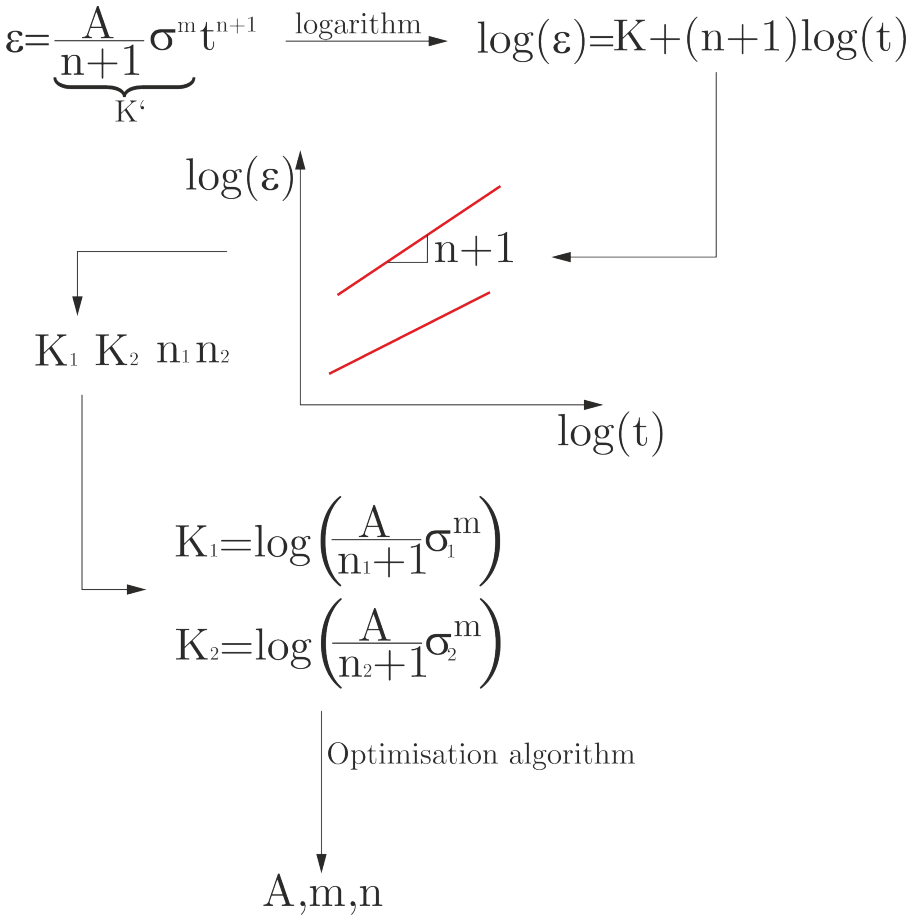

Figure 2.4: Principle of determining the parameters of the creep model

2.2.6 Viscoelasticity

Viscoelasticity describes the time dependent elastic behaviour of polymers. Viscoelasticity is only valid as long as the yield strength of the material is not reached. The constitutive law for linear viscoelasticity is shown in the equation 2.35 below.

$$\sigma_{ij}(t) = \int_0^t \left[K(t-\tau)\dot{\varepsilon}^{(vol)}\delta_{ij} + 2G(t-\tau)\dot{\varepsilon}_{ij}^{(dev)} \right] \mathrm{d}\tau \tag{2.35}$$

where $K(t-\tau)$ is the time dependent bulk modulus, $\dot{\varepsilon}^{(vol)}$ is the volumetric strain rate, δ_{ij} is the Kronecker delta, $G(t-\tau)$ is the shear modulus and $\dot{\varepsilon}_{ij}^{(dev)}$ is the deviatoric strain rate tensor. The relaxation time spectrum describes the change of the bulk modulus as well as the shear modulus for the entire time range. However, the relaxation time spectrum is usually unknown. Therefore, the continuous spectrum is replaced by a discrete series, the so-called Prony series. The problem with using the Prony series is that the creep of the material over time is only predictable up to the time range for which measured values are available.

$$K(t) = \sum_{i=1}^{n} K_i e^{-\frac{t}{\tau_i}} \tag{2.36}$$

$$G(t) = \sum_{i=1}^{n} G_i e^{-\frac{t}{\tau_i}} \tag{2.37}$$

By applying temperature shift approaches, the temperature dependence of the material behaviour is also taken into account. A large variety of temperature shift functions exist in the literature. For more detailed information about the temperature shift approaches, please refer to [6], [20].

The measurement data in figure 4.46 are determined in the creep test. An uniaxial tensile stress state is present in the test specimen. The packing ring is in a multiaxial stress state with a high hydrostatic stress component. Detailed information on the influence of hydrostatic pressure can be found in [16]. Further information on the (non-linear) creep behaviour of polymeric materials can be found in [13] and [3].

Chapter 3

Modelling

3.1 Mechanical model of the packing ring

Due to the symmetry in geometry and loading of the packing ring, an axi-symmetric model is sufficient (see [**?**]). Because of the high contrast in the elastic constants between the steel parts (rod and packing housing) and the polymer packing ring, it is possible to model the piston rod and the packing housing as rigid bodies, whereas the packing ring is modelled as deformable body. This simplification reduces the computation time but also guarantees a high degree of accuracy (see [**?**]). Figure 3.1 shows a sketch of the axisymmetric model, a cut is made through the packing ring in the r-z-plane. p_1 and p_2 are the pressures from the working chamber- and atmospheric-side acting on the packing ring. g is the gap between the piston rod and the packing house. RRT is the radial ring thickness, d_i is the inner radius of the packing ring and b is the axial tickness of the packing ring. μ is the friction coefficient between packing ring and piston rod or packing housing. u_{rod} denotes the oscillating displacement of the piston rod during operation.

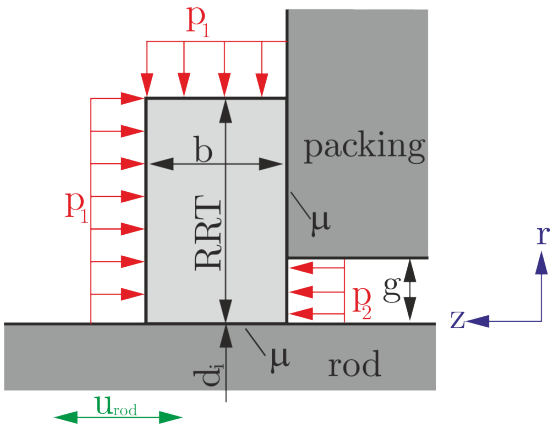

Figure 3.1: Schematic of the axisymmetric model with the relevant model parameters

3.1.1 3D-model of the packing ring

A fully axisymmetric model is no longer admissible if the influence of pressure compensation elements (grooves or bores) and the influence of asymmetry in the pressure gap need to be taken into account. For this reason, a 3D model of the packing ring has to be provided for these analyses. However, some symmetries still apply and can thus be taken advantage of. This means it is sufficient to model only a sector of the entire packing rather than the full 360°. Figure 3.2 and Figure 3.3 show the modelled part of the packing ring with the pressure balancing bores. The geometry definition of the model requires additional parameters, i.e., the diameters of the pressure compensation bores, the distance between the bores and their distance from the edges. This 3D model is also used to determine the influence from the asymmetry of the gap. The asymmetry is created by a displacement of the packing housing in radial direction.

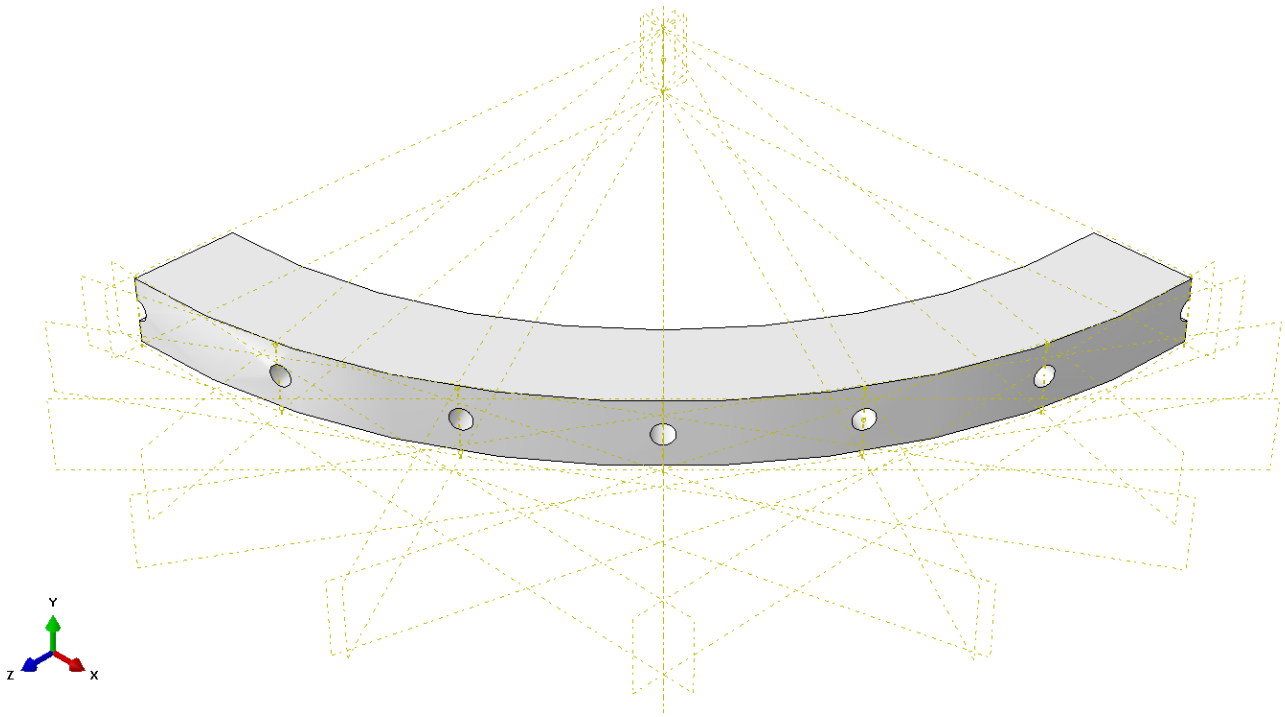

Figure 3.2: 3D-model of the packing ring with the pressure balance holes

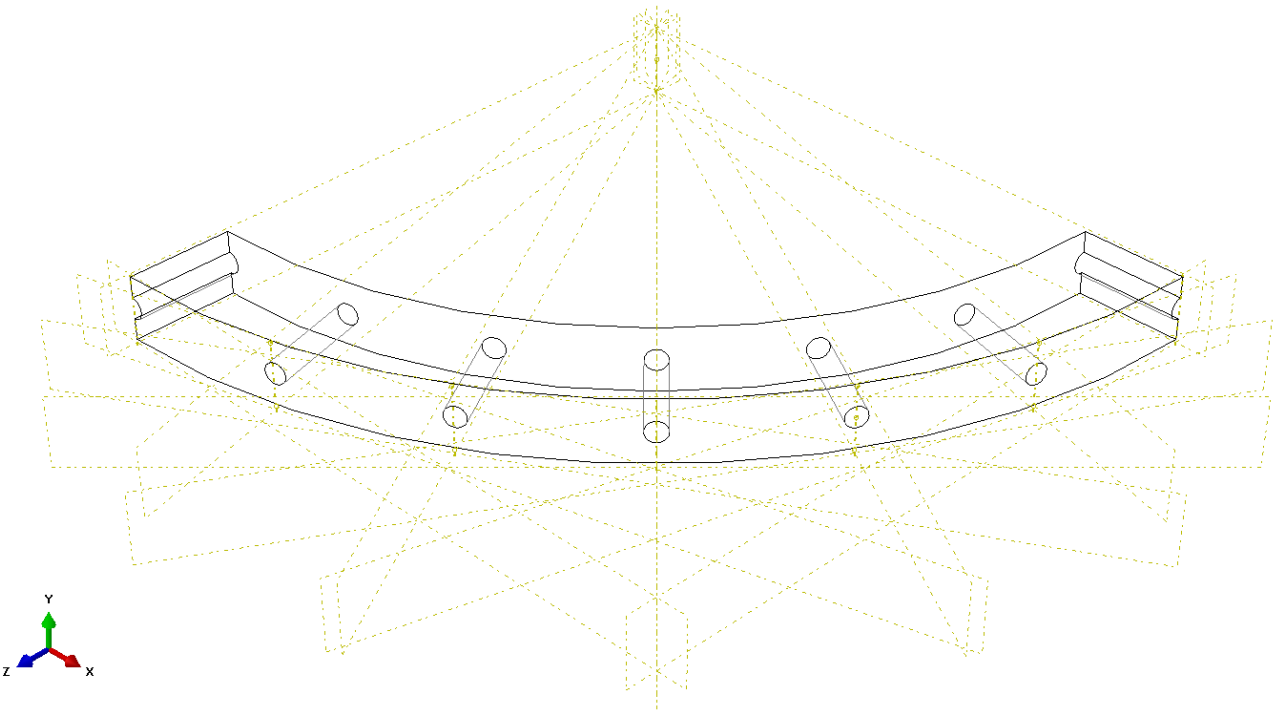

Figure 3.3: 3D-model of the packing ring with the pressure balance holes as wire-frame model

3.1.2 Load definition

The loads due to the acting mechanical pressures are modelled as pressures. After consultation with HOERBIGER Wien GmbH about the temporal development of the acting pressures, they are considered to be constant. In the pack, the suction pressure is sealed. The last packing rings no longer notice the pressure fluctuations, so constant pressure is expected. Here, the pressure is applied in the load application step and then kept constant. The load is applied in Abaqus in a step with the procedure type "STATIC", whereas simulating the time-dependent creep process requires the procedure type "VISCO". The load application phase is therefore executed as a "STATIC" step, as this is numerically more stable than the "VISCO" step and therefore no convergence problems occur.

3.1.3 Piston Rod Movement

This subchapter is purely valid for the simulations with moving piston rod. The boundary conditions of the piston rod are designed in such a way that displacement in the radial direction is blocked (xsym). Only displacement in the axial direction is permitted. The movement of the piston rod is modelled as a sinusoidal displacement signal. This displacement is characterised by the frequency f_{rod} and the amplitude u_{rod}. For the implementation in Abaqus the actual displacement history (see chapter 1.2.2) is approximated by a Fourier series.

3.1.4 Boundary Conditions

The boundary conditions of the rigidly modelled piston rod and packing housing are modelled in the axisymmetric model as well as in the 3D model by a fixed clamping (encastre) of a reference point. Since only a section of the 3D model is modelled, symmetric boundary conditions must be applied at the bounding planes.

3.1.5 Contact

The normal contact is modelled as a "hard" contact. For the tangential contact a penalty formulation is used. More detailed information about the different contact types and formulation options can be found in the Abaqus User Manual [1]. According to [14], [17], [4], the coefficient of friction grows with increasing temperature. According to [14], increasing contact pressure has a friction-reducing effect (i.e., it reduces the coefficient of friction). Increasing the speed at the contact point also has a friction-reducing effect. Although the packing rings are not made of PA but of PTFE, this paper explains in great detail the dependence of the coefficient of friction on temperature, contact pressure and relative velocity. The results are not easily transferable to PTFE. This requires practical material tests. Since no information is available on the influence of these variables on the coefficient of friction between the packing ring and the steel rod, it is for the sake of simplicity subsequently assumed to be constant.

3.2 Selection of analysis method

The selection of a suitable analysis method is important to guarantee useful results in acceptable time or to ensure convergence of the results. In general, a decision has to be made between an implicit or and explicit analysis.

3.2.1 Implicit analysis

An implicit analysis is based on equilibrium iterations. The internal forces $\underline{S}$ corresponding to a first guess of the displacement state $\underline{u}^*$ are generally different from the external forces $\underline{S}^*$ in a nonlinear behavior.

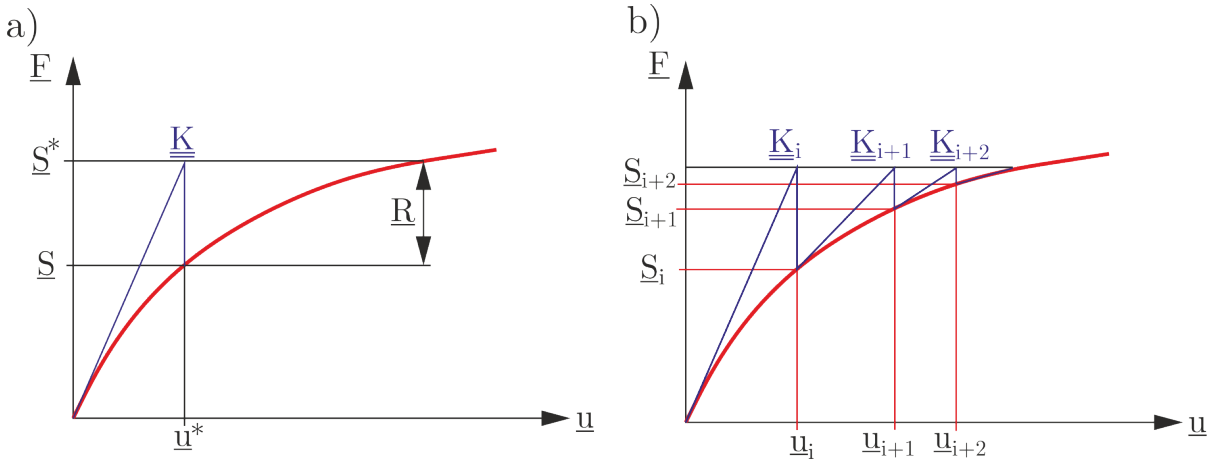

Figure 3.4: a.) Principle of implicit methods
a) Residuum after the first iteration step
b) Equilibrium iterations according to the Newton-Raphson procedure

The fundamental equation of the FE method reads,

$$\underline{S}^* = \underline{\underline{K}}\,\underline{u} \tag{3.1}$$

with the linearised displacement $\underline{u}^*$ instead of the displacement $\underline{u}$ at equilibrium. It is recognisable in Figure 3.4 that the internal $\underline{S}$ and external forces $\underline{S}^*$ are not in equilibrium, i.e., a residual $\underline{R}$ occurs. The task is to determine the displacement such that the residual becomes sufficiently small. This is typically done in an iterative manner using classical solution methods such as the Newton-Raphson scheme.

$$\underline{R} = \underline{S}^* - \underline{S} \tag{3.2}$$

There are many variations of the Netwon-Raphson scheme in the literature which will not be discussed here. The aim of this subchapter is to select an analysis method for the subsequent simulations. For more detailed information, please refer to [21]. Since the stiffness matrix has to be recalculated for each iteration, these methods become ineffective if many time increments are necessary. The great advantage of implicit time methods is there is no constraint on the size of the time increment, i.e., the method is unconditionally stable, which means that convergence is possible after only a few increments. This makes these methods particularly suitable for non-linear quasi-static problems. Since there are no restrictions on the size of the

time increments, implicit analysis is particularly suitable for analysing the long-term behaviour of the material. The largest disadvantage is that convergence issues may arise, depending on the degree of nonlinearity of the problem. This is especially true if contact conditions change during the process.

3.2.2 Explicit analysis

In this case, explicit methods may be the better choice. Figure 3.5 shows the basic principle of explicit procedures.Explicit methods do not require the system of equations to be resolved, as in these methods the load path is approximated stepwise with the tangent stiffness matrix (see Figure 3.5). The absence of equilibrium iterations, however, requires the time increment to satisfy the Courant-Friedrichs-Levy condition, i.e., it has to be less than a critical value which depends on the mesh size and the speed of sound, which in turn is a function of the elastic constants and the density of the material. For the investigated model the maximum allowable time increment is in the order of $\Delta t_{inc} = 10^{-5}$s.

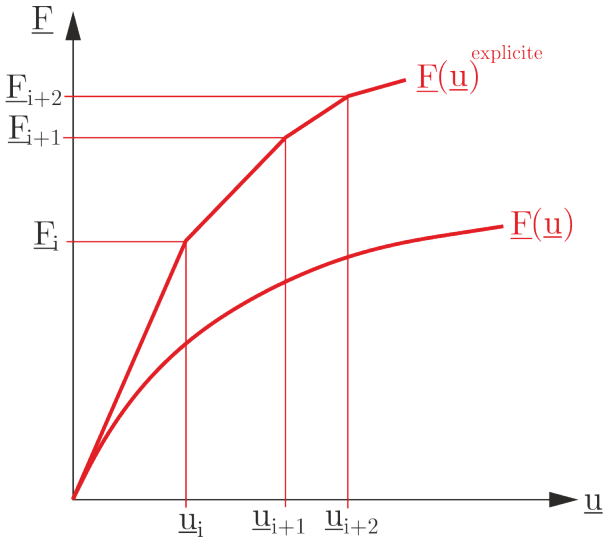

Figure 3.5: Principle of explicit analysis

Explicit analyses are much more suitable than implicit analysis for efficiently investigating the influence of the moving piston rod. On the one hand, there is a non-linearity due to the frictional contact, on the other hand, the increments must be chosen small enough to resolve the motion anyway. However, the small time increments of ($\Delta t_{inc} = 10^{-5}$s) entail excessively many increments and thus long computation times. They can be shortened by mass scaling, i.e. by artificially increasing the density of the material, without degrading the accuracy of the results. This is possible here because the influence of inertial forces is negligible.
The explicit analysis is only used in this Master's thesis for the simulations considering the moving piston rod. Implicit analysis are used for all other simulations.

3.3 Element selection

3.3.1 Element selection for the mechanical problem

The choice of a suitable element type is highly important for the accuracy of a FE simulation. Since there are several contact points in the present problem, it is recommended to use elements with linear interpolation functions in the present mechanical problem. Thus, for the axisymmetric model, axisymmetric continuum elements with linear interpolation functions (CAX4) are chosen. For the 3D geometry, 3D continuum elements with linear interpolation functions (C3D8) are used. Elements with reduced integration should not be used in the present problem since they may cause numerical artifacts such as hourglassing. Figure 3.6 shows the meshing of the axisymmetric Fe model. In the area of the pressure gap, the mesh is finer in order to resolve the displacements more precisely.

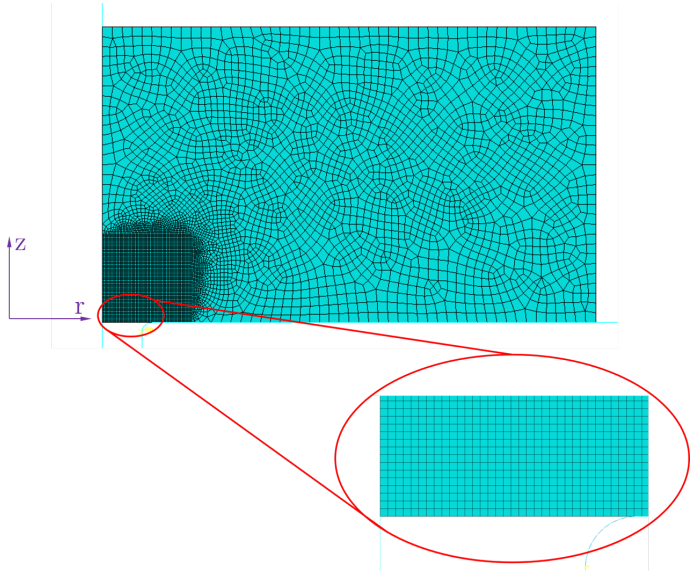

Figure 3.6: Meshing of the axisymmetric model of the packing ring using a finer meshing in the area of the pressure gap

3.3.2 Element selection for the thermal problem

The packing ring is not subjected to a cyclic mechanical load. This means that there are no mechanical hysteresis losses. In this case, the temperature profile in the cylinder ring results from the heat conduction between the cylinder ring and the packing housing as well as the dissipated frictional heat at the contact between the packing ring and the piston rod. Since the piston rod speed as well as the contact pressure influence the friction coefficient and thus the dissipated power, technically a fully thermo-mechanically coupled problem has to be dealt with. However, for the considered case it is sufficiently accurate to calculate the temperature field beforehand and impose it on the mechanical analysis in a decoupled manner. For the thermal analysis DAX4 elements are used as the element type. These are elements for axially-symmetric heat conduction problems with (bi-)linear interpolation function.

3.3.3 Remeshing for large mesh deformations

Due to the time-dependent viscoelastic/viscoplastic yield, large distortions of the FE mesh occur. As a result, the time increments are gradually reduced to guarantee convergence. This continues until the simulation aborts because of excessively distorting elements. To avoid this, it is necessary to remesh, i.e., to redefine the mesh during the simulation. ABAQUS CAE allows several options for remeshing.

ALE adaptive meshing

With the help of the ALE (Arbitrary Lagrangian-Eulerian) remeshing concept, the element distortions can be controlled. When remeshing, the deformed FE mesh is smoothed. This is done by slightly repositioning the nodes without altering the element connectivities. This method is only useful if a single FE mesh is usable throughout the entire analysis. For more detailed information, see [1]

Adaptive meshing

The adaptive remeshing algorithm is normally used to control the accuracy of the results. Within an iterative process, the FE mesh is optimised with respect to a good ratio between accuracy and simulation time. This iterative process is performed separately from the analysis steps. Furthermore, adaptive remeshing is not intended to control element distortion.

Mesh to mesh solution mapping

This adaptation technique is particularly suitable if large element distortions occur. Remeshing takes place between the analysis steps. The principle is simple: As soon as the element distortion becomes unacceptable, the simulation is interrupted. Then a remeshing takes place in the deformed state and all solution variables of the previous analysis step are mapped onto the new mesh. Afterwards, further loading takes place.

Selection of a suitable remeshing concept

The only remeshing concept that is useful for the problem at hand is mesh to mesh solution mapping. However, this method has the disadvantage that it is not automatable and requires a lot of manual intervention.

3.4 Material characterisation

Either a viscoelastic material model or a creep model is used to describe the long-term material behavior of thermoplastic polymers. The problem associated with the use of the viscoelastic material model is the discrete description of the time dependence using the Prony series. With the help of the Prony series, the behaviour is only reasonably predictable in the time decade of the measurement data used for material modelling. At the end of the time decade, the creep compliance converges and no longer changes. Furthermore, the viscoelastic material model is not able to represent viscoplastic flow. The plastically deformed areas, which are located in the area of the manufacturing radius on the housing, creep significantly more than the elastically deformed areas of the packing ring.

3.4.1 Calibration of the Creep parameters

Figure 3.7 shows the calibrated Norton-Bailey model for the material at a temperature of $140°$C. The calibrated model shows good agreement with the measured data. As Figure 3.7 shows, the material model minimally underestimates the real measured values. The creep behaviour of the materials is strongly dependent on temperature. With increasing temperature, the material stiffness decreases and the creep rate increases at the same load level. Thus, it is necessary to calibrate the creep parameters for several temperatures.

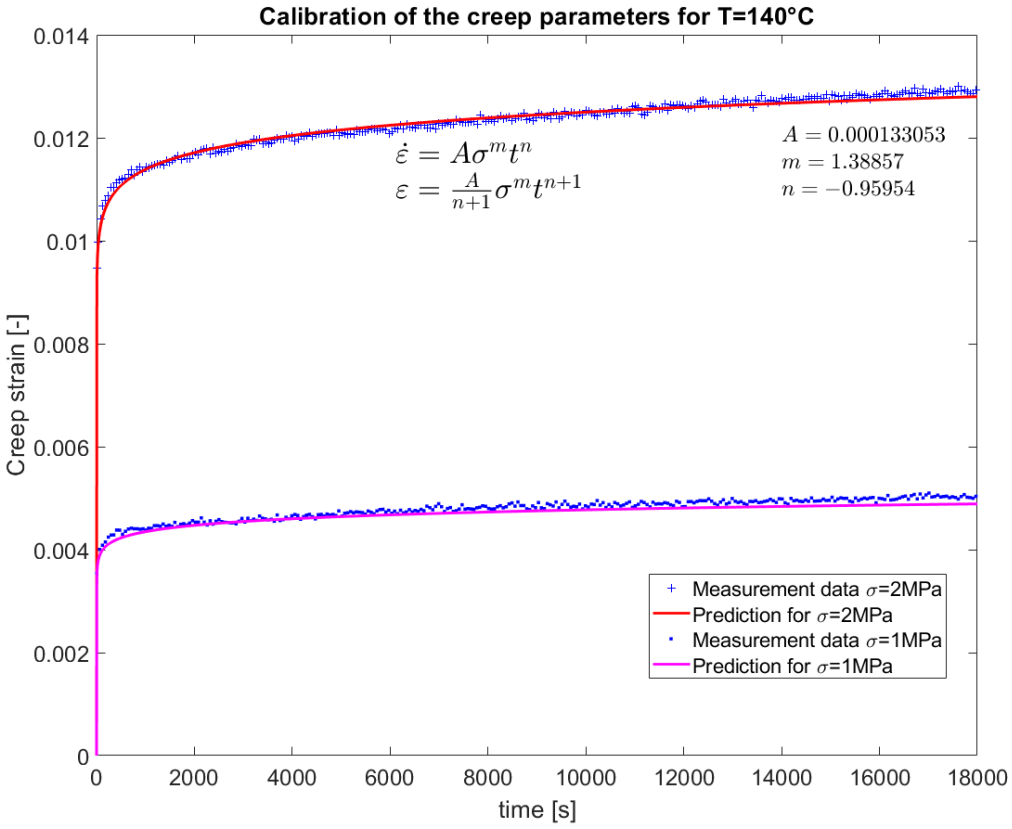

Figure 3.7: Determination of the creep parameters at a temperature of T=140°C

Figure 3.8 shows the calibration of the Norton-Bailey creep model of the material at a temperature of $T = 110°\text{C}$. The calibrated model shows good agreement with the measurement data. The measured data are minimally overestimated with the calibrated material model.

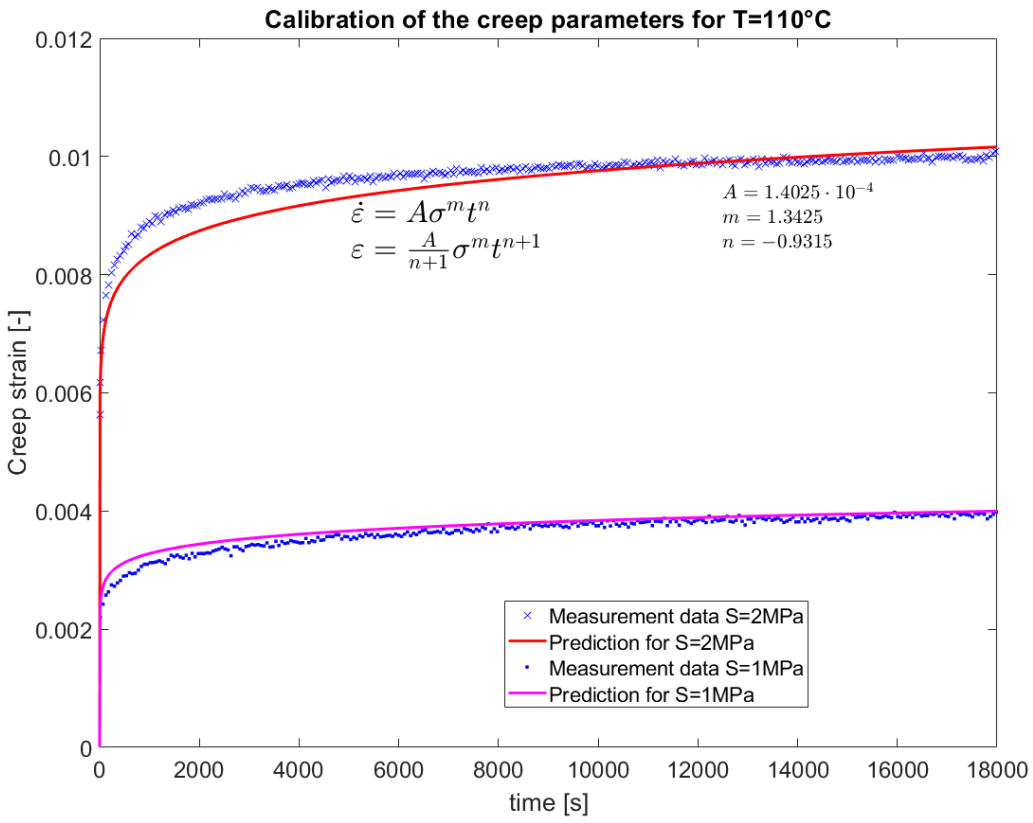

Figure 3.8: Determination of the creep parameters at a temperature of T=110°C

Figure 3.9 shows the calibration of the Norton-Bailey creep model of the material at a temperature of $T = 80°C$. At this temperature, measurement data is available at three different stress levels. The quality of the calibrated material model is sufficiently good for all stress levels. At a stress level of $\sigma = 5$MPa the response of the material is well predicted. For a load of $\sigma = 1MPa$, the material response to the load is somewhat underestimated. For $\sigma = 2$ the material response is slightly overestimated. The material model is calibrated with the load levels of $\sigma = 5$MPa and $\sigma = 2$MPa.

A perfect prediction for all load levels is not possible already from a mathematical point of view. When determining the material parameters based on the measurement data, a mathematically overdetermined system of equations exists. These equations have to be solved by regression methods, e.g. based on a least squares approach.

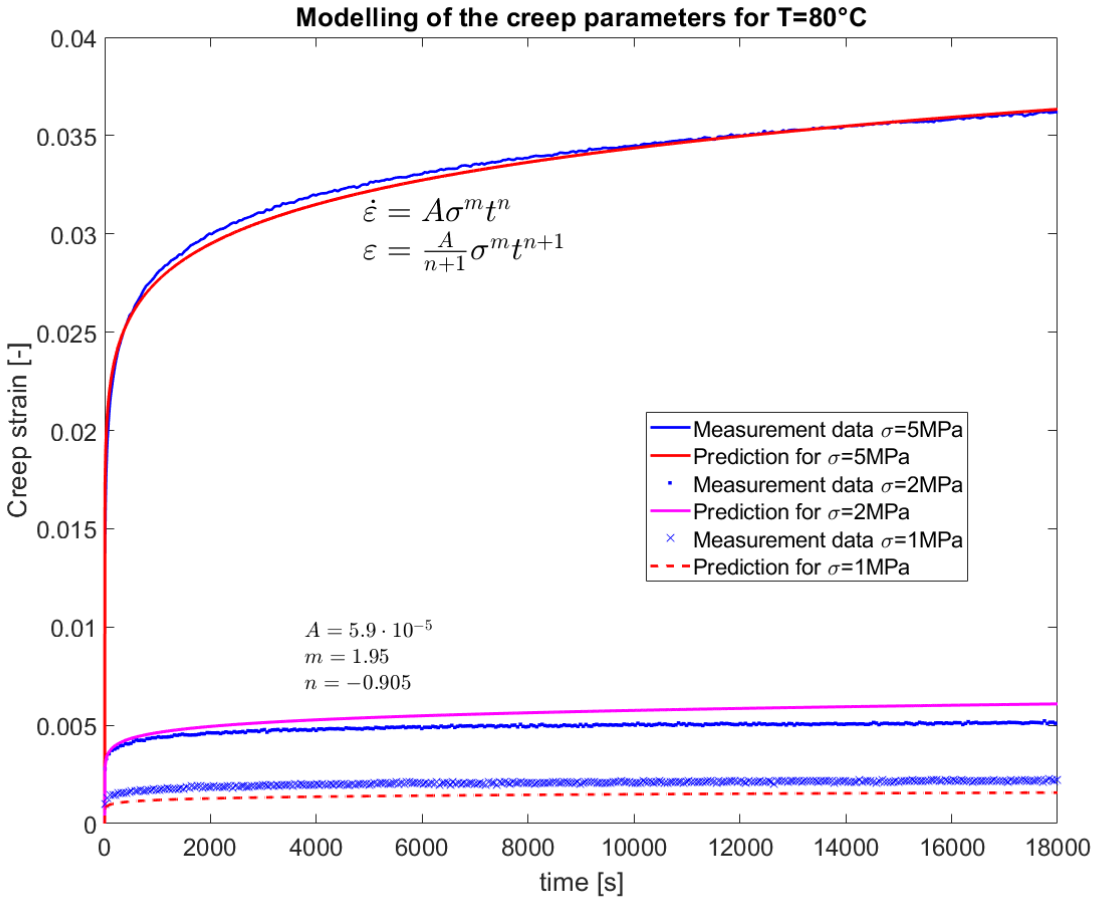

Figure 3.9: Determination of the creep parameters at a temperature of T=80°C

Figure 3.10 shows the calibrated material model and the test data used to calibrate the material model for a temperature of $T = 55°C$. The material model shows small deviations from the test data at all three stress levels. Consequently, load levels that lie in this range are also well approximated. The reasons are discussed in the "Discussion" chapter.

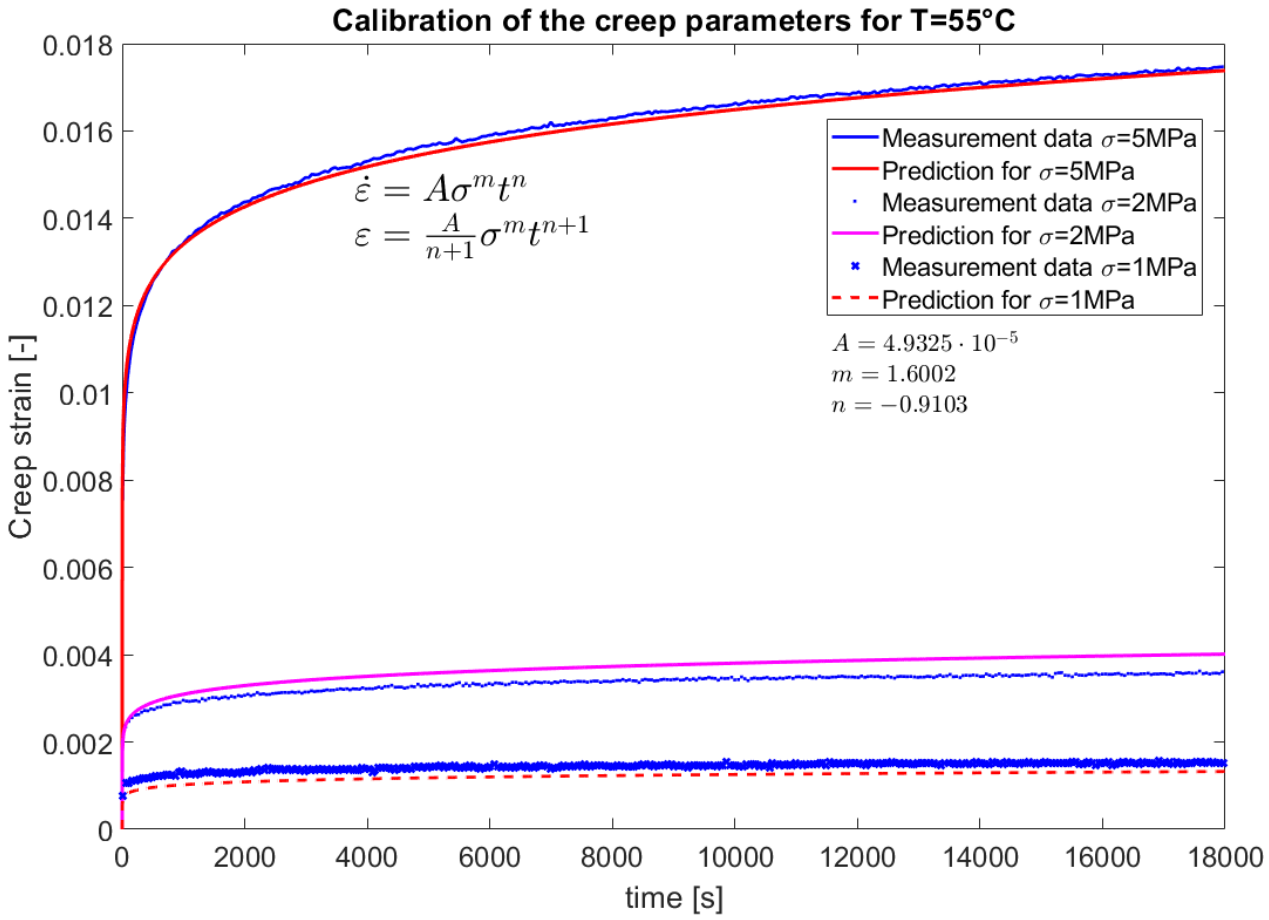

Figure 3.10: Determination of the creep parameters for a temperature of T=55°C

Figure 3.11 shows the calibrated material model and the test data used to calibrate the material model for a temperature of $T = 23°C$. The material model shows good agreement with the test data at all three stress levels. Consequently, load levels that lie in this range are also well approximated.

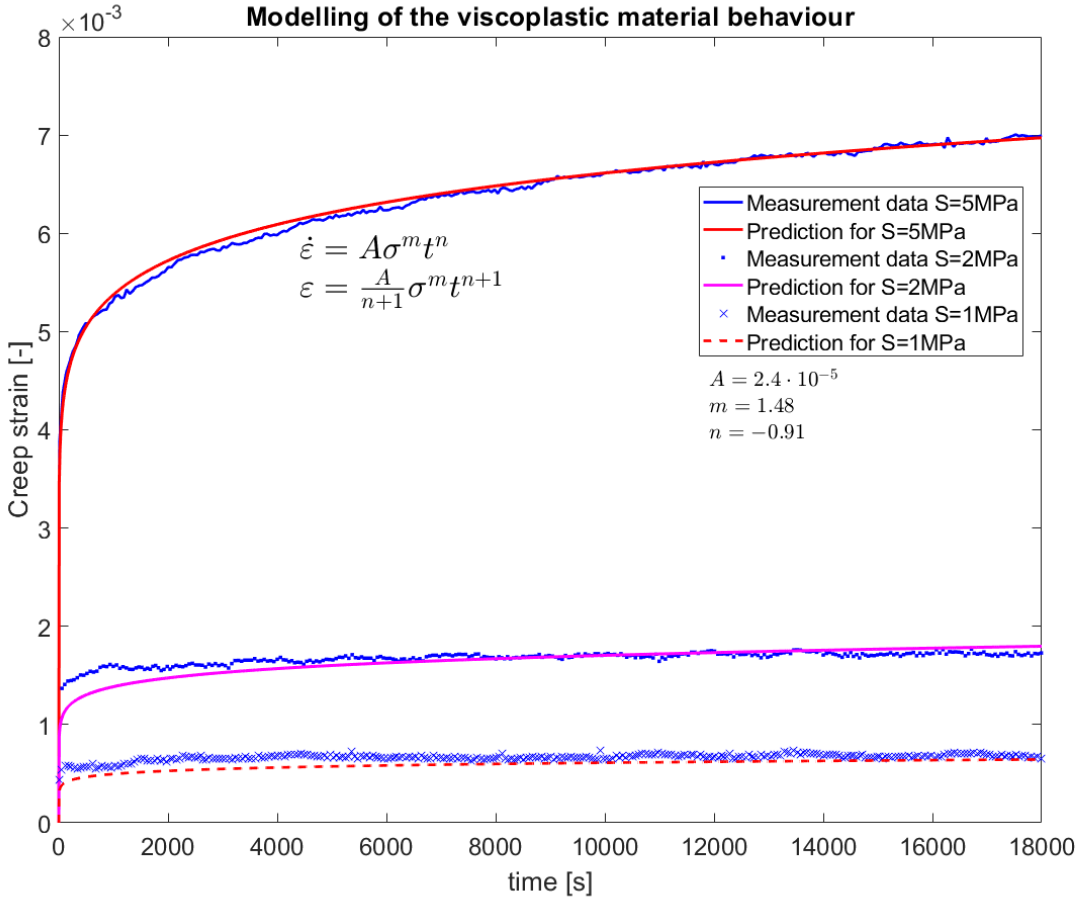

Figure 3.11: Determination of the creep parameters for a temperature of T=23°C

Chapter 4

Results

4.1 Influence of friction on the deformation

The purpose of this chapter is to determine the influence of friction between the piston rod and packing ring on the maximum displacement into the pressure gap.

4.1.1 Influence of friction for the static case

Figure 4.1 shows the influence of friction between the piston rod and packing ring on the displacement into the pressure gap for the static case (no movement of the piston rod) and Δp=40bar. Figure 4.1 shows the deformed contour of the packing ring across the pressure gap (which in this analysis is assumed to be 0.2mm) for four different friction coefficients. As Figure 4.1 shows, an increase in the friction coefficient μ leads to a reduction in the maximum displacement into the pressure gap. The maximum displacements occur when there is no friction. For a friction coefficient of $\mu = 0.2$, the maximum displacement is almost half of the one evaluated for the frictionless case.

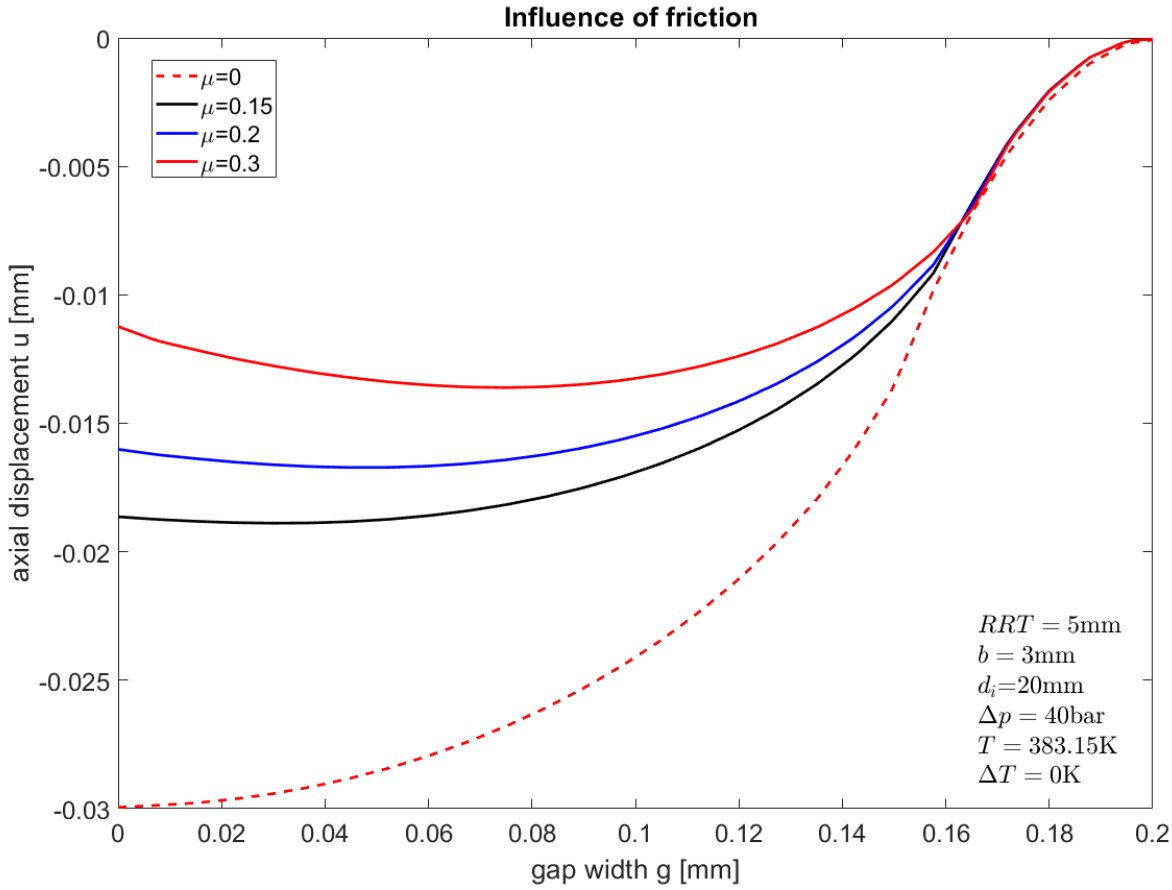

Figure 4.1: Contour of the packing ring across the pressure gap for different friction coefficients for the static case.

As Figure 4.2 shows for the case of Δp=100bar, the friction between the piston rod and the packing ring has a significant influence on the position of the maximum displacement. As expected, in the frictionless case (see Figure 4.1) it is directly at the contact point between packing ring and piston rod. As Figure 4.2 shows an increasing frictional influence leads to a stronger bulging of the displacement curve. The position of the maximum displacement shifts with increasing frictional influence in the direction of the packing housing.

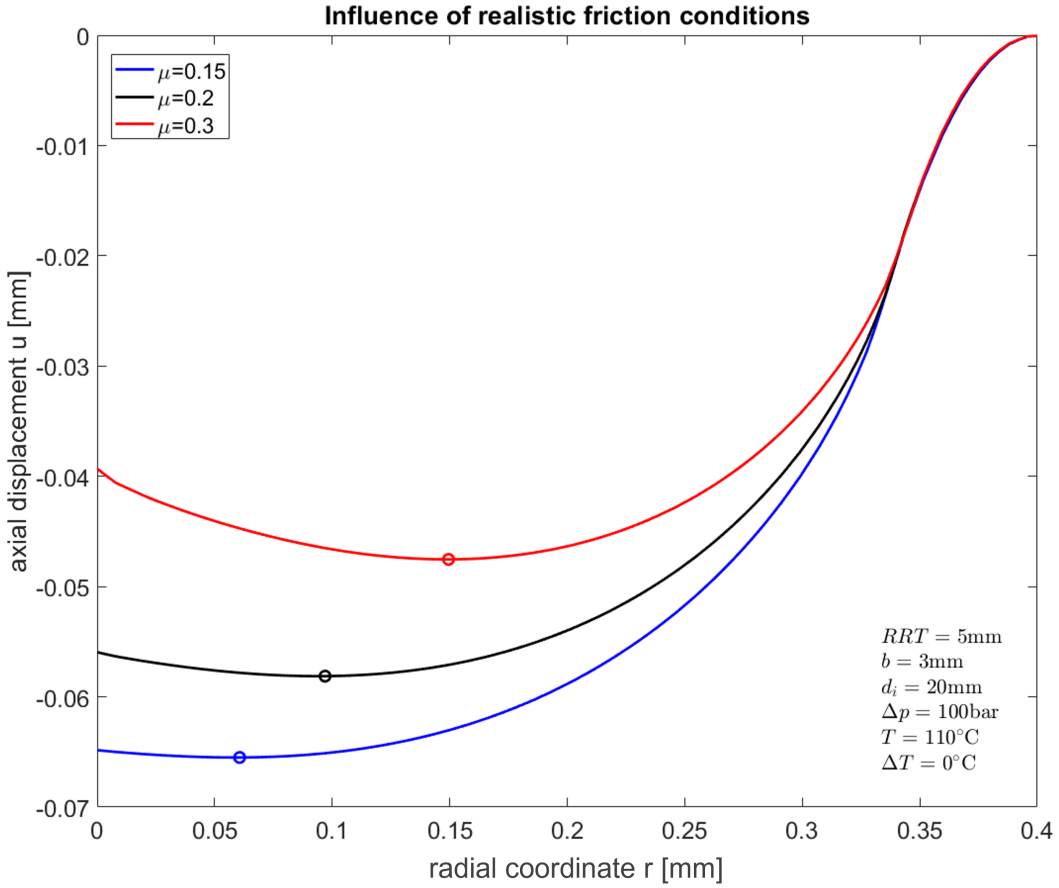

Figure 4.2: Influence of friction on the position of maximum displacement for the static case

4.1.2 Influence of friction for the dynamic case

In the following simulation results, it must be noted that ABAQUS CAE does not distinguish between static friction coefficient and dynamic friction coefficient. This means that as soon as the sticking friction is overcome sliding occurs with the same coefficient of friction. In reality, the coefficient of dynamic friction is slightly lower than the coefficient of static friction.

Figure 4.3 shows the evolution of the displacement of the contact point between the piston rod and the packing ring as a function of time. The linear increase of the displacement at the beginning is due to the load application phase (load application step). The movement of the piston rod is added in the Creep step. The course of the displacement indicates stick-slip effects (see Figure 4.4). This means that during the upward or downward movement of the piston rod, there is initially adhesion between the packing ring and the piston rod and the material point moves with the piston rod. At a certain point, the adhesion condition is violated and the packing ring begins to slide on the piston rod. As soon as the piston has reached the top or bottom dead center and the piston rod changes its direction of movement, adhesion is initially restored. The process is repeated, but in the opposite direction.

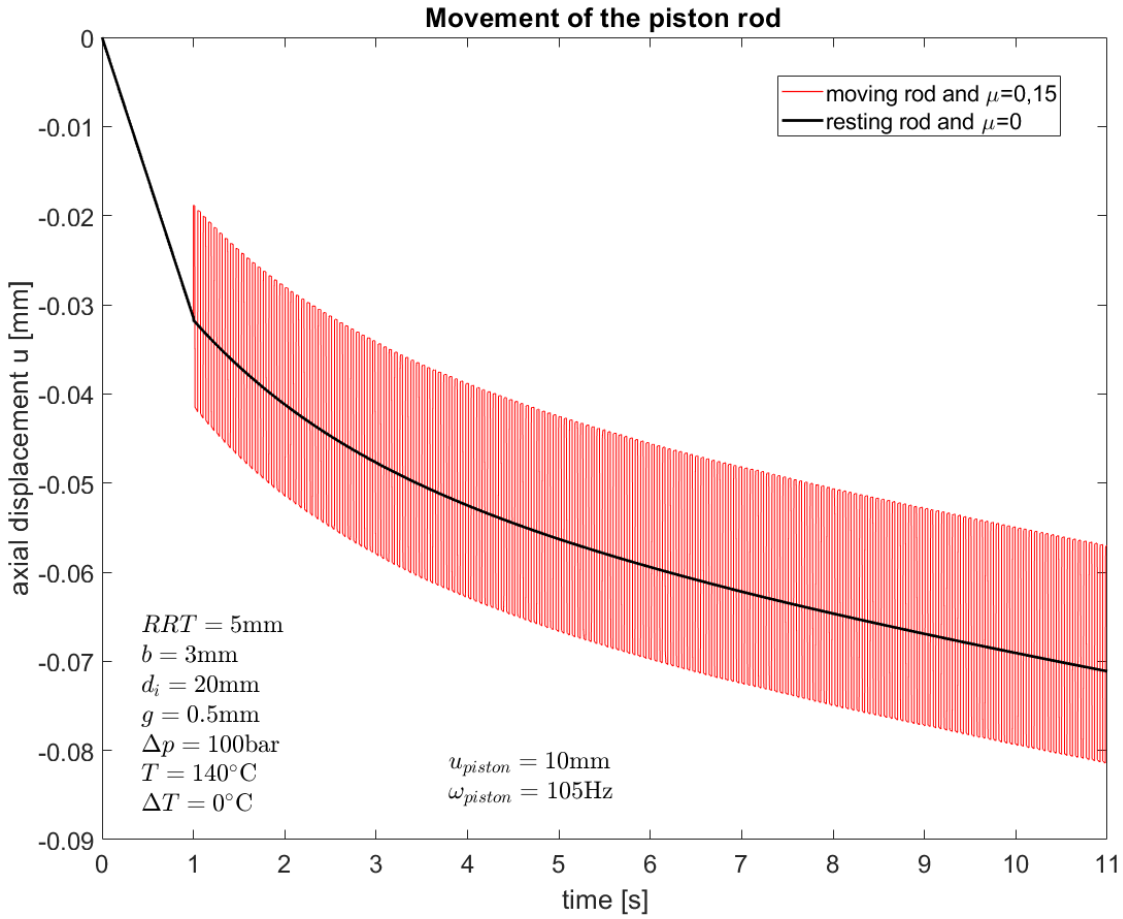

Figure 4.3: Influence of the frictional contact with the piston rod in motion on the displacement of the rod-ring contact point.

As figure 4.3 shows, when the piston rod is moving, the displacement does not oscillate around the corresponding displacement curve when the piston rod is stationary (same friction coefficient). The displacement oscillates around the displacement curve with the piston rod at rest and frictionless contact.

Figure 4.4 shows the evolution of the displacement from Figure 4.3 in more detail. The stick-slip effect is recognisable here. For linear elastic material behaviour, the slip zone would therefore be at the same displacement level after one stroke of the piston. Due to the creep of the material, during the slip the displacement curve exhibits a negative slope. Furthermore, the displacements are no longer at the same level after a stroke of the piston as a result of the creep process.

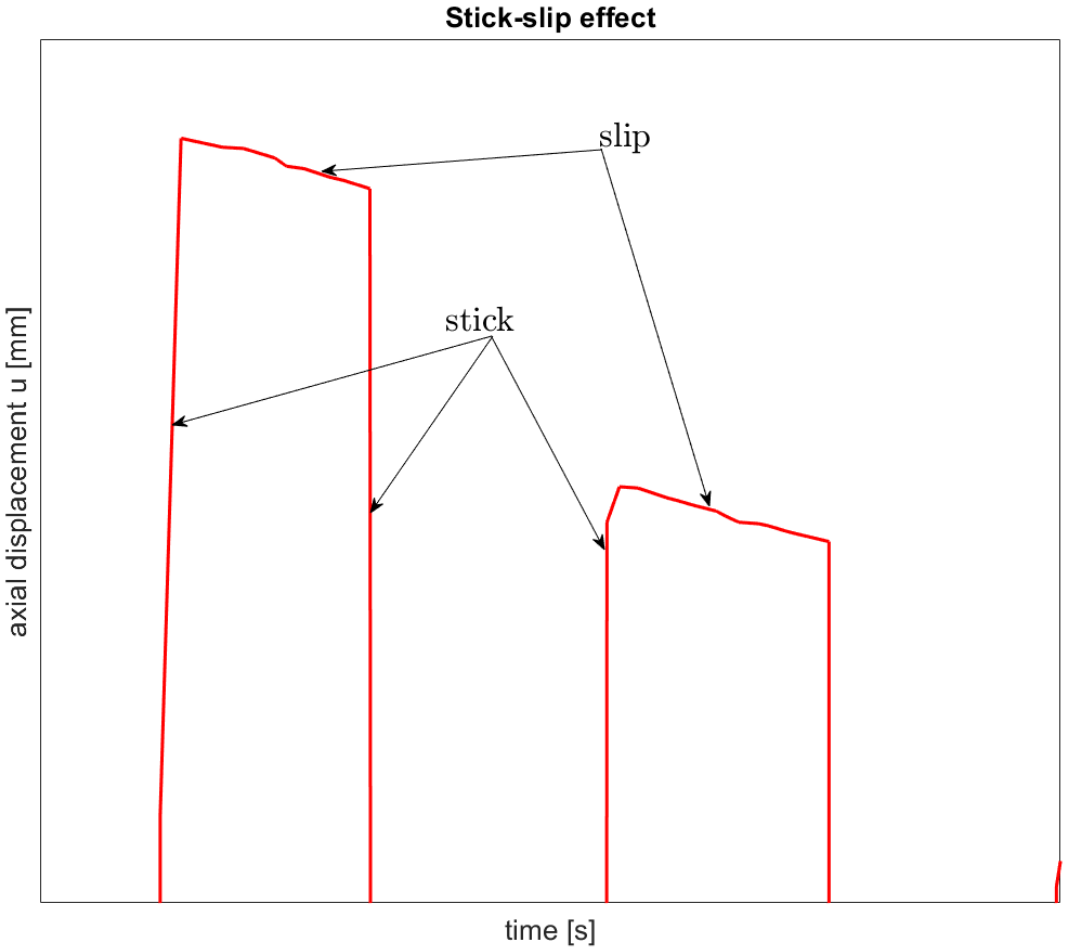

Figure 4.4: Stick-slip effect between packing ring and piston rod during the piston rod movement

Figure 4.5 shows the contour of the packing ring across the pressure gap at three different times (red curves) and for a pressure gap of g=0.5mm. At time $t = 9.962$s, the piston is near crank end (CE). Consequently, the packing ring bulges further into the gap. At time $t = 9.979s$, the piston moves towards head end (HE). As a result of the adhesion between the packing ring and the piston rod, the ring contour shifts upwards. At time $t = 10$s the piston rod continues to move upwards and the adhesion between packing ring and piston rod still acts or the adhesion condition has been violated shortly before and sliding occurs. The blue curve shows the ring contour for the frictionless case and stationary piston rod after a time of 10s.

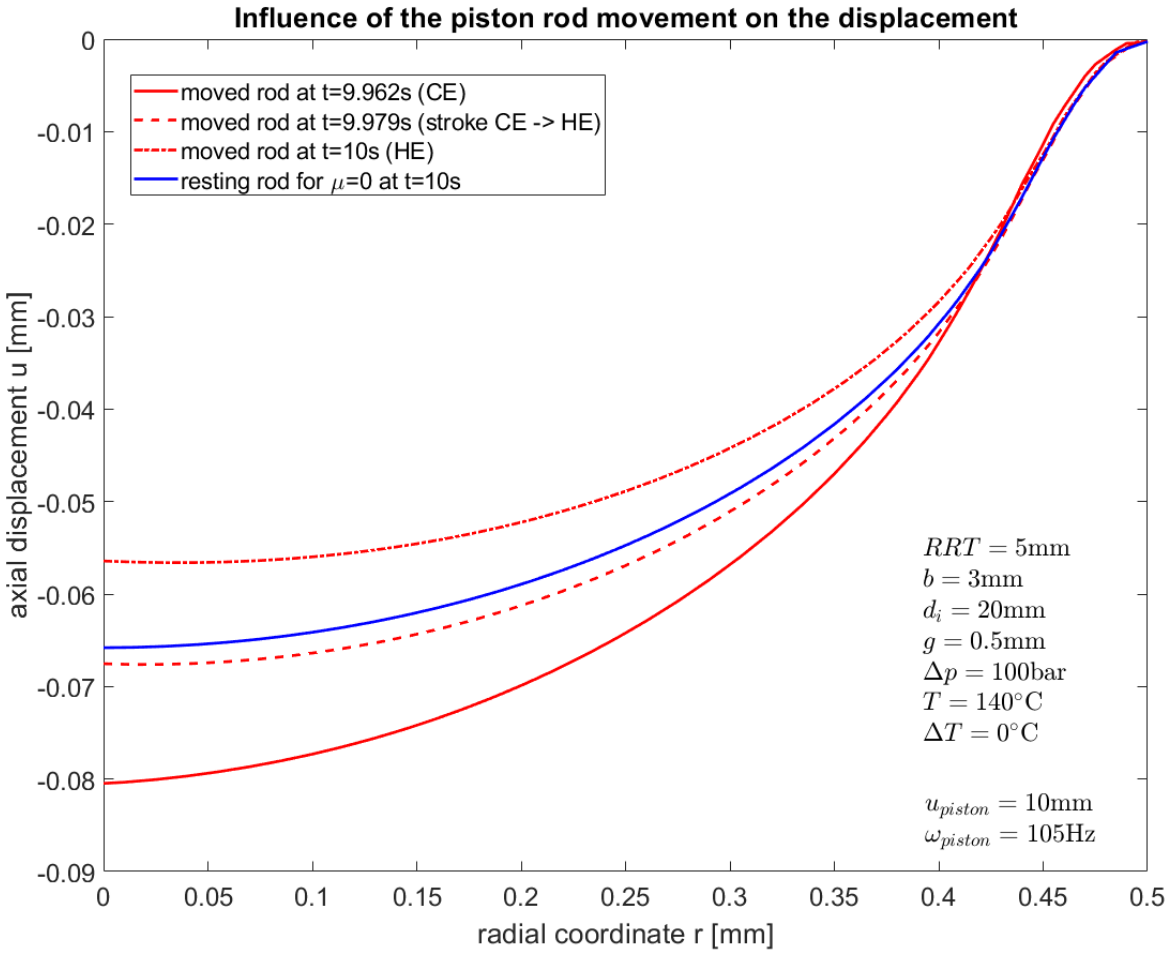

Figure 4.5: Influence of the piston rod movement on the displacement of the ring contour across the pressure gap at different times just before and at 10s.

Figure 4.6 shows the influence of the friction coefficient on the time course of the displacement of the rod-ring contact point. It is recognisable that the amplitude of the oscillation becomes larger with increasing friction. This is explained by the fact that with increasing friction coefficient the adhesion condition remains fulfilled longer and the contact surface on the packing ring is displaced more by the piston rod. Furthermore, Figure 4.6 shows that the displacements oscillate around the same values corresponding to the displacement curve without any friction. This is not surprising, since it is clearly recognisable that the friction only influences the amplitude of the oscillation but not its mean value.

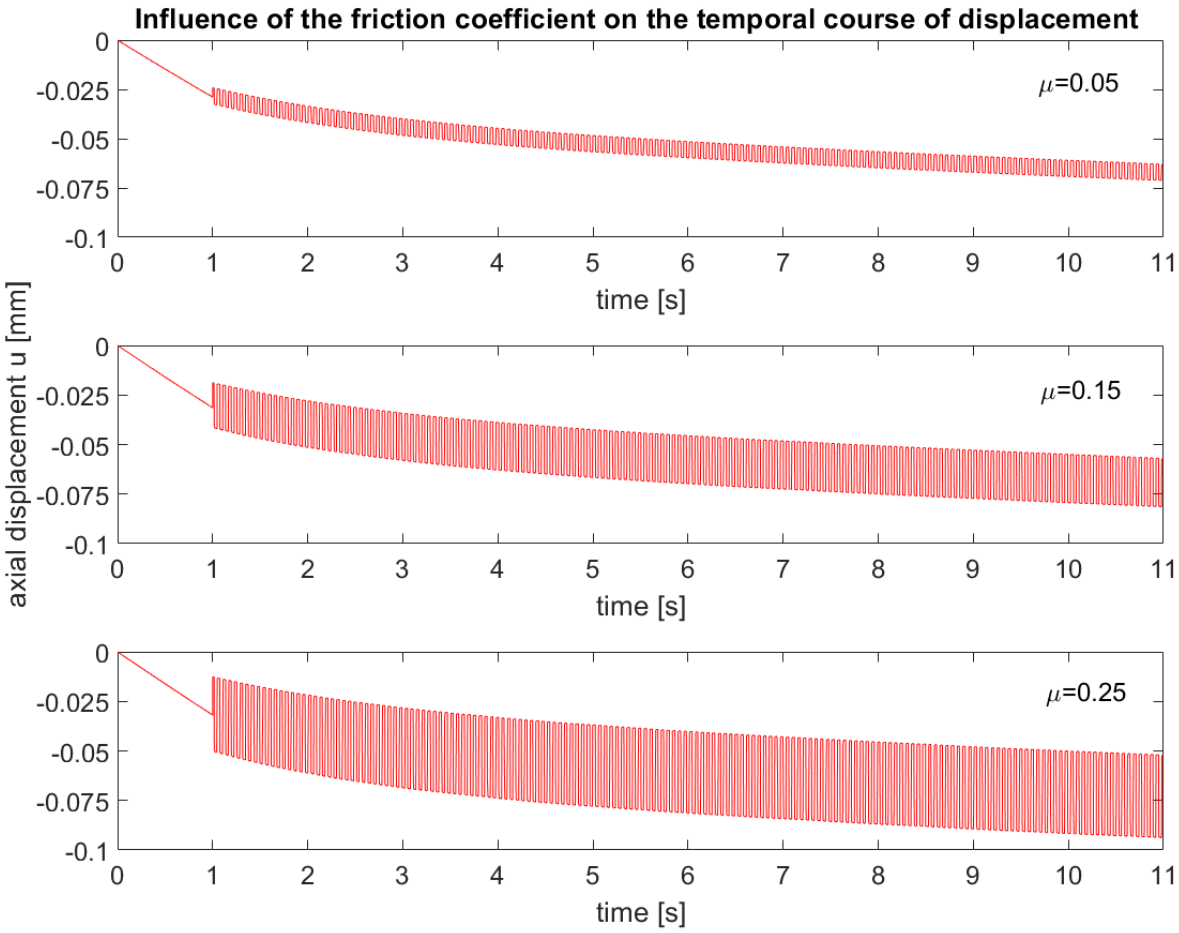

Figure 4.6: Influence of the friction coefficient on the time-evolution of the displacement of the ring-rod contact point.

Consequently, it is permissible to calculate further simulations quasistatically and frictionless. This is permissible because with friction contact and a moving piston rod, the displacement oscillates around the value when the piston rod is stationary and frictionless.

4.2 Influence of the geometry

The initial simulations are performed assuming a linear elastic material model. When using the linear elastic material model, temporal effects such as creep are not captured. The aim of these first simulations is to capture the influence of the geometry on the maximum stresses that occur, as well as the spontaneous elastic deformations. The axisymmetric model is defined by three geometrical parameters, i.e., the radial ring thickness RRT, the axial ring thickness b and the inner radius of the packing ring d_i.

4.2.1 Influence of geometry parameters for linear elastic behaviour

Figure 4.7 shows the influence of b on the maximum Mises stresses. It is evident that the maximum stresses decrease with increasing b. For smaller dimensions, the influence of b is more pronounced. With increasing ring thicknesses, the influence decreases and stabilizes at an axial thickness of 10mm. Larger thicknesses no longer have any influence on the maximum Mises stress.

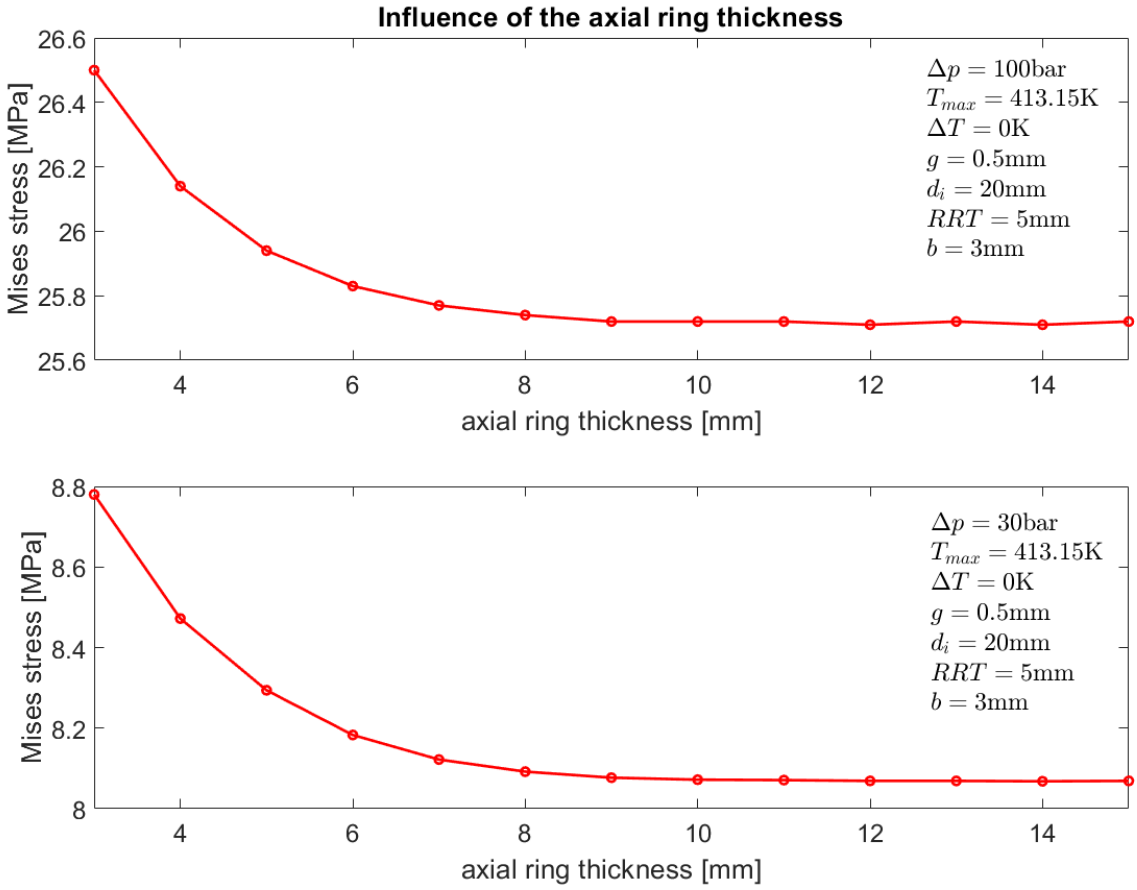

Figure 4.7: Influence of the axial ring thickness on the maximum occurring Mises stress

In addition to the maximum Mises stress, the axial ring thickness also influences the maximum deformation.

Figure 4.8 shows the influence of the d_i on the maximum Mises equivalent stress under the assumption of a linear elastic material behaviour. It is evident that an increase in d_i leads to an increase in the equivalent stress. Figure 4.8 shows that the increase of the Mises stress slows down with increasing d_i.

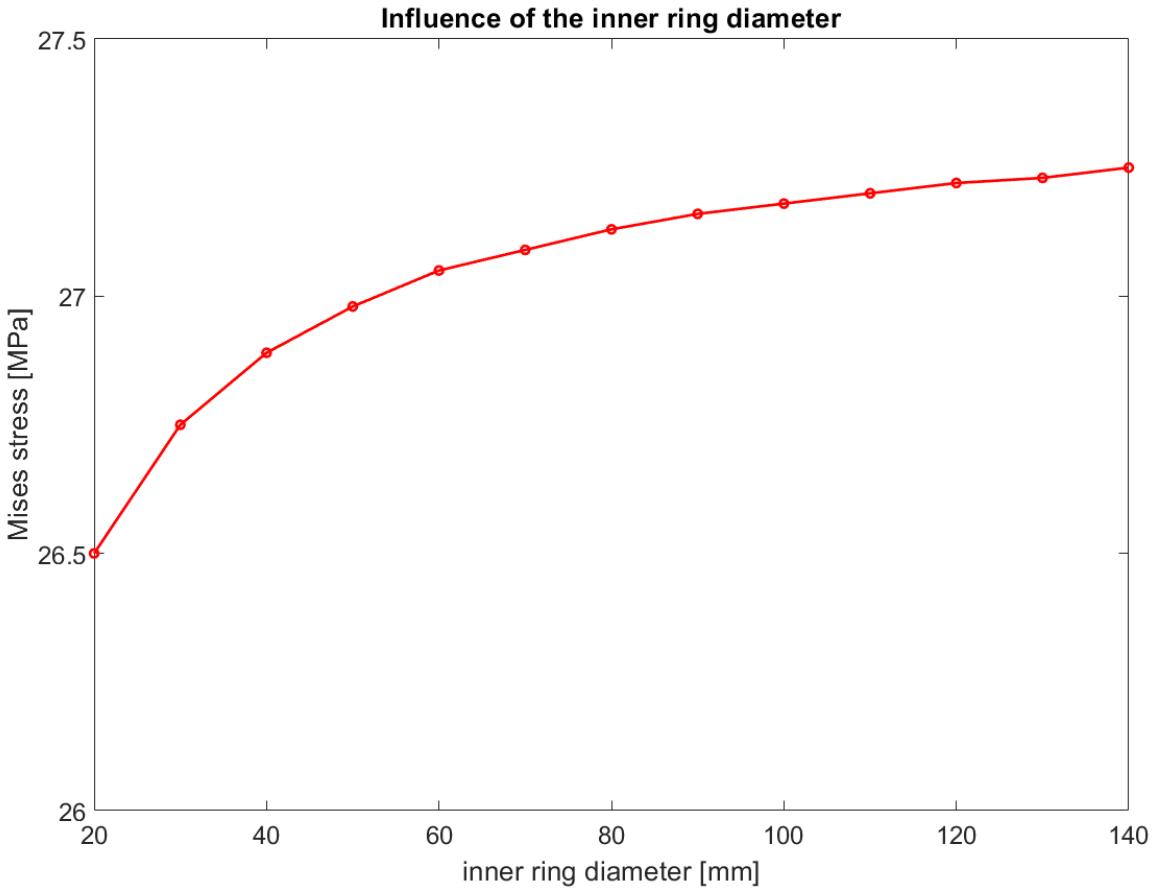

Figure 4.8: Influence of the inner ring diameter on the maximum Mises stress for linear elastic material behaviour

4.2.2 Influence of geometry using a realistic material model

Figure 4.9 shows the influence of the axial ring thickness on the maximum displacements into the pressure gap. Evidently, that influence is significant. An increase in b leads to an increase in the bending rigidity of the system. This reduces the displacements. The results in Figure 4.9 confirm the results in Figure 4.7. From an axial ring thickness of $b = 10\text{mm}$, the maximum Mises stress no longer changes in the linear elastic case. In the case of the more realistic material model, no changes in the maximum displacements occur for larger axial thicknesses.

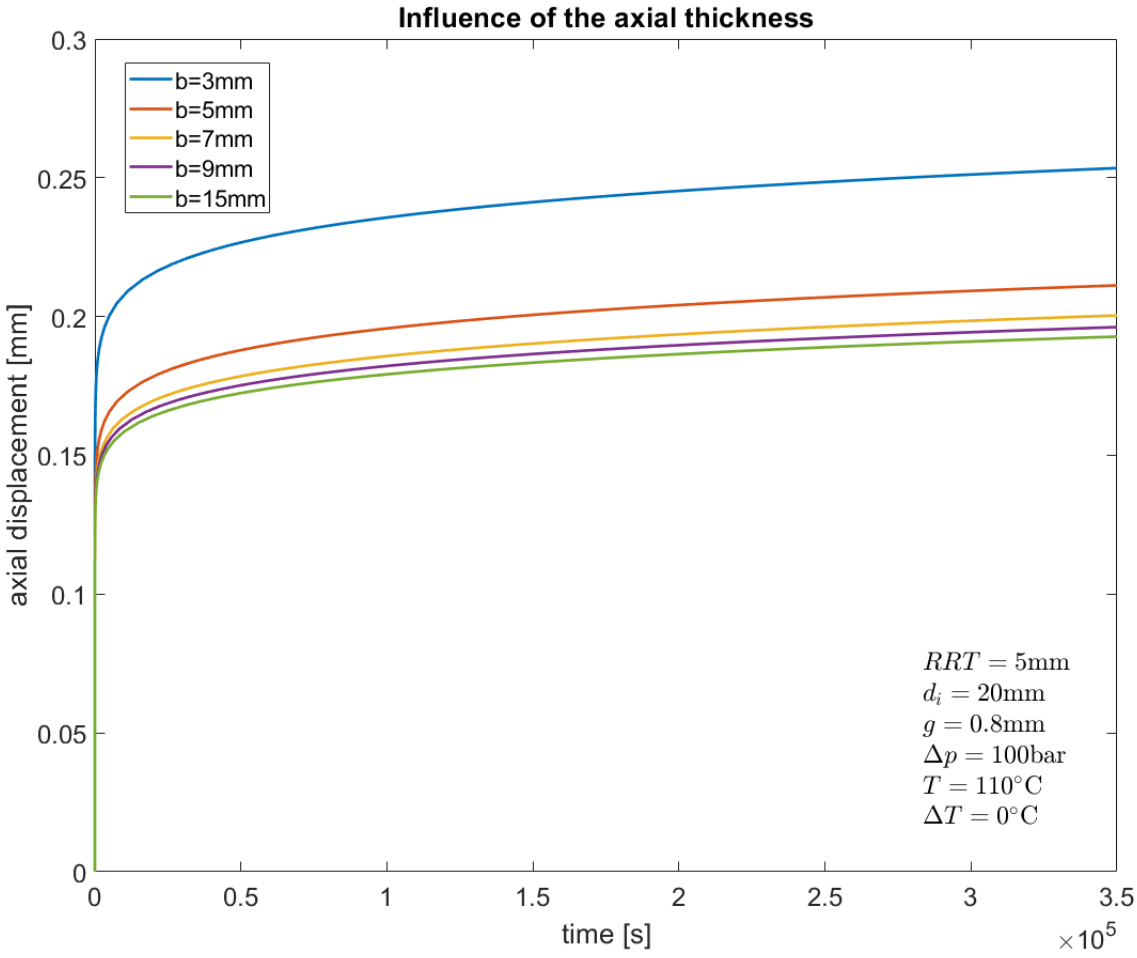

Figure 4.9: Influence of the axial ring thickness on the maximum displacement into the pressure gap using a creep model

With larger pressure gaps and larger pressure differences, the packing ring begins to collapse into the pressure gap, resulting in partial lifting of the packing ring. This is avoided by increasing the axial ring thickness.

Figure 4.10 shows the influence of the inner packing ring diameter on the maximum displacement into the pressure gap using the full material model including plasticity as well as creep effects. An increase in the inner diameter results in an increase in the maximum displacement. This phenomenon is explained by the reduction of the structural stiffness with increasing inner ring diameter, since RRT does not grow along with it. However, figure 4.10 shows that the influence of the inner ring diameter is small compared to the influence of the axial ring thickness. Evidently, the influence of the inner ring diameter is only pronounced in the range between $d_i = 20\text{mm}$ and $d_i = 50\text{mm}$. For larger dimensions, the maximum displacement changes very little.

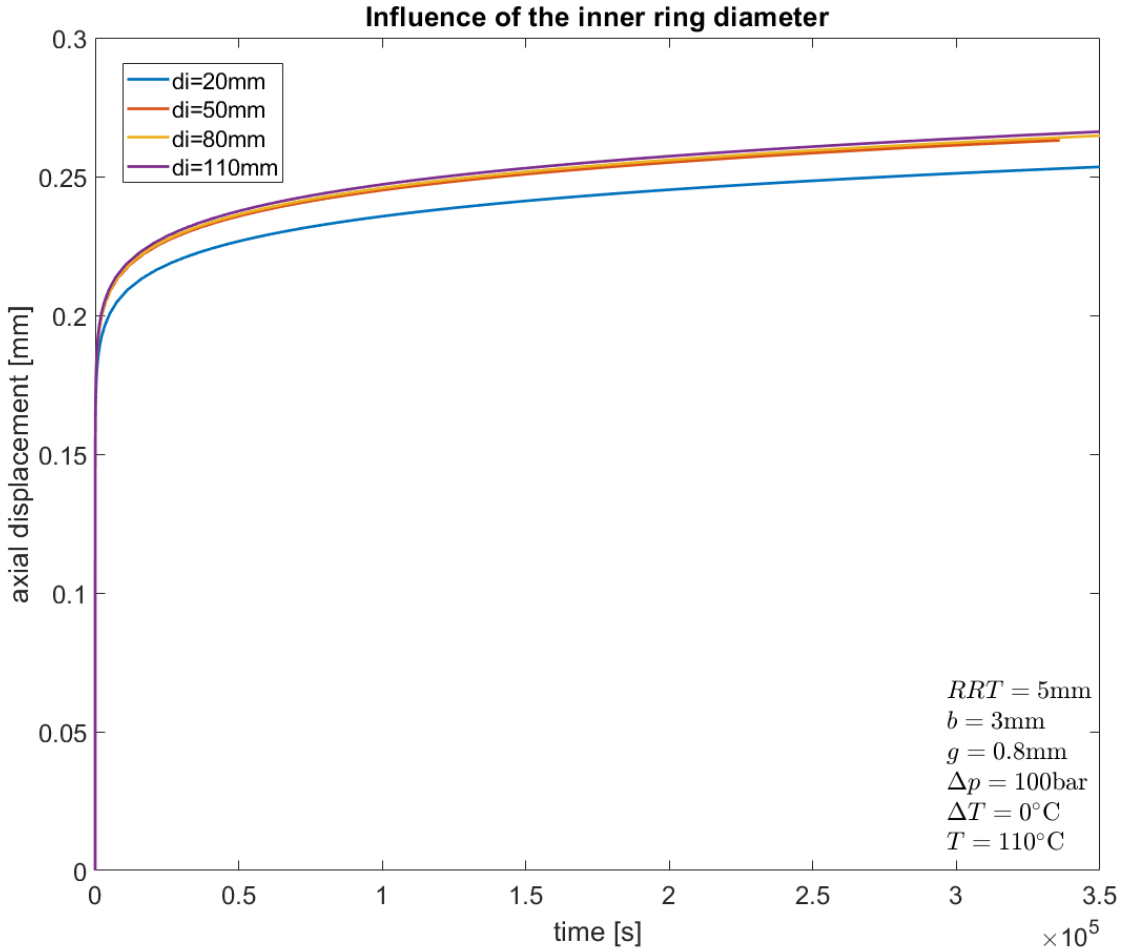

Figure 4.10: Influence of the inner ring diameter on the maximum displacement into the pressure simulated with the full material model including plasticity and creep effects.

Figure 4.11 shows the influence of RRT on the maximum displacement into the pressure gap. The displacement increases minimally with increasing radial thickness. This is explained by the reduction in structural stiffness. Compared with the influence of the axial ring thickness, the influence of the radial ring thickness is negligible.

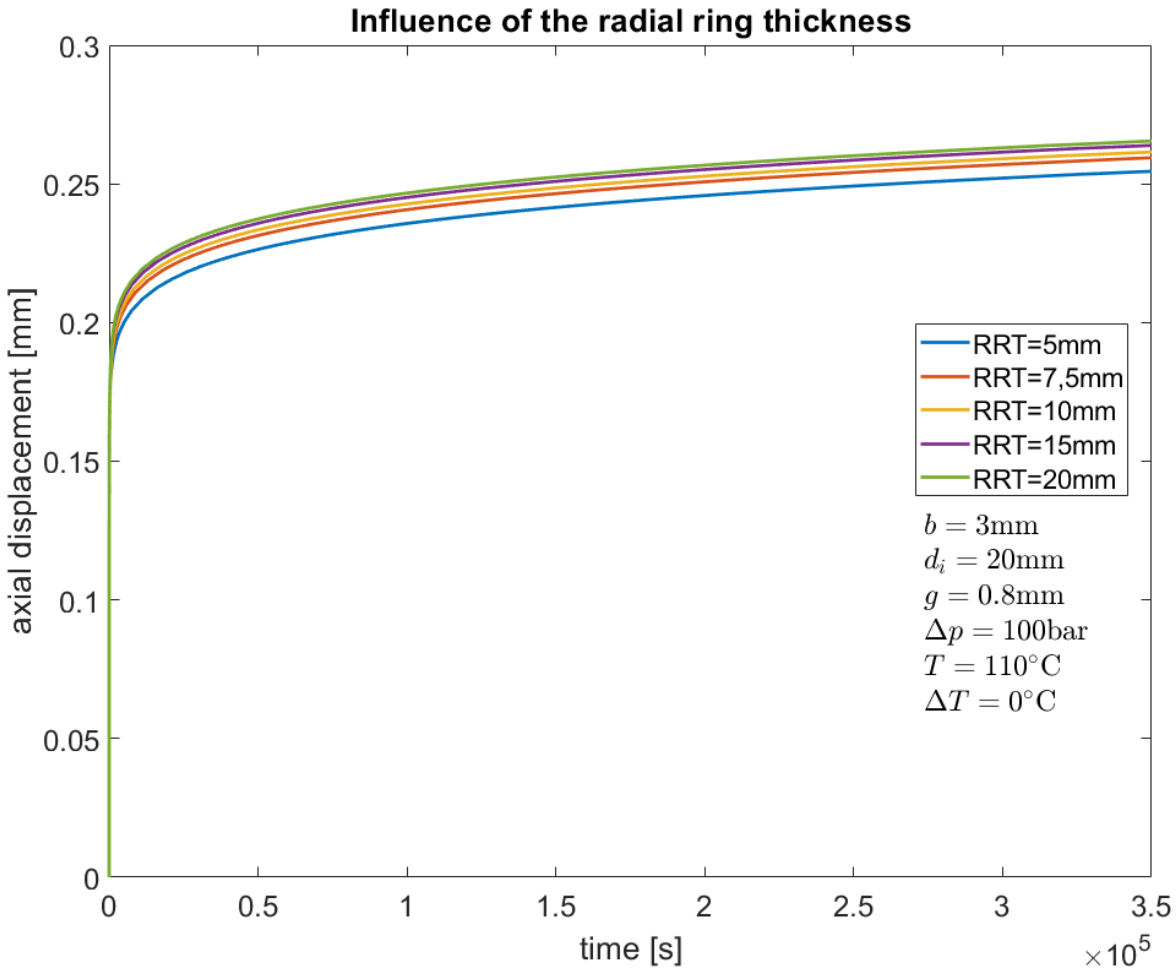

Figure 4.11: Influence of the radial ring thickness on the maximum displacement into the pressure gap using a creep model

4.2.3 Influence of the geometry – Conclusion

The geometry analysis demonstrated above indicates that only the influence of the axial ring thickness needs to be taken into account. The axial ring thickness has a significant influence on the maximum displacement into the pressure gap. The influence of the radial ring thickness and the inner ring diameter is negligible and is therefore not taken into account in the following.

4.3 Influence of the temperature

Temperature has several influences in the present problem. On the one hand, an increase in temperature causes a decrease in material stiffness. On the other hand, the yield strength of the material is reduced. In the case of an isotropic thermal expansion behaviour, no additional thermal stresses are induced in the case of a change of a homogeneous temperature field. However, since the materials used exhibit an orthotropic expansion behaviour, thermal stresses are induced even in the case of a homogeneous temperature field.

4.3.1 Influence of the temperature on the maximum displacement

Figure 4.12 shows the influence of temperature and gap width on the maximum displacement in the direction of the gap between piston rod and packing housing. These simulations are performed using a linear elastic material model. However, the use of a linear elastic material model is unsuitable for dimensioning the compression gap, since the influence of time on the deformation is not considered. Only the temperature dependence of the Young's modulus is recorded. As the temperature increases, the stiffness of the material decreases, resulting in larger displacements. The displacement increases strongly non-linearly with increasing pressure gap. This is due to the dependence of the bending on the gap.

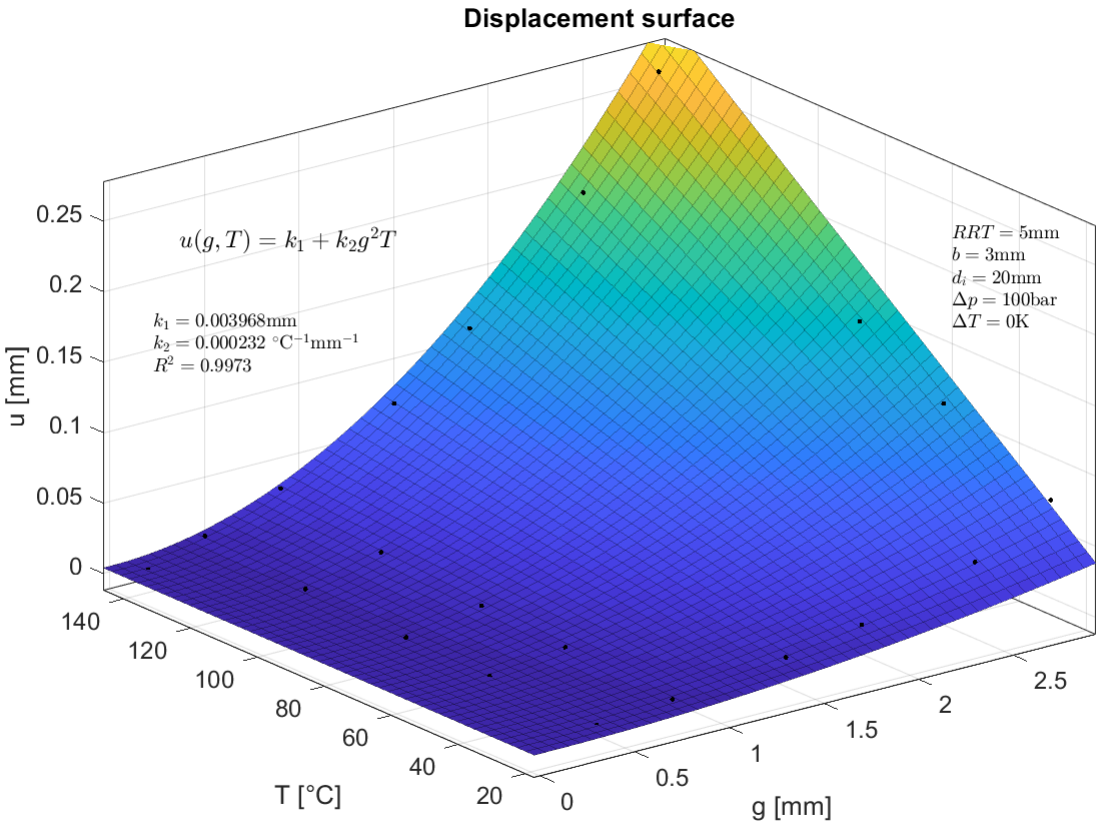

Figure 4.12: Influence of the temperature and the gap on the maximum displacement assuming a temperature dependent linear elastic material behaviour

An interpolation surface can be fitted to the simulation data. For linear elasticity, it can be determined by the following equation 4.1,

$$u(g,T) = k_1 + k_2 g^2 T \tag{4.1}$$

where u is the displacement, T is the temperature, g ist the pressure gap width, k_1 and k_2 are coefficients of the interpolation function. The coefficients of the interpolation function are shown in figure 4.12.
Figure 4.13 shows the contour plot of the interpolation surface 4.12. Although the simulations are performed with the linear elastic material model, the maximum displacements for the given conditions are already large in the upper temperature window and for larger gaps.

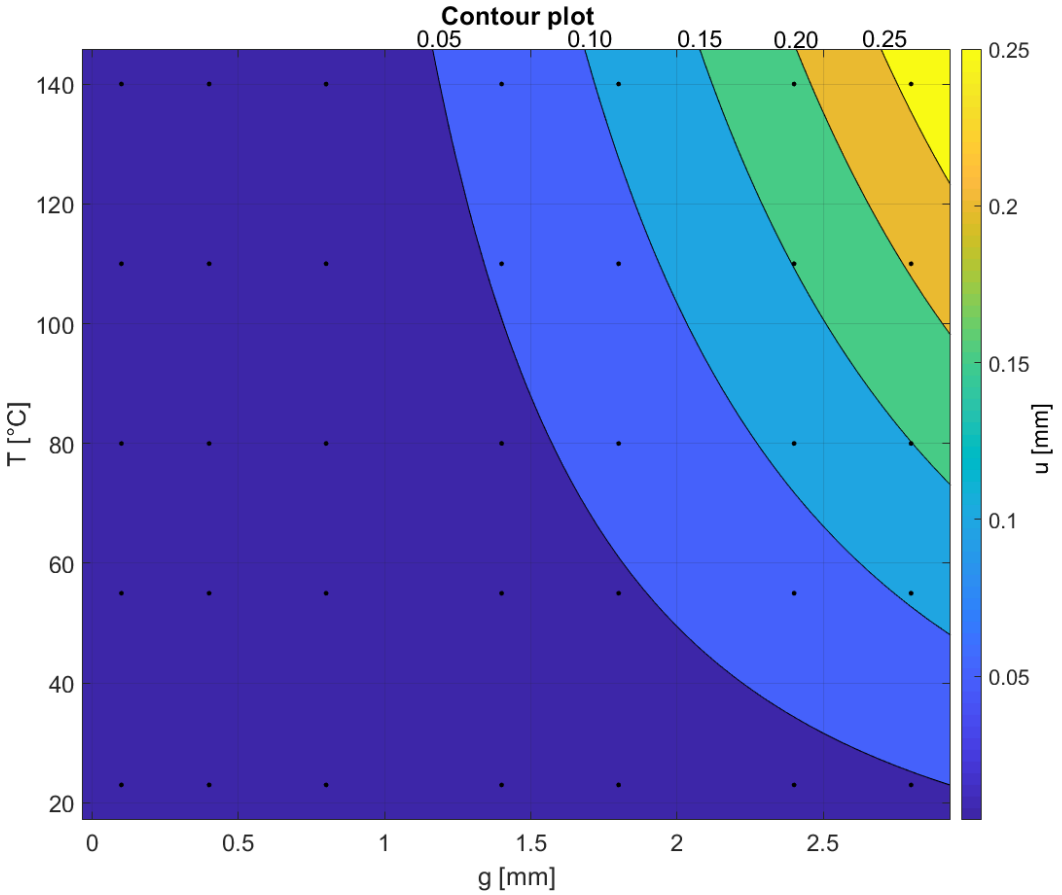

Figure 4.13: Contour plot of the displacement-temperature-gap surface shown in figure 4.12

4.3.2 Thermal stresses and displacements

Due to the orthotropic thermal expansion, additional stresses are induced in the packing ring. Figure 4.14 and 4.15 show the thermal stresses assuming a homogeneous temperature field and a temperature increase of 60K. No additional stresses are induced in axial direction. The orthotropic behaviour does not cause any additional shear stresses, only normal stresses. The greatest stresses appear in the circumferential direction. Tensile stresses occur at the inner edge and compressive stresses at the outer edge (see Figure 4.15).

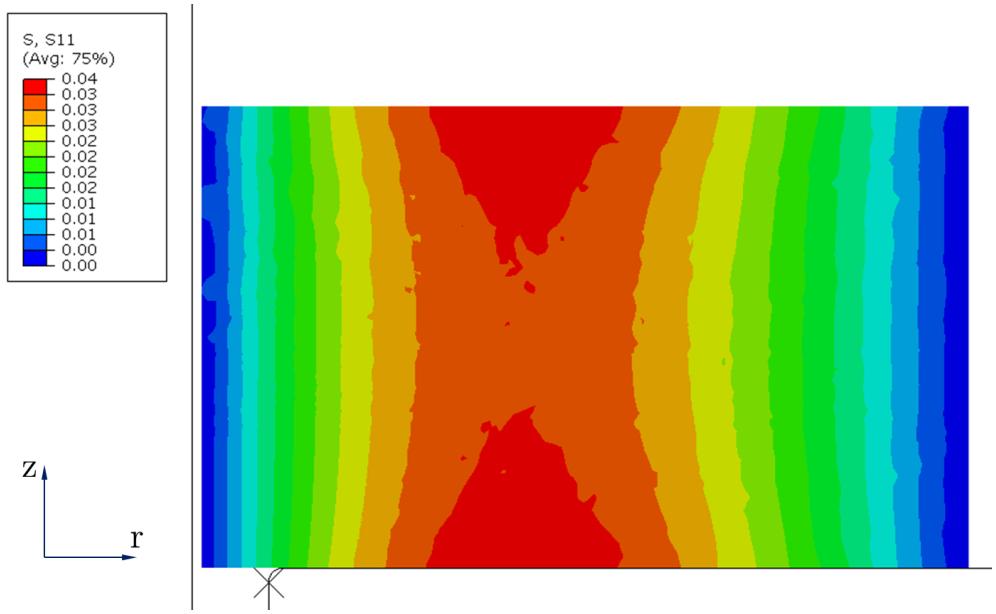

Figure 4.14: Additional thermal stresses (in MPa) in radial direction through thermal expansion

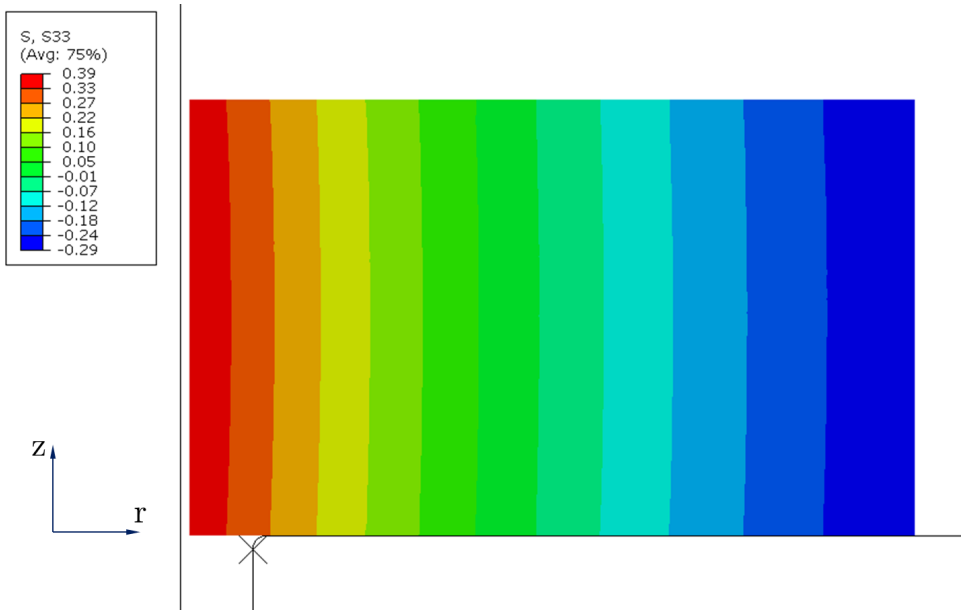

Figure 4.15: Additional thermal stresses (in MPa) in circumferential direction through thermal expansion

Due to the orthotropic thermal expansion properties of the material, stresses result even when the temperature field changes homogeneously. In the case of isotropic thermal expansion behavior, the homogeneous change of the temperature field does not result in additional stresses. In case of orthotropic expansion, the stresses are induced due to the non-uniform thermal expansion. These stresses are residual stresses. Consequently, it is necessary that the forces and moments resulting from the induced stresses are in equilibrium.

$$\underline{F} = \int_A \underline{\sigma}_n \mathrm{d}A = \underline{0} \tag{4.2}$$

where $\underline{F}$ is the resulting force vector and $\underline{\sigma}_n$ is the stress vector.

Franz-Josef-Str. 18/III, 8700 Leoben
mechanik@unileoben.ac.at
Chair of Mechanics

4.3.3 Influence of the real temperature field

Until now, the temperature field inside the packing ring is considered to be constant. The piston rod and the packing housing generally have different temperatures. From the heat conduction in the packing ring, an inhomogeneous temperature field results. Additional stresses and distortions result from the inhomogeneous temperature field.

Figure 4.16 shows the temperature field in the packing ring in the steady state. It is obvious that the maximum temperatures occur at the contact to the piston rod, while the lowest temperatures occur at the contact to the housing wall. Due to the frictional contact between the piston rod and the packing ring, energy is dissipated during the movement of the piston rod.

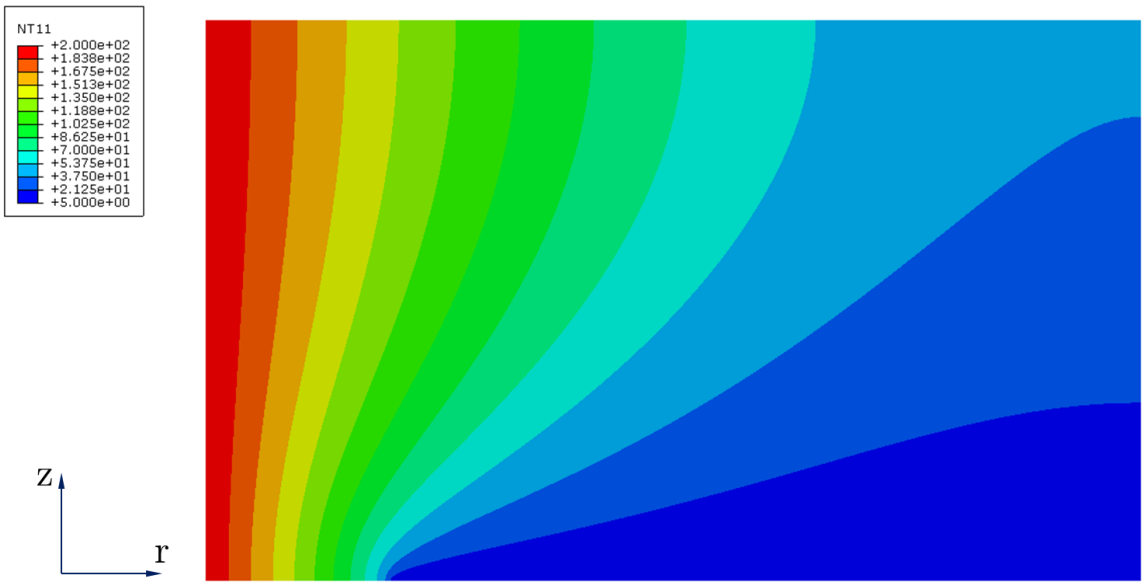

Figure 4.16: Temperature field in °C inside the packing ring due to heat conduction for HY54

Figure 4.17 shows the maximum displacement into the gap as a function of the temperature of the piston rod as well as the temperature of the packing housing. Figure 4.17 shows that the temperature of the piston rod has a greater influence on the maximum displacement than the temperature of the packing house. The simulations are performed under the conditions shown in 4.17 and the full material model. The maximum displacements occur for the case of homogeneous heating of the packing ring. For this reason, a homogeneous temperature field is used to determine the critical pressure gap width (chapter 4.8). Figure 4.18 shows the contour plot of the displacement surface in Figure 4.17.

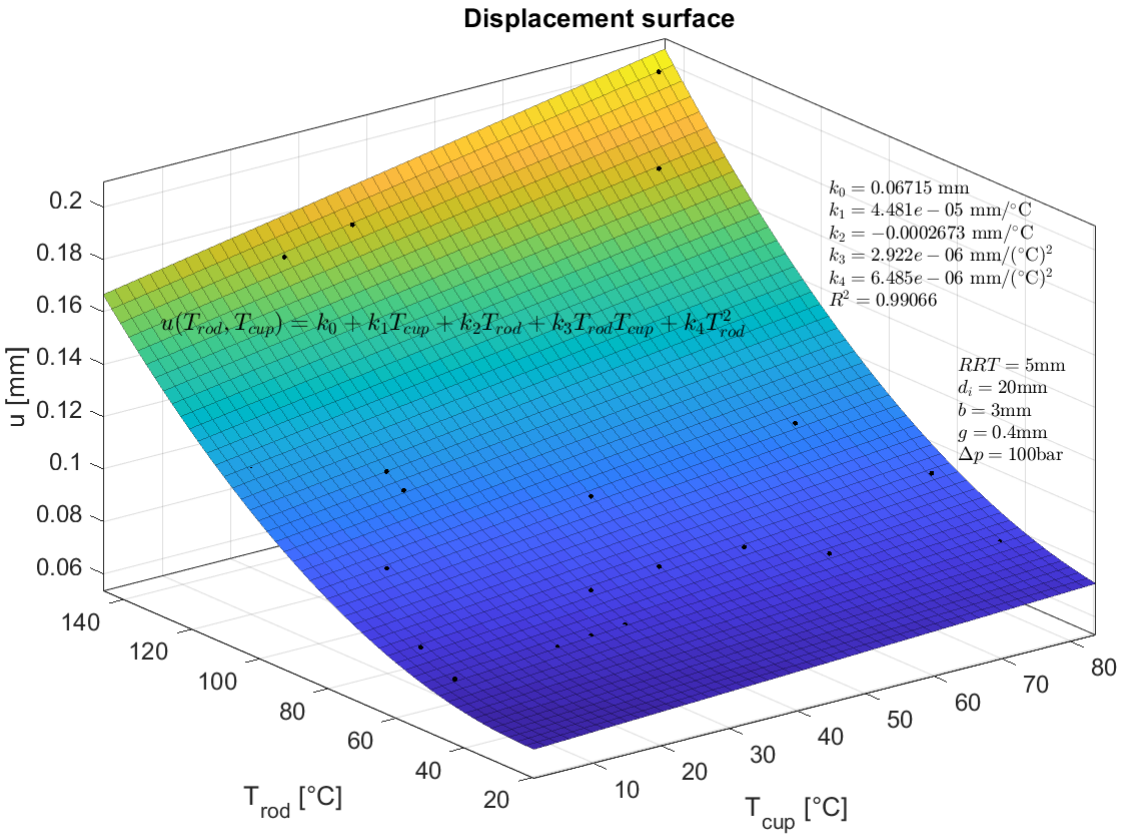

Figure 4.17: Influence of the temperatures of the rod and the packing on the maximum displacement into the pressure gap

The maximum displacement as a function of rod and packing house temperature is well described by the following interpolation function,

$$u(T_{rod}, T_{cup}) = k_1 + k_2 T_{rod} + k_3 T_{rod} T_{cup} + k_4 T_{rod}^2 \tag{4.3}$$

where $k_1 ... k_4$ are the coefficients of the interpolations polynomial, T_{rod} is the temperature of the piston rod and T_{cup} is the temperature of the packing house.

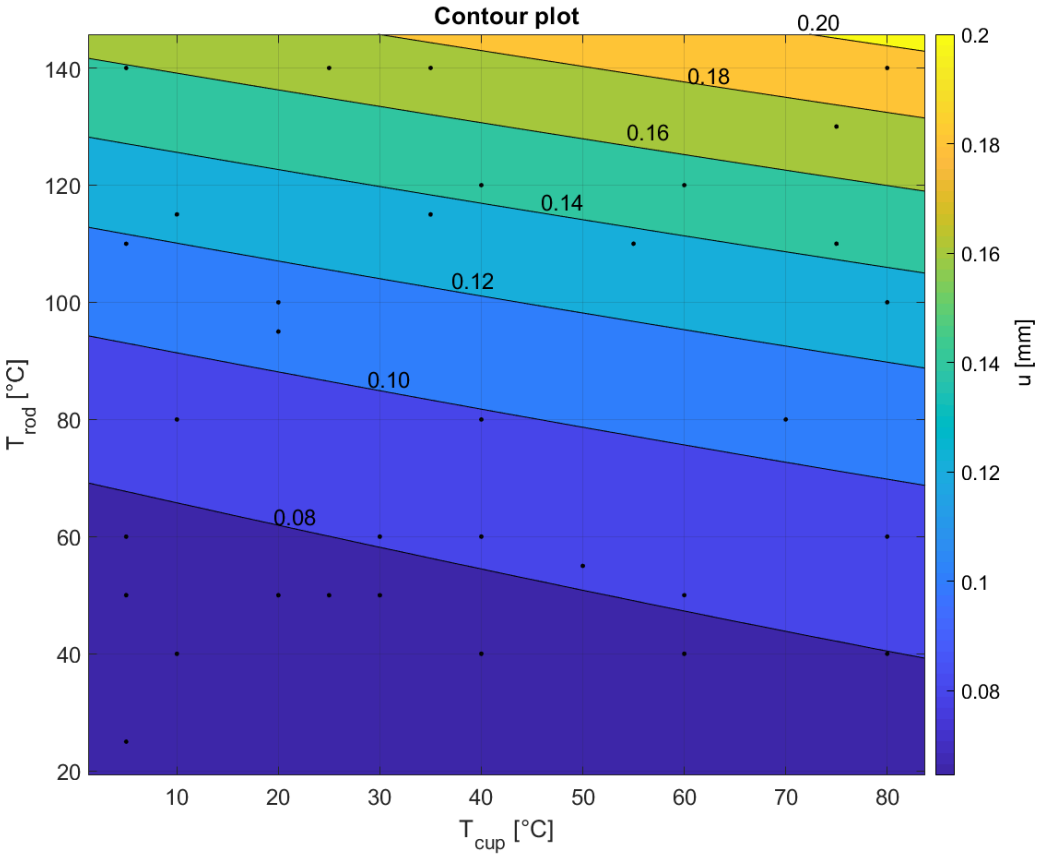

Figure 4.18: Contour plot of the displacement surface shown in 4.17

4.3.4 Influence of the temperature to creep displacements

Figure 4.19 shows the influence of a homogeneous temperature field on the maximum displacement of the packing ring into the pressure gap. As the temperature rises, the displacement increases strongly due to a more pronounced creep of the material. With increasing temperature, not only the stiffness of the material decreases, but also its yield strength. Thus, at higher temperatures, a larger area of the material plastifies resulting in a stronger creep.

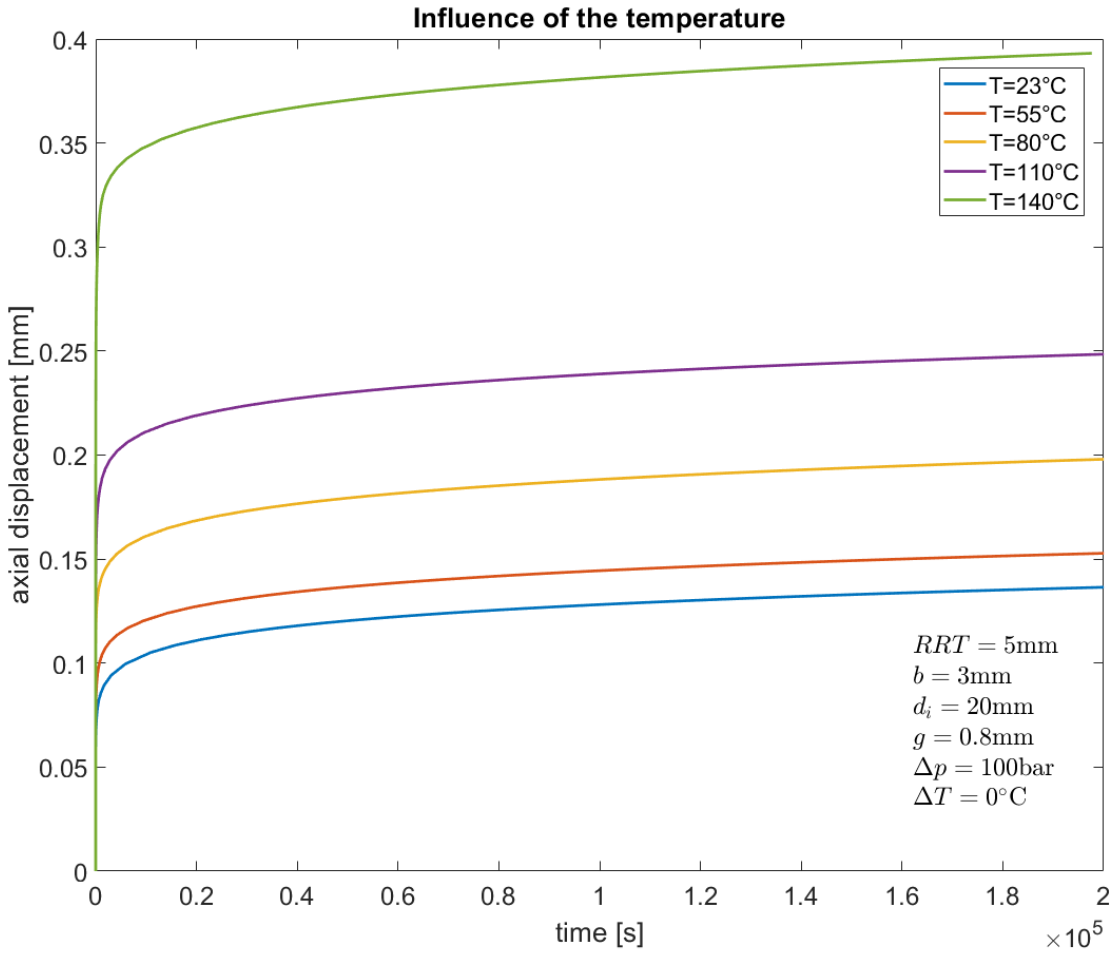

Figure 4.19: Influence of the temperature on the maximum deformation into the pressure gap

4.4 Influence of the pressure difference

Figure 4.20 shows the influence of the pressure difference on the maximum displacement into the gap between piston rod and pressure housing. As expected, the maximum displacement increases with increasing pressure difference (load). The correlation is non-linear. Doubling the pressure does not lead to a doubling of the displacement. This is due to the load dependence of the creep model. Besides the pressure gap width and the temperature, the pressure difference has the largest influence on the displacements into the pressure gap. The influences of the geometry parameters are significantly smaller.

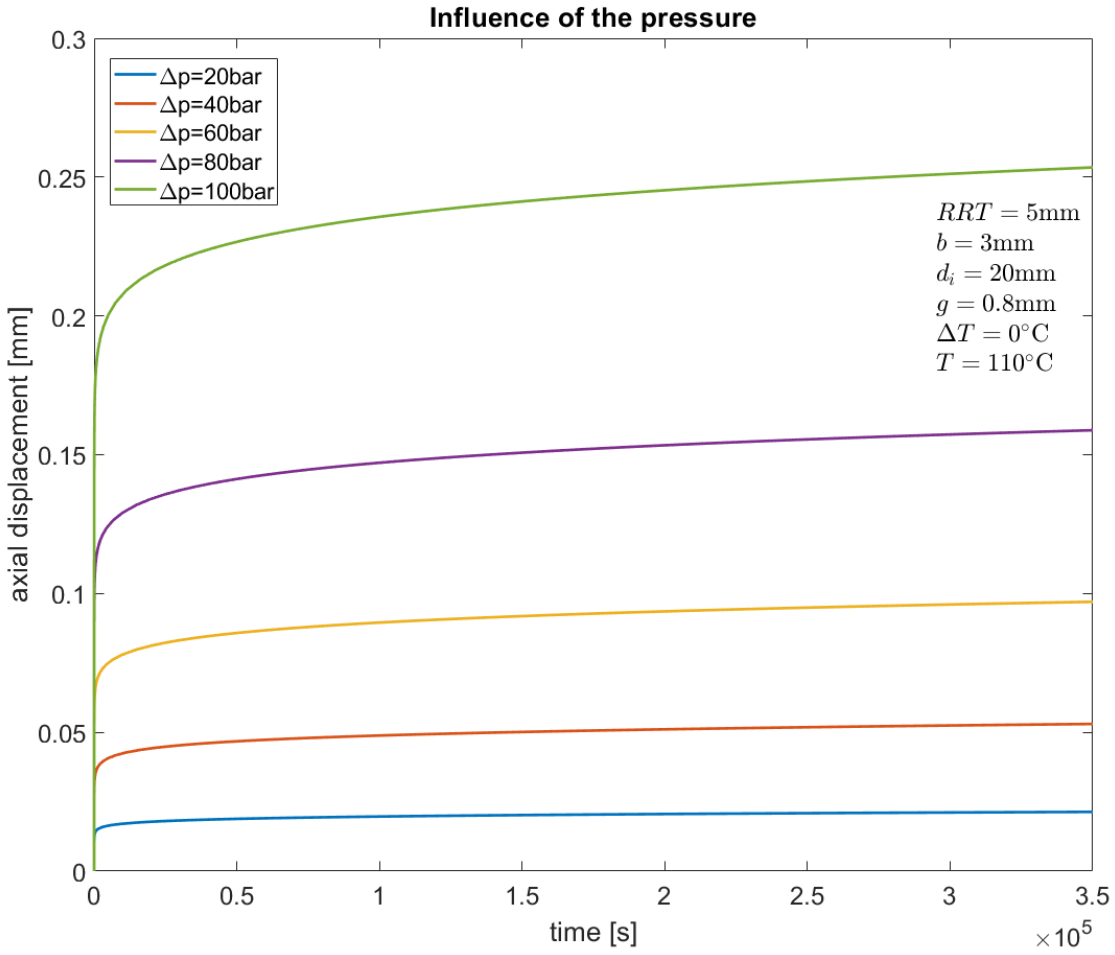

Figure 4.20: Influence of the pressure difference on the maximum displacement into the gap between piston rod and pressure housing

4.4.1 Influence of pressure and temperature on displacement

Figure **??** shows the influence of the pressure difference on the maximum displacement at three different temperatures. The maximum displacement increases more steeply with increasing pressure at higher temperatures than at lower temperatures. This is due to the fact that at higher temperatures both the material stiffness and the yield strength are reduced.

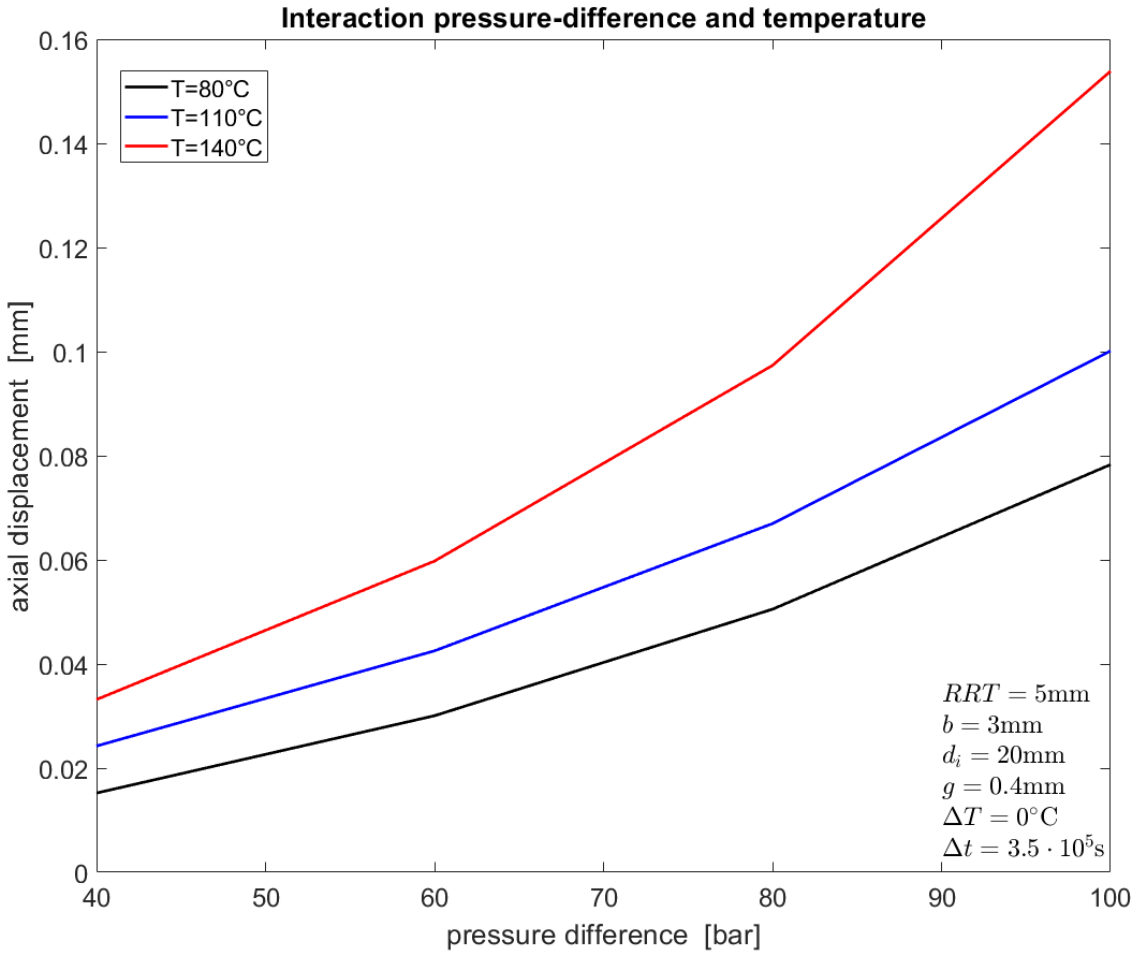

Figure 4.21: Influence of the pressure difference and the temperature on the maximum displacement into the pressure gap for a homogeneous temperature field

4.5 Influence of the gap between piston rod and housing

Figure 4.22 shows the influence of the pressure gap width on the maximum displacements into the gap. It is recognisable that the time-evolution of the maximum displacement increases with increasing gap width. The displacement is composed of a bending component and a shear component. As the gap increases, the influence of the bending dominates over the shear influence. For the gaps relevant for practical applications, the displacement component due to the shear is significantly larger than the component due to bending. The simulated range is chosen as $\Delta t = 3.5 \cdot 10^5$s. In principle, a longer time period is also possible. The aim of the parameter study is to determine the influence of the different system parameters on the creep displacement. For qualitative statements regarding the influence of a parameter, it is not necessary to simulate the entire period of use.

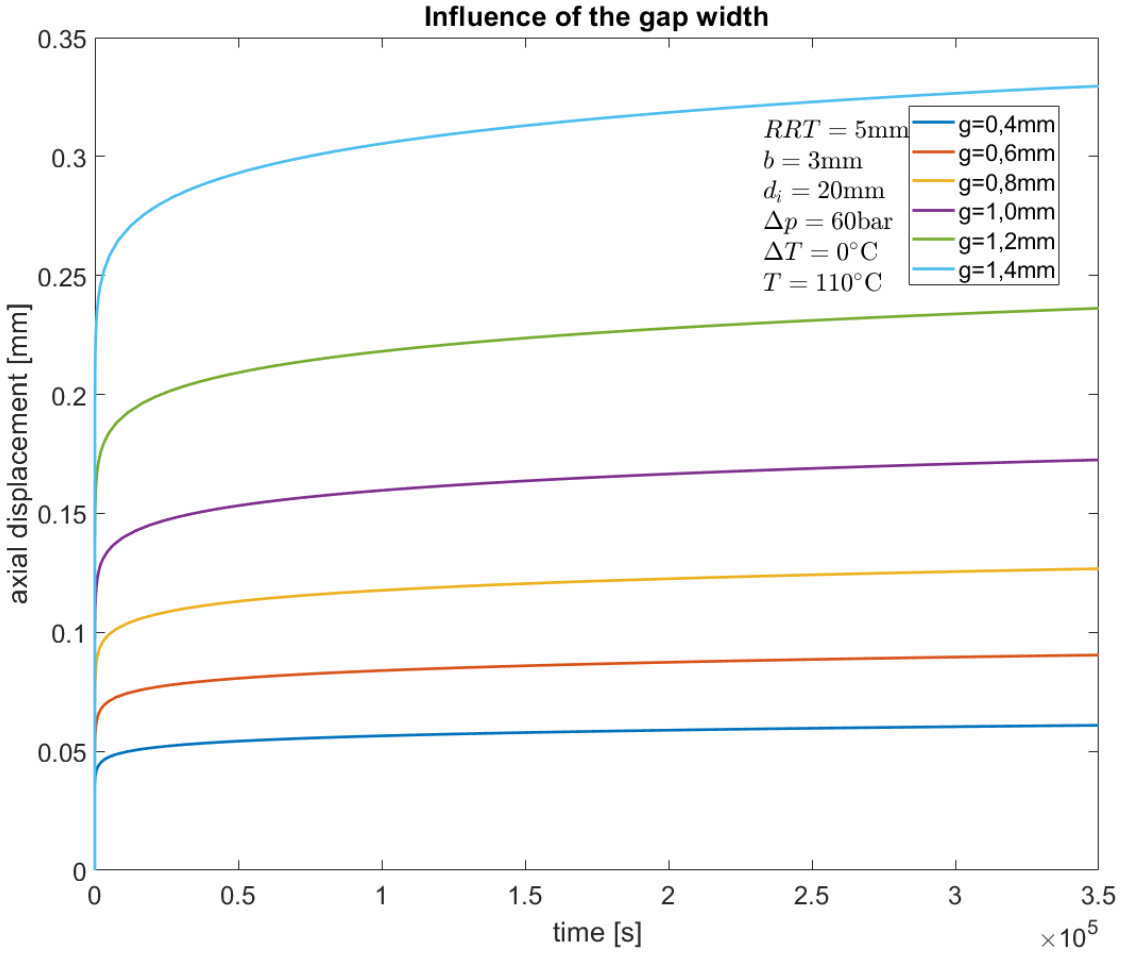

Figure 4.22: Influence of the gap width on the evolution of the maximum displacement into the gap

4.5.1 Influence of gap width and temperature on the displacement

Figure 4.21 shows the influence of the gap width on the maximum displacement for two different homogeneous temperatures $T = 110°\text{C}$ and $T = 140°\text{C}$. The maximum displacement increases more steeply with increasing gap between piston rod and packing housing at higher temperatures than at lower temperatures. This is due to the fact that at higher temperatures both the material stiffness and the yield strength are reduced.

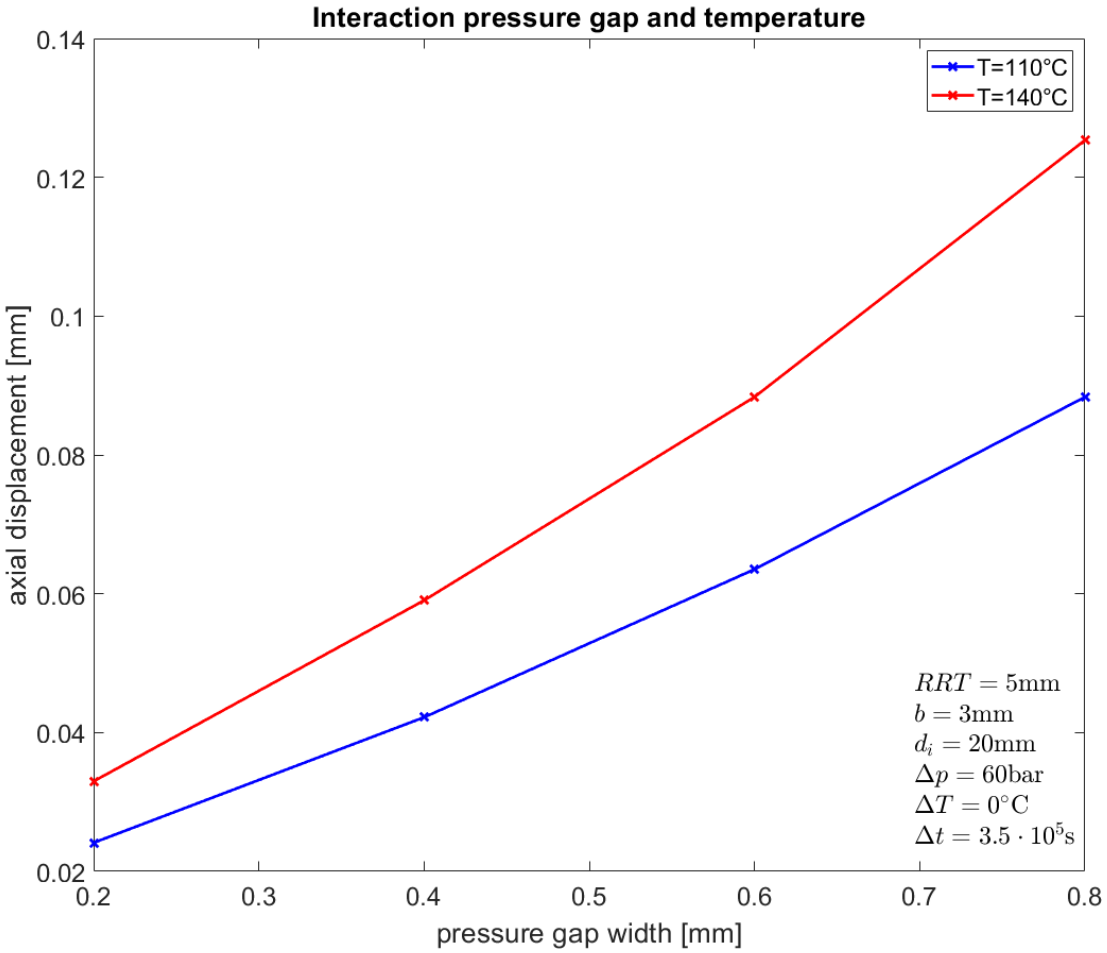

Figure 4.23: Influence of the pressure gap width and the temperature on the maximum displacement into the pressure gap

4.5.2 Influence of gap width and geometry on the displacement

Further simulations show the interactions between the different geometrical parameters of the packing ring and the pressure gap. Figure 4.24 shows the influence of the pressure gap width on the maximum displacement of the packing ring into the pressure gap for three different inner ring diameters evaluated after a period of $\Delta t = 3.5 \cdot 10^5$s.

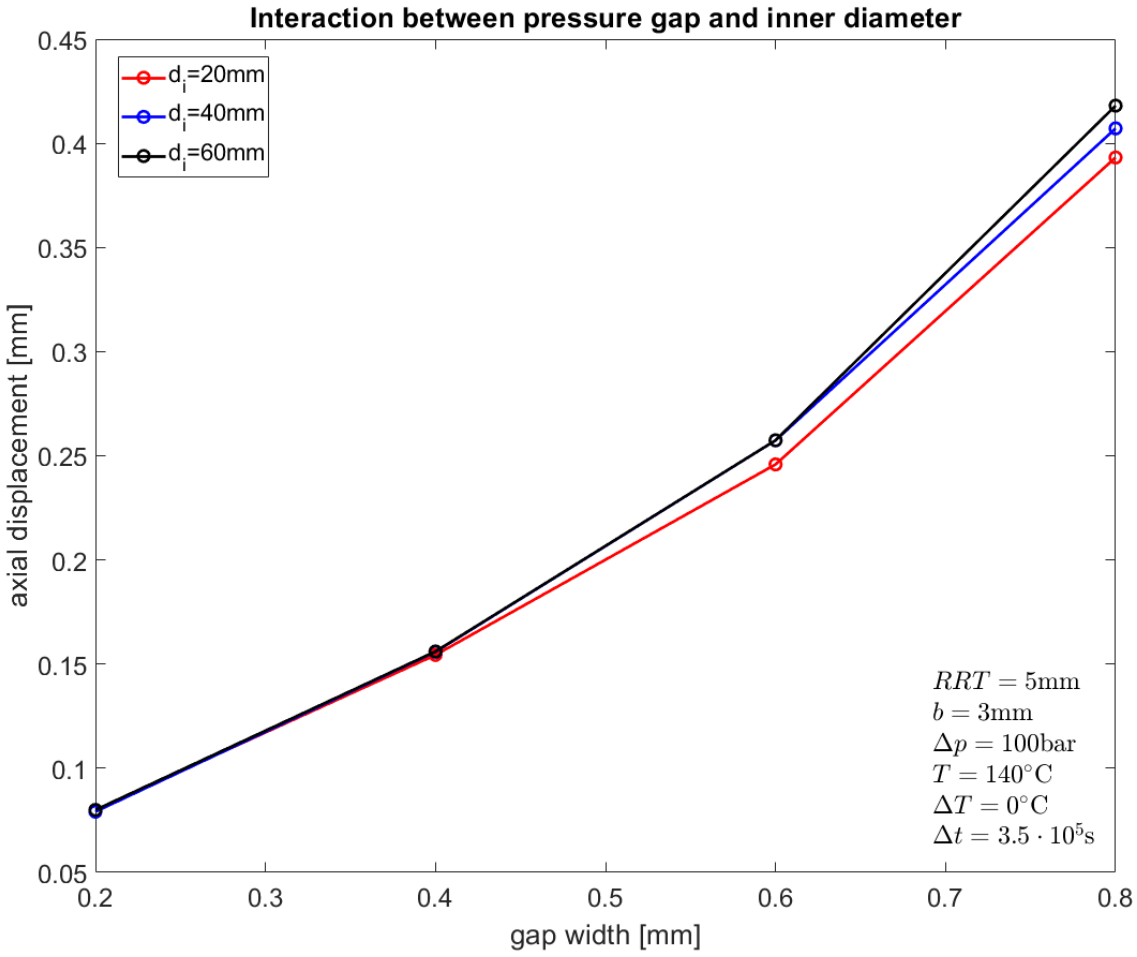

Figure 4.24: Influence of the pressure gap and the inner diameter on the axial displacementafter $\Delta t = 3.5 \cdot 10^5$s

Figure 4.25 shows the influence of the pressure gap width on the maximum displacement of the packing ring into the pressure gap for three different axial thicknesses evaluated after a period of $\Delta t = 3.5 \cdot 10^5$s. Figure 4.25 also shows that the influence of the pressure gap is greater when the axial thickness of the packing ring is smaller. The correlation is also non-linear here.

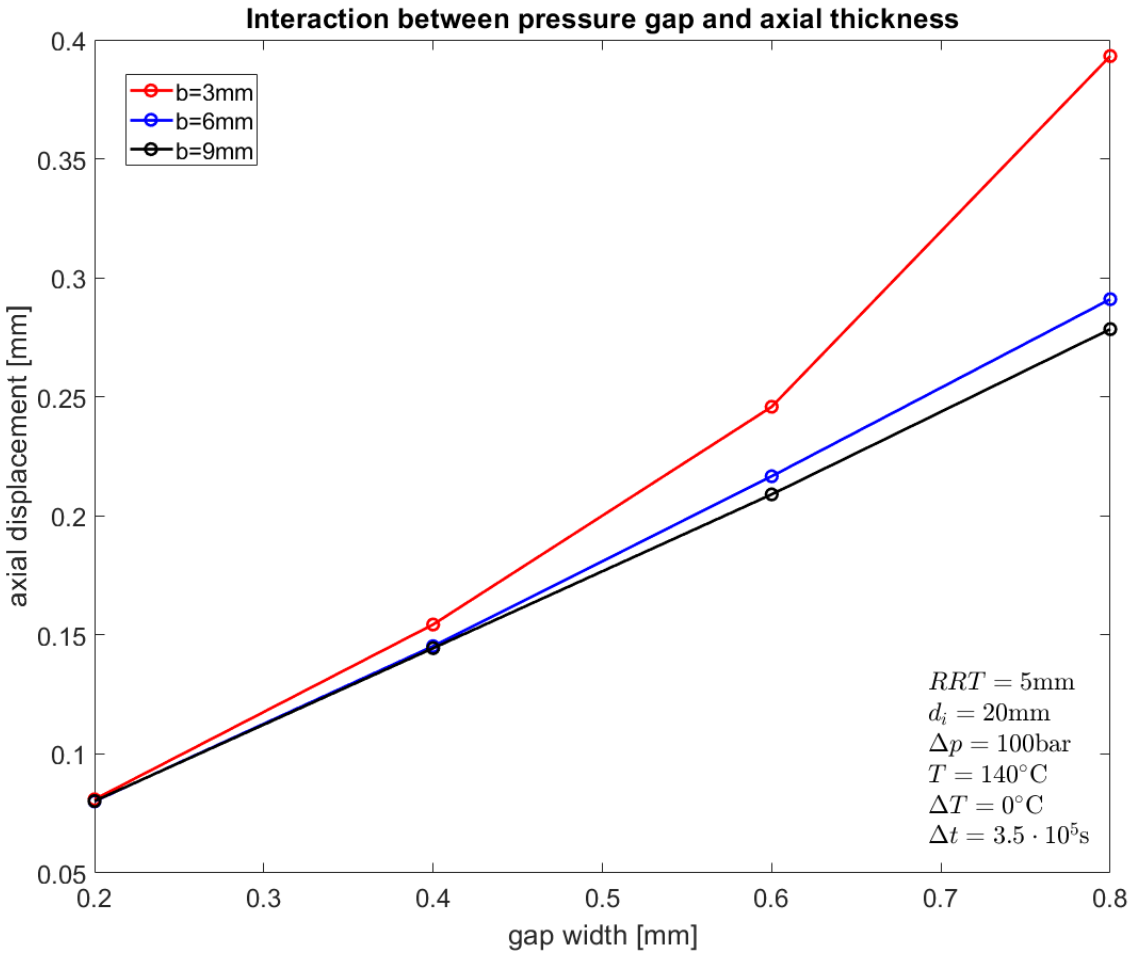

Figure 4.25: Influence of the pressure gap and the axial ring thickness on the axial displacement after $\Delta t = 3.5 \cdot 10^5$s

4.6 Criterion for maximum pressure gap

The objective of this subchapter is to select a suitable criterion for the maximum pressure gap. In principle, a distinction is made between stress-based design and deformation-based design.

4.6.1 Stress-based design

The stress-based design of machine components is usually carried out according to the FKM guideline. Dimensioning is based on the degree of utilization. The static utilization factor a_{stat} is defined as in equation (4.4).

$$a_{stat} = \frac{\sigma_{Vmax}}{\sigma_{lim}} \leq 1 \tag{4.4}$$

where σ_{Vmax} is the maximum equivalent stress and σ_{lim} is the permissible stress. For stress-related dimensioning according to the FKM guideline, exceeding the yield point of the material is not permitted. However, this means that the permissible pressure gaps would be very small.

4.6.2 Deformation based design

In deformation-based design, a maximum deformation is defined as a limit value. When the yield point is exceeded, the material creeps further and further and does not reach a stationary value within finite time. The limit value of the displacement after the operating time is then calculated according to equation 4.5, where

$$u_{max} = u_{t=28.8 \cdot 10^6 \mathrm{s}} \tag{4.5}$$

u_{max} is the displacement after the operation time of $t = 8000\mathrm{h}$. One influencing factor that is difficult to detect is the rate dependence of the mechanical behaviour. Polymeric materials show a strong dependence on the strain rate. Various material models, such as the Johnson-Cook model, are able to take strain rate dependence into account. However, the problem is that the strain rates in creep are several orders of magnitude lower than in the tensile test, with whose data the material model is calibrated.
In contrast to the stress-based design, plastic deformation zones are permitted here.

4.6.3 Stress and strain fields in the packing ring

Figure 4.26 shows the stress field in the packing ring in the area of the pressure gap. The maximum stresses occur directly in the area of the cup edge. In contrast to the linear-elastic material behaviour, the maximum stresses do not occur below the surface here, but in a larger area due to yielding. As a result of exceeding the yield point of the material, hardening of the material occurs. A complex multi-axial stress state appears around the cup edge of the packing housing.

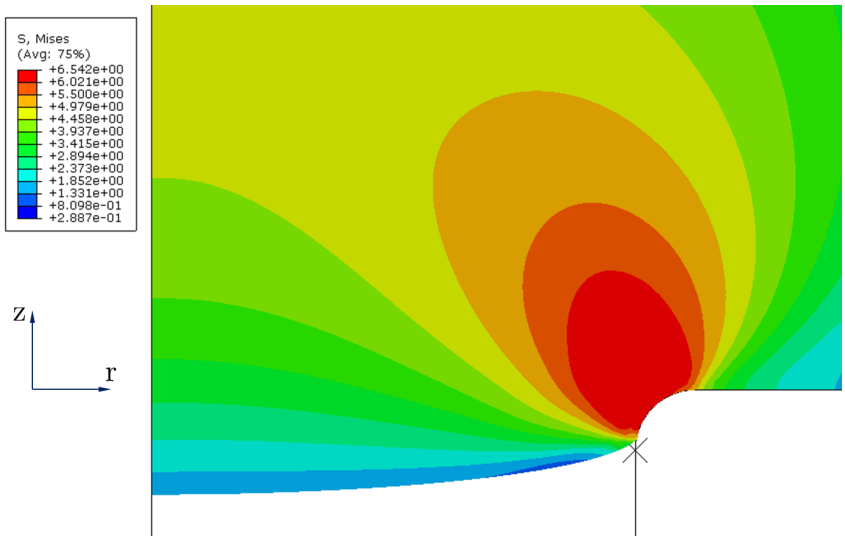

Figure 4.26: Stress field (in MPa) inside the packing ring in the region of the pressure gap

Figure 4.27 shows the equivalent creep strain in the area of the pressure gap. The maximum creep strains appear in the zone of maximum stresses.

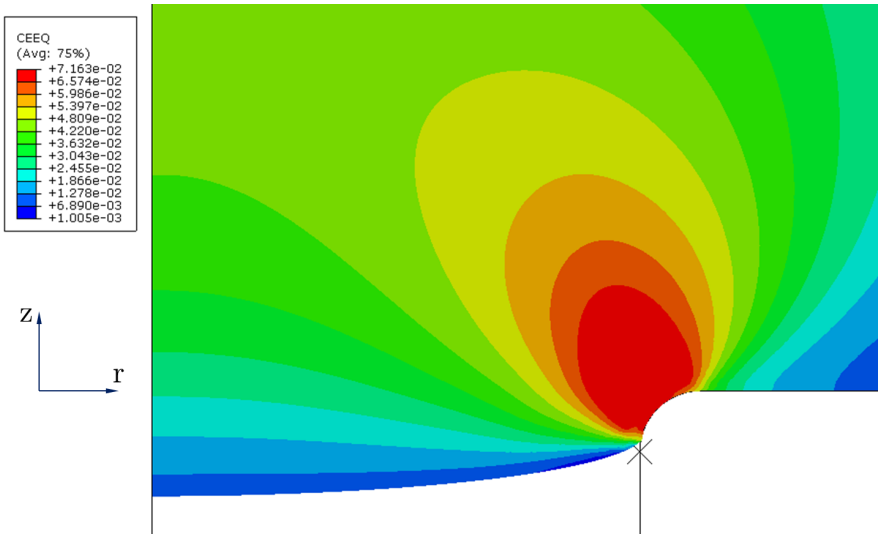

Figure 4.27: Equivalent creep strain in the packing ring in the region of the pressure gap

Figure 4.28 shows the equivalent plastic strain in the area of the pressure gap. Significant plastic deformation occurs in the area of the transition to the pressure gap. The strongest creep of the material takes place in this area.

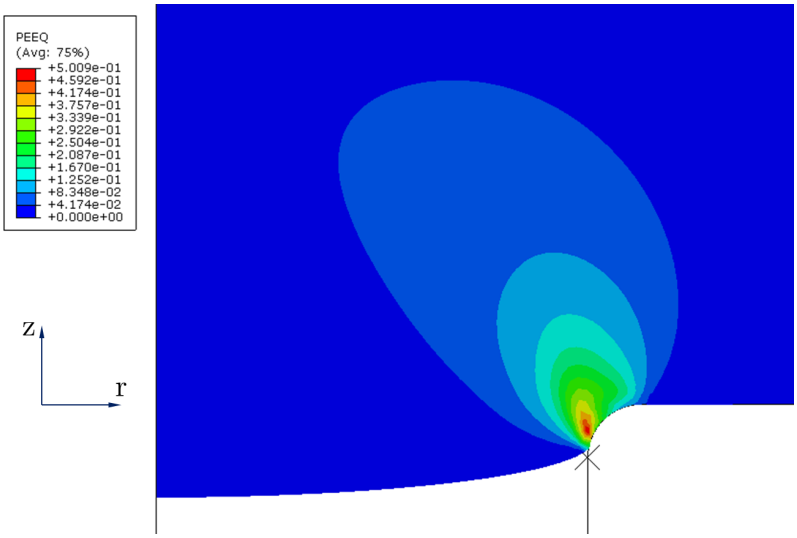

Figure 4.28: Equivalent plastic strain in the packing ring in the region of the pressure gap

The equivalent plastic strain rate is calculated from the double contraction of the plastic strain rates.

$$\dot{\varepsilon}^{pl} = \sqrt{\frac{2}{3}\dot{\varepsilon}_{ij}^{pl}\dot{\varepsilon}_{ij}^{pl}} \tag{4.6}$$

where, $\dot{\varepsilon}_{ij}^{pl}$ is the plastic strain rate tensor. The double contraction of the tensors is defined as follows.

$$\dot{\varepsilon}_{ij}^{pl}\dot{\varepsilon}_{ij}^{pl} = \dot{\underline{\underline{\varepsilon}}}^{pl} : \dot{\underline{\underline{\varepsilon}}}^{pl} = \dot{\varepsilon}_{11}^{pl}\dot{\varepsilon}_{11}^{pl} + \dot{\varepsilon}_{12}^{pl}\dot{\varepsilon}_{12}^{pl} + ... + \dot{\varepsilon}_{33}^{pl}\dot{\varepsilon}_{33}^{pl} \tag{4.7}$$

The plastic equivalent strain is then obtained by integrating the equation 4.6 over time.

$$\varepsilon^{pl} = \int_0^t \dot{\varepsilon}^{pl}\mathrm{d}t \tag{4.8}$$

The equivalent plastic strain is therefore the plastic strain accumulated over time.

4.6.4 Extrapolation of the simulation data

After long creep durations and increasing displacments, some elements become severely distorted. These distortions lead to a significant reduction of the time increments until it is no longer tenable to continue the analysis. There are several ways to remedy this problem. On the one hand, during the simulation, remeshing can be performed and the results obtained thus far mapped onto the new mesh. On the other hand, the maximum displacement at $t = 8000h$ can be approximated using reasonable time extrapolation functions. The time history of creep strain is defined by the Norton-Bailey law. Thus, the time evolution of the displacement can be estimated reasonably well.

Figure 4.29 shows the simulation result of the evolution of the maximum displacement over a period of 10^6s which can well be approximated by the fit curve provided in the figure. The regression coefficient is $R^2 = 0.9984$, which means that the temporal evolution of the displacement is almost exactly described by the fit function.

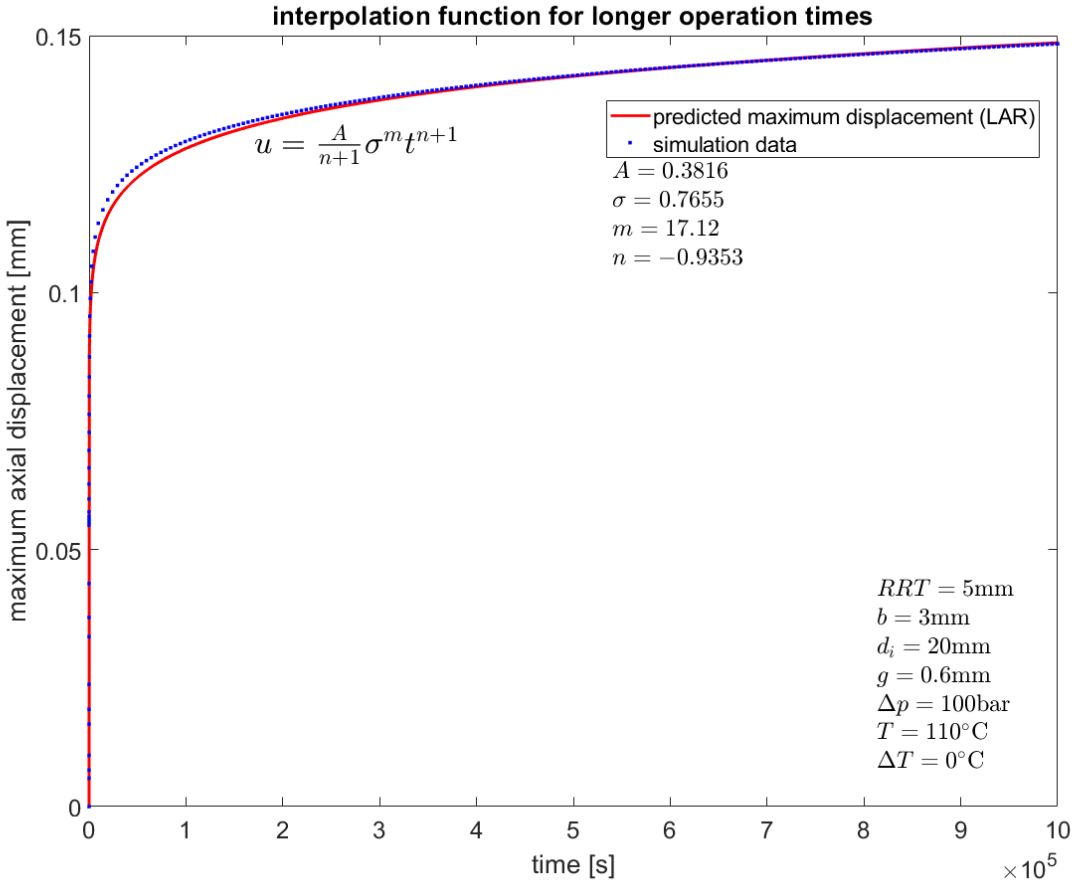

Figure 4.29: Interpolation function for the simulation data in a time range of 10^6s

Figure 4.30 shows the quality of the fit with the parameters shown in Figure 4.29 by comparision with a full FE simulation (including multiple remeshing steps) over the entire operating time of $t = 28.8 \cdot 10^6 \mathrm{s}$. The fit-function proposed in Figure 4.29 shows excellent agreement with the FE results. The relative error is $\Delta u[\%] = 0.53$ when extrapolating to operating time.

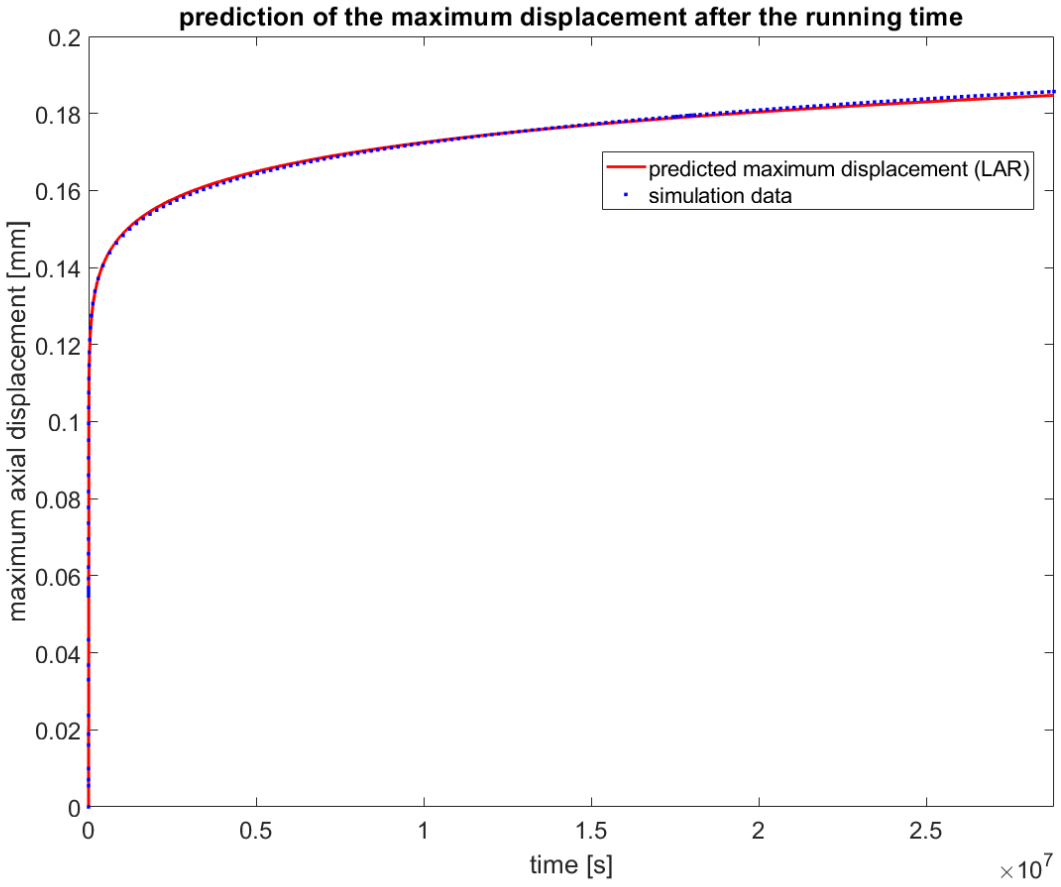

Figure 4.30: Extrapolation of the maximum axial displacement for the whole operation time of the packing ring

The validity of the fit-function is further checked in the following figure for other load levels and pressure gaps.

The simulation data generally shows that the prediction accuracies are also good at other load levels or pressure gap widths. In the right part of the figure 4.31 the simulation stops after $\Delta t = 3 \cdot 10^5$s. By remeshing several times, the total operating time of $\Delta t_{op} = 28.8 \cdot 10^6$s is achieved. However, remeshing requires manual mesh to mesh solution mapping and is thus very time intensive, so the data up until $\Delta t = 3 \cdot 10^5$s is used for finding the fit-function. This obviously gives poorer results than a fit based on a duration of $\Delta t = 10^6$s, but it still allows sufficiently accurate extrapolations.

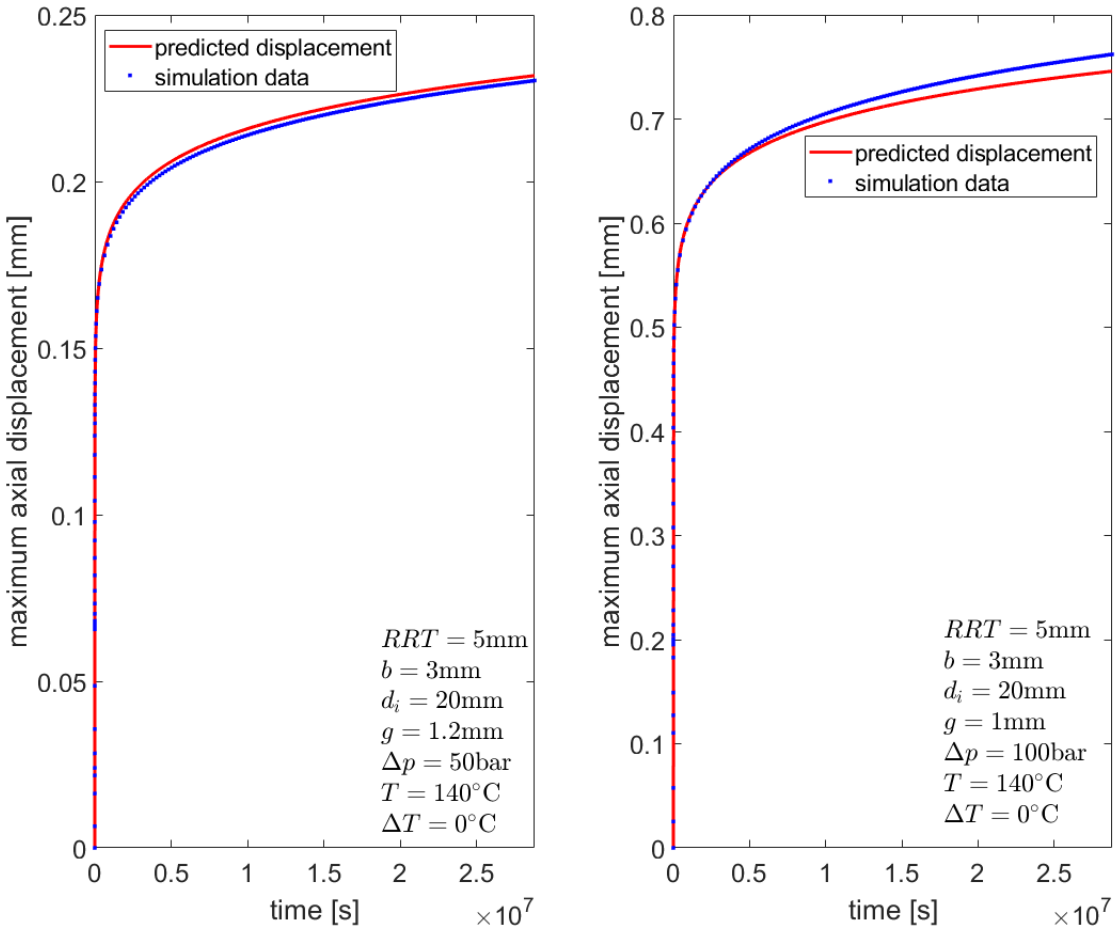

Figure 4.31: Extrapolation of the simulation data for other pressure differences, other load levels and other temperatures

The advantage of this extrapolation method is that the full operating time does not have to be simulated. This requires repeated manual remeshing and is therefore very expensive in terms of time. The extrapolation method also provides values that are sufficiently accurate.

4.7 Dimensioning of the gap width

With the simulation data, a suitable function to describe the influence of different factors is established. This interpolation function is used to determine the permissible limit curve (pressure difference-gap width). As Figure 4.32 shows, the displacement surface as a function of pressure difference and gap width between piston rod and packing housing. The coefficient of determination R^2 is close to 1.

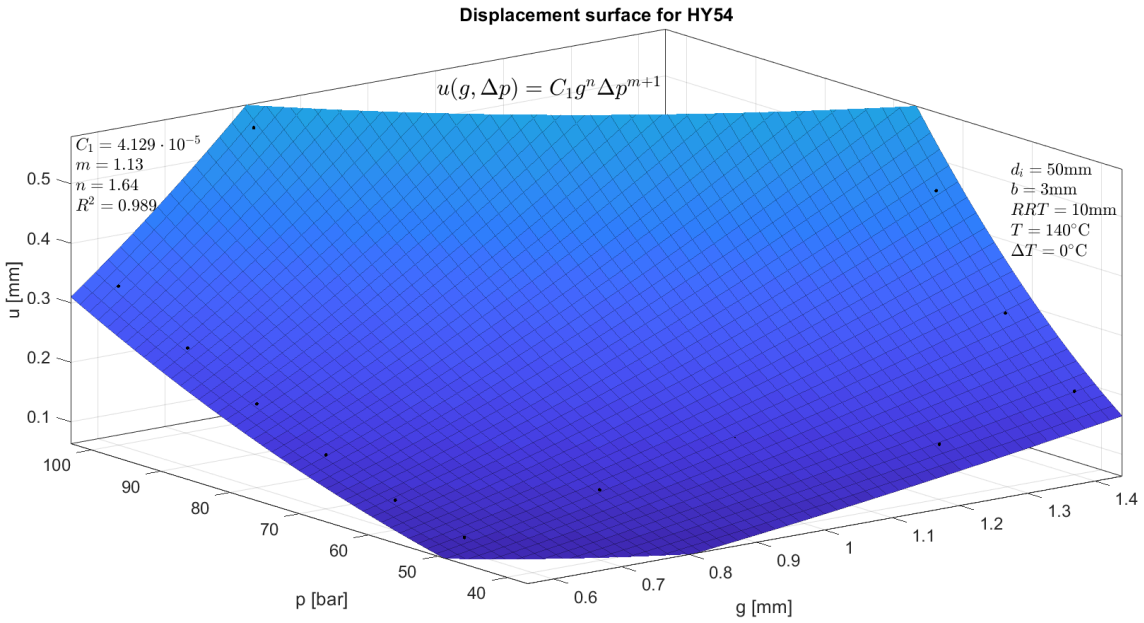

Figure 4.32: Displacement surface as a function of pressure difference and pressure gap width

This displacement surface is well described by the determined interpolation function 4.9. The best mathematical description of the displacement surface is described by a power law.

$$u(\Delta p, g) = C_1 \Delta p^{m+1} g^n \tag{4.9}$$

where u is the maximum displacement, C_1 is the coefficients of the interpolation function, m as well as n are the exponents of the interpolation function. If a maximum permissible value is specified for the displacement, the permissible pressure difference is described as a function of the pressure gap width with the interpolation function 4.9.

$$\Delta p(g) = \left(\frac{u}{C_1 g^n} \right)^{\frac{1}{m+1}} \tag{4.10}$$

4.7.1 Permissible gap widths for the worst case scenario

Figure 4.33 shows the isodisplacement curves for the material after the full operating time at a temperature of $T = 140°\text{C}$. The pressure difference is plotted over the gap width. Figure 4.33 and Figure 4.34 shows that with increasing pressure gap the pressure difference has to be reduced to obtain the same displacement.

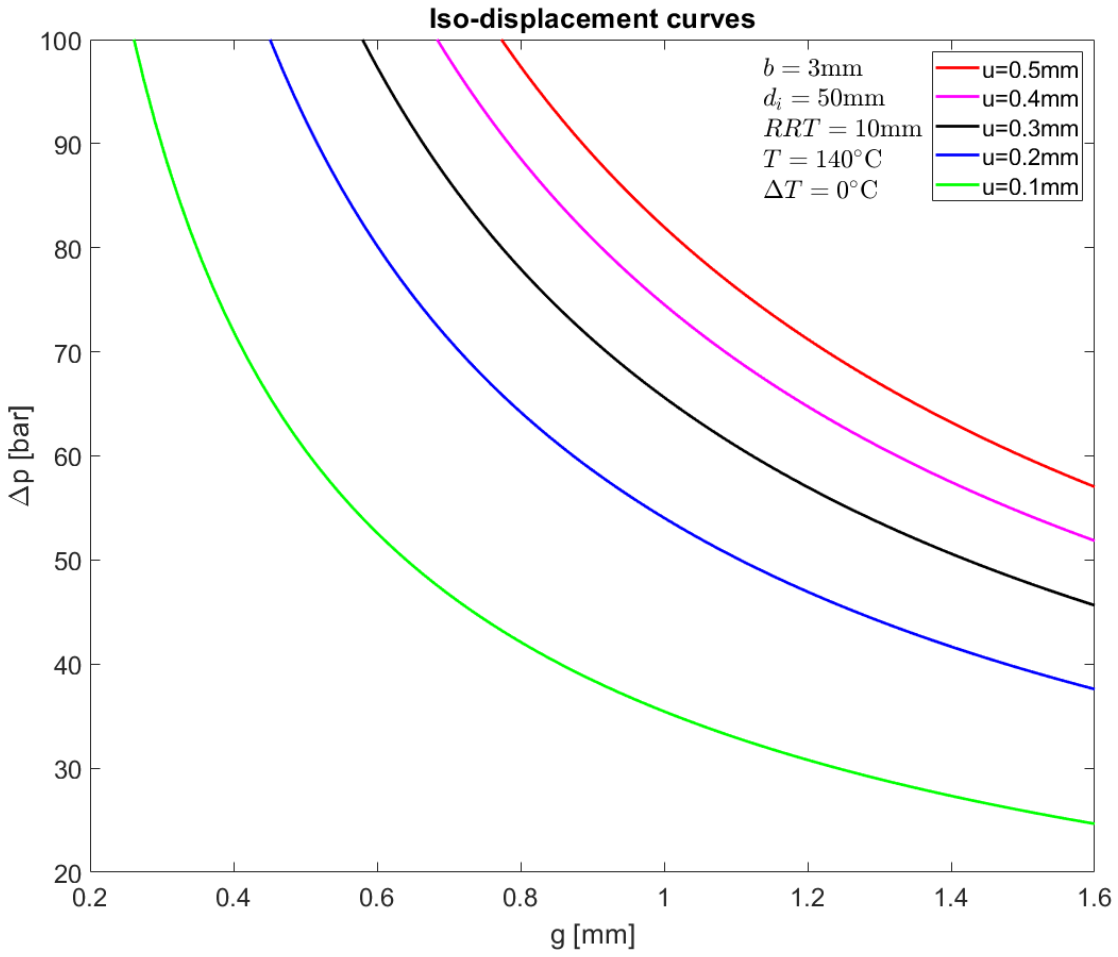

Figure 4.33: Iso-displacement curves as a function of pressure difference and gap width

Figure 4.33 shows that e.g. for a maximum axial displacement of $u = 0.5\text{mm}$ at the maximum pressure difference of $\Delta p = 100\text{bar}$ a maximum pressure gap of $g = 0.78\text{mm}$ is permissible.

Figure 4.34 shows the logarithmic representation of the iso-displacement lines shown in Figure 4.33. For practical dimensioning of the pressure gap, the logarithmic representation of these isocurves is more suitable. This display allows quick and easy reading of the permissible pressure gap widths.

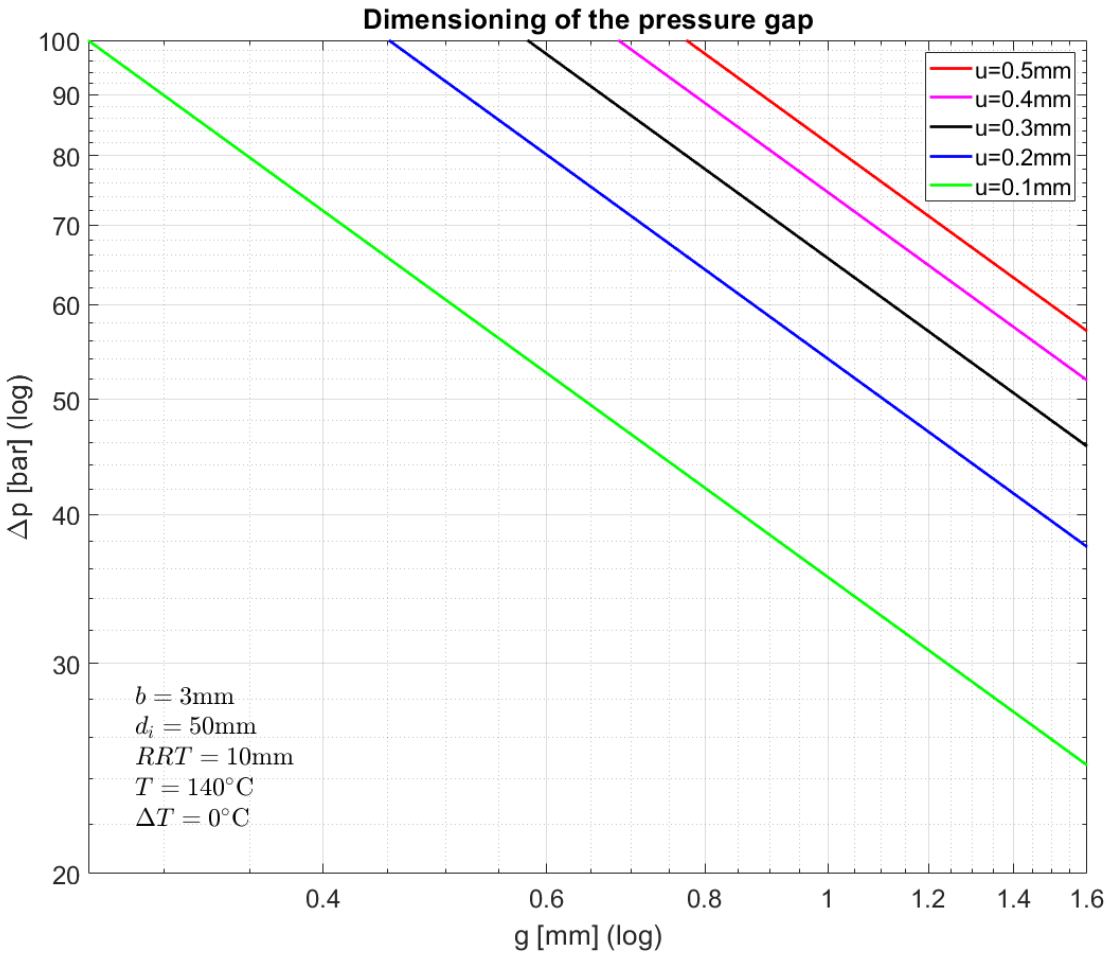

Figure 4.34: Logarithmised representation of the iso-displacement curves

4.7.2 Consideration of the temperature influence

As Figure 4.21 and Figure 4.23 show, the parameters Δp and g of the interpolation function 4.9 are in general a function of the temperature T.

$$u = u(\Delta p(T), g(T)) \tag{4.11}$$

To account for the influence of temperature, this function has to be described as a function of temperature. An exponential approach is suitable for describing the temperature dependence. This can be justified on the basics of polymer physics. Arrhenius approaches are often used to describe the temperature dependence of semi-crystalline polymers. The Arrhenius approach is based on the activation energy. The coefficient K_0 is used to scale the function, since $C_1(T = 140°\mathrm{C}) = 4.129 \cdot 10^{-5}$. By combining equation 4.9 as well as equation **??**, the description of the displacement surface as a function of temperature, pressure and pressure gap width follows.

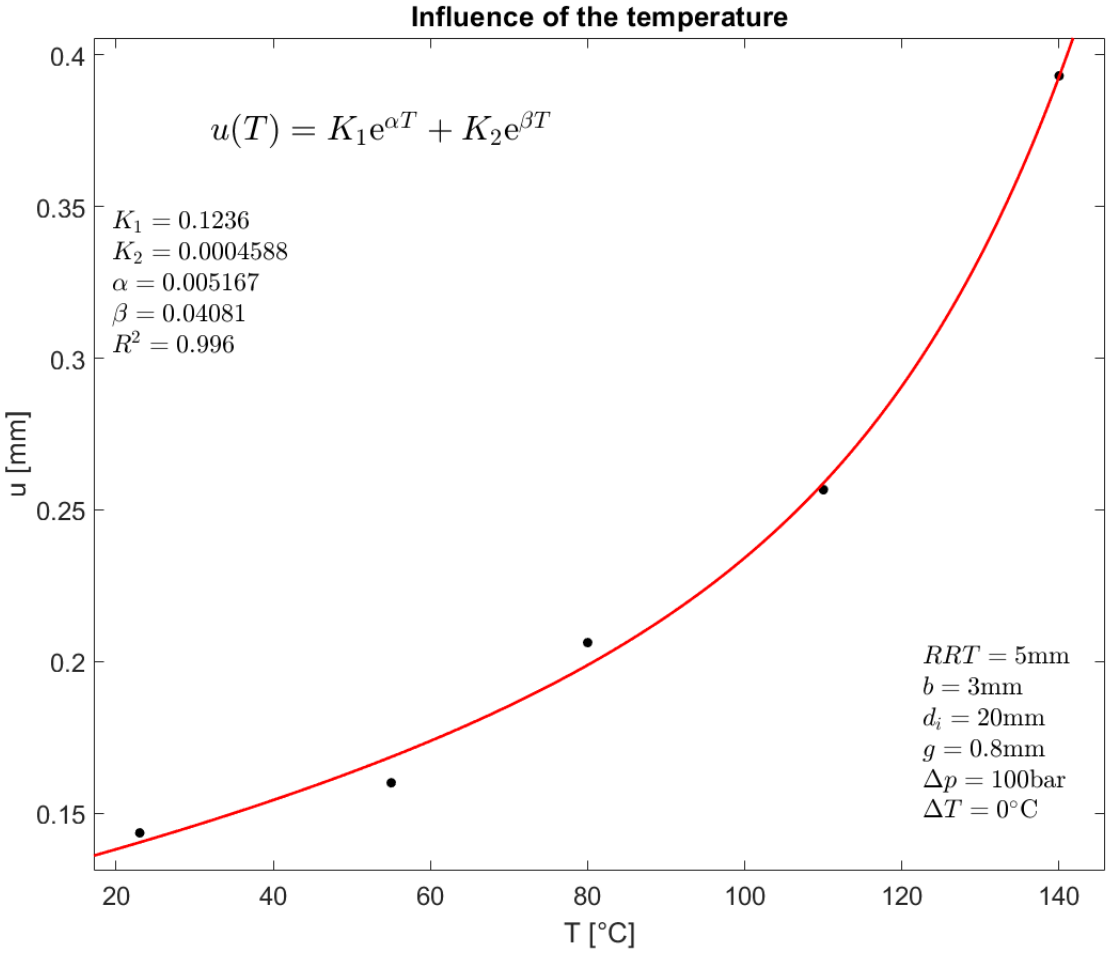

Figure 4.35: Mathematical description of the temperature-dependency of the the maximum displacement

$$u(T, \Delta p, g) = K_0 \Delta p^{m+1} g^n \left(K_1 e^{\alpha T} + K_2 e^{\beta T}\right)^{m+n+1} \tag{4.12}$$

4.7.3 Permissible gap widths at $180°$C

Practical results show that the actual pressure gaps must be significantly smaller than the results of Figure 4.34. The reason for this is that significantly higher temperatures might occur during operation. No material data are available for temperatures of approx. $T = 180°$C which might appear very locally at the rod-ring contact. The reason is that at this temperature, problems occur with the clamping of the specimens in common tensile testing devices due to the high compliance of the material. Therefore, equation 4.9 is used to extrapolate the displacements to $T = 180°$. Figure 4.36 shows the iso-displacement curves for a temperature of $T = 180°$C. It has to be treated with caution since equation 4.12 has been calibrated in a temperature interval ranging from room temperature to $T = 140°$C. At $T = 180°$C phenomena may occur that are not taken care of by a simple extrapolation of equation 4.12.

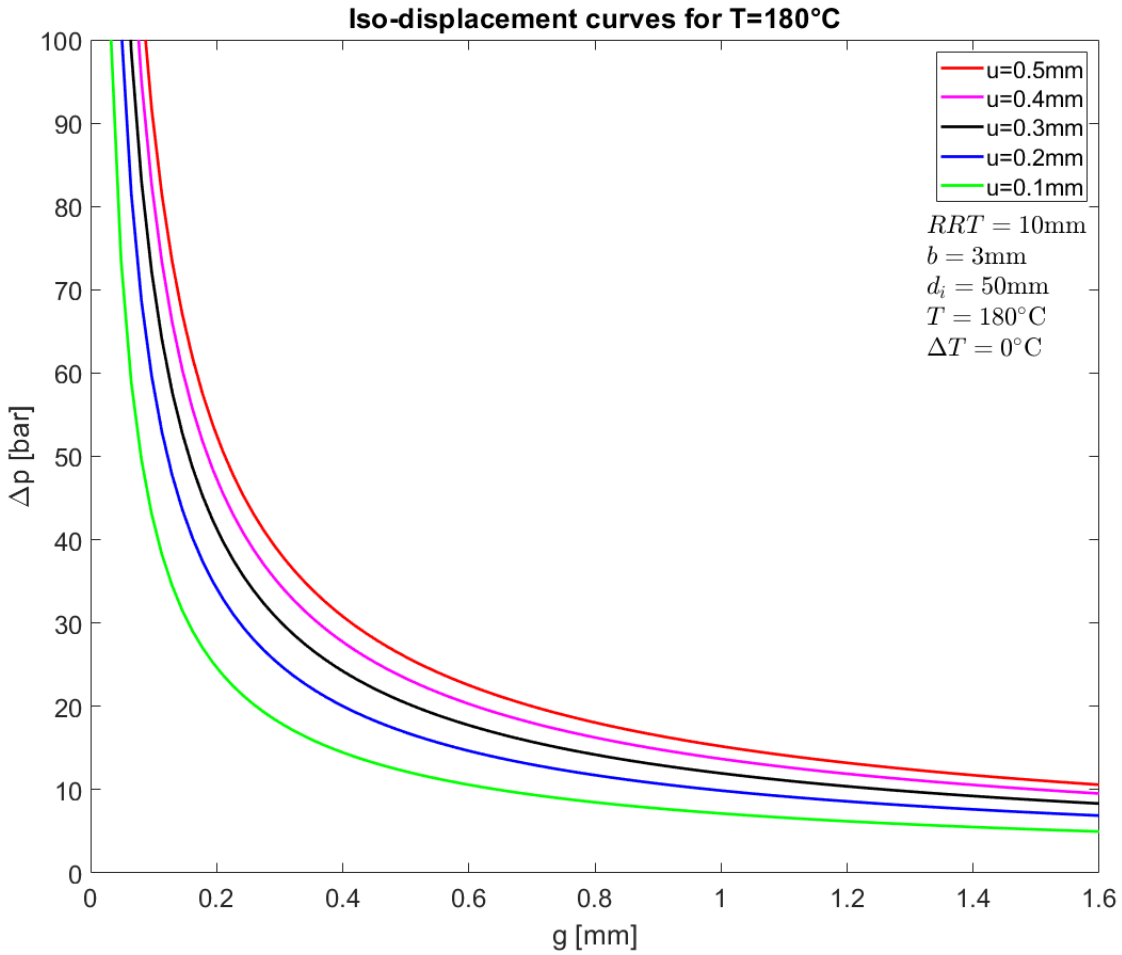

Figure 4.36: Extrapolated iso-displacement curves for at a temperature of $180°$C

Figure 4.37 shows the logarithmised plot of the iso displacement lines at a temperature of $T = 180°C$. The comparison of Figure 4.34 and Figure 4.37 shows that the permissibale pressure gap at a temperature of $180°C$ has to be reduced significantly compared to a temperature of $140°C$.

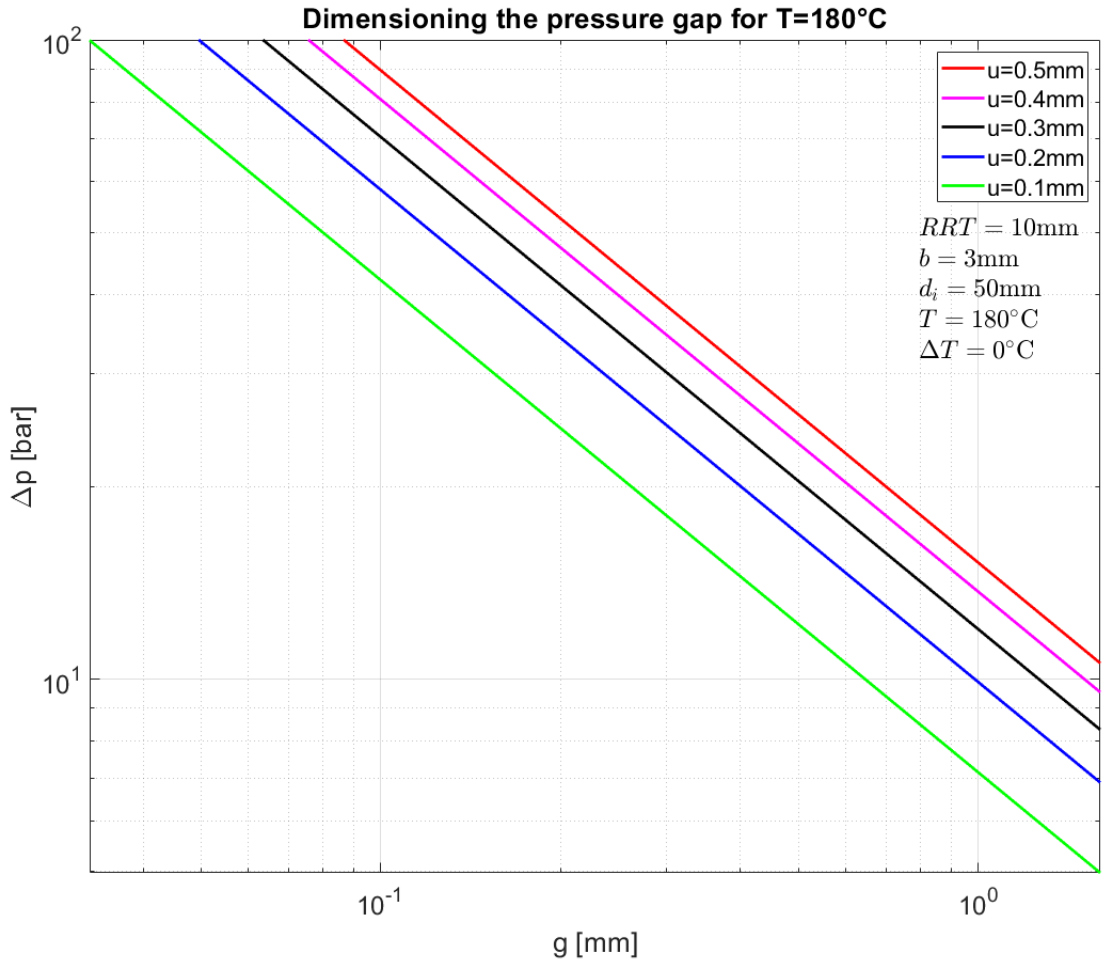

Figure 4.37: Logarithmised representation of the iso-displacement curves for HY54 at a temperature of $180°C$

The parameters of the mathematical model according to equation 4.12 are briefly summarised again here in tabular form.

Table 4.1: Input parameters and for equation 4.12

Formula symbol	value
K_0	0.0014
m	1.13
n	1.64
K_1	0.1236
α	0.005167
K_2	0.0004588
β	0.04081

4.7.4 Permissible gap widths for the best case scenario

Figure 4.7.4 shows the displacement surface, as well as the residuals plot for the best case scenario with respect to the geometric dimensions at $T = 140°\text{C}$. Geometrically best case means that the axial ring thickness $b \geq 10\text{mm}$. This is the best case because in this case smaller displacements into the pressure gap result with the same mechanical and thermal load. Nevertheless, in this case the material requirement is increased.

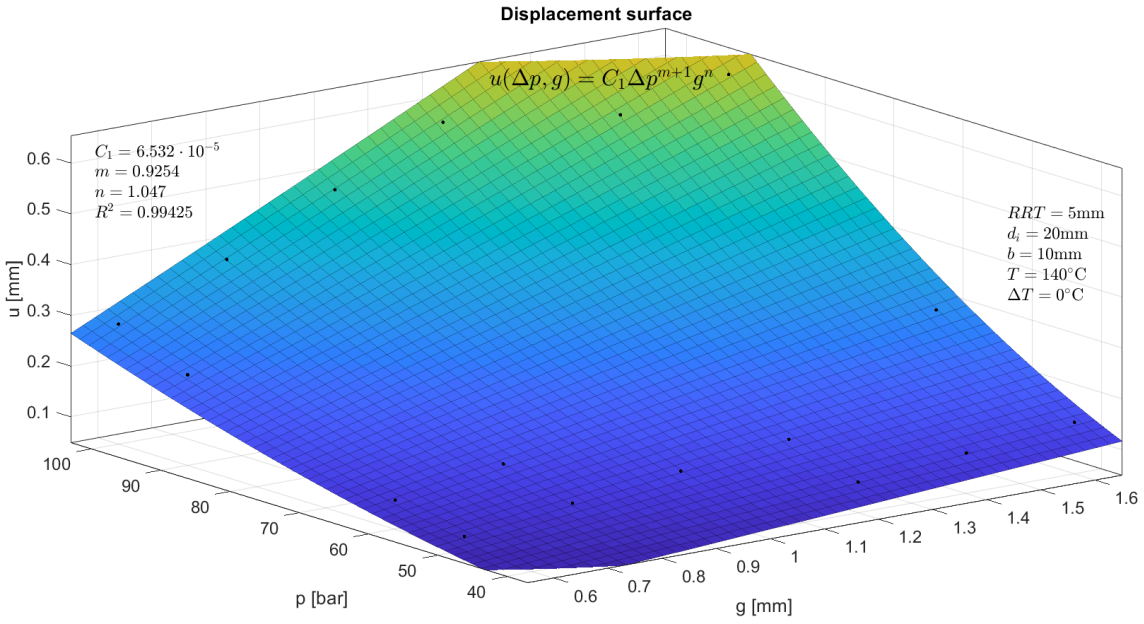

Figure 4.38: Displacement surface and the parameter that describe this surface

Figure 4.39 shows the logarithmic representation of the iso-displacement curves after the full operating time at a temperature of $T = 140°\text{C}$ and for $b \geq 10\text{mm}$. The pressure difference is plotted over the permissible pressure gap. Figure 4.39 shows that with increasing gap between piston rod and packing housing the pressure difference has to be reduced to obtain the same displacement.

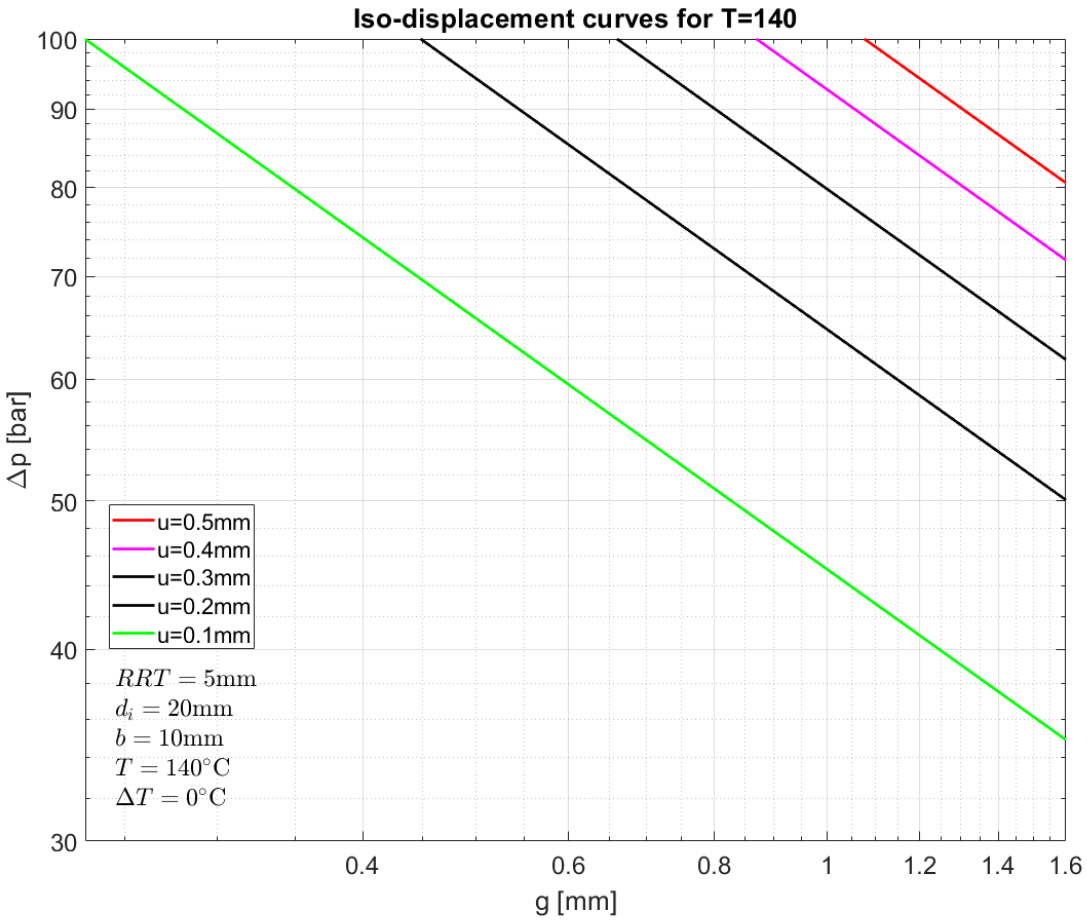

Figure 4.39: Logarithmised representation of the iso-displacement curves for at a temperature of $140°\text{C}$ for larger axial thicknesses

The parameters of the mathematical model according to equation 4.12 are briefly summarised again here in tabular form for $b \geq 10\text{mm}$.

Table 4.2: Input parameters and for equation 4.12

Formula symbol	value
K_0	0.0014
m	1.13
n	1.64

4.8 Influence of pressure balancing elements

The aim of this section is to determine the influence of pressure compensation elements on the creep behaviour of the packing rings. In addition to bores, pressure compensation elements are also available in the form of grooves. However, the focus of this Master's thesis is on the bore design.

4.8.1 Stress field in the ring due to the pressure balancing elements

The pressure balancing bores have an influence on the local stress field in the packing ring. To analyse the stress state in the packing ring, purely linear elastic calculations are carried out first in order to reduce computing time. Figure 4.40 shows the influence of the pressure balancing bores on the stress field at the back of the packing ring. As with axially symmetrical models, the stress field at the back of the packing ring is influenced by the pressure gap. A periodic pattern appears in the stress field. It is recognisable that the influence of a single hole on the local stress field quickly decays (principle of Saint Venant).

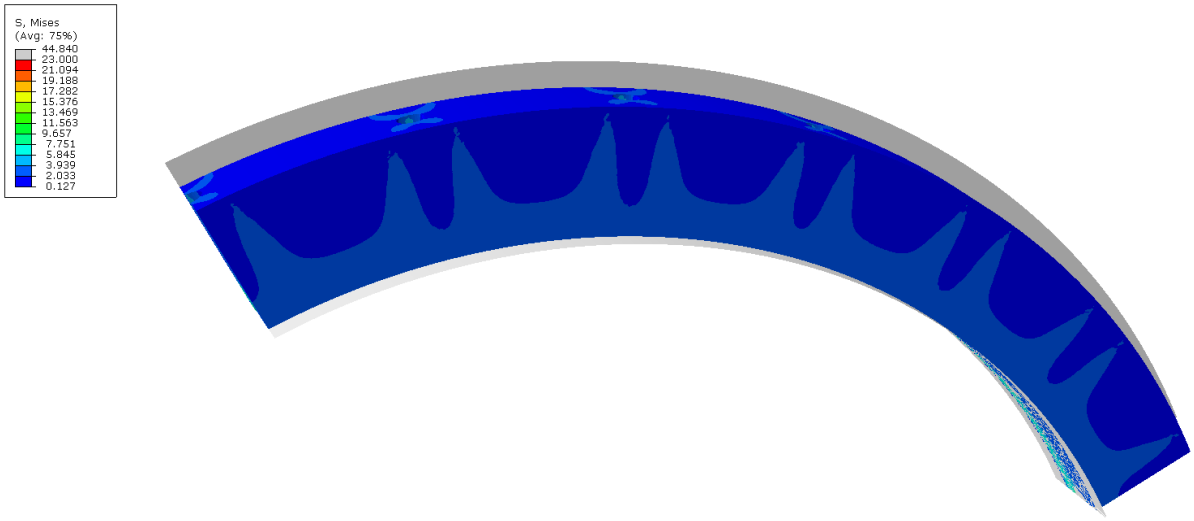

Figure 4.40: Stress field (in MPa) in the back of the packing ring due to the influence of the pressure balancing bores for linear elastic material behaviour

Like in the axially symmetrical model, the maximum stresses occur near the contact point between the pressure gap and the packing ring.

Figure 4.41 shows the distribution of Mises stresses near the pressure balancing bores from a different viewpoint

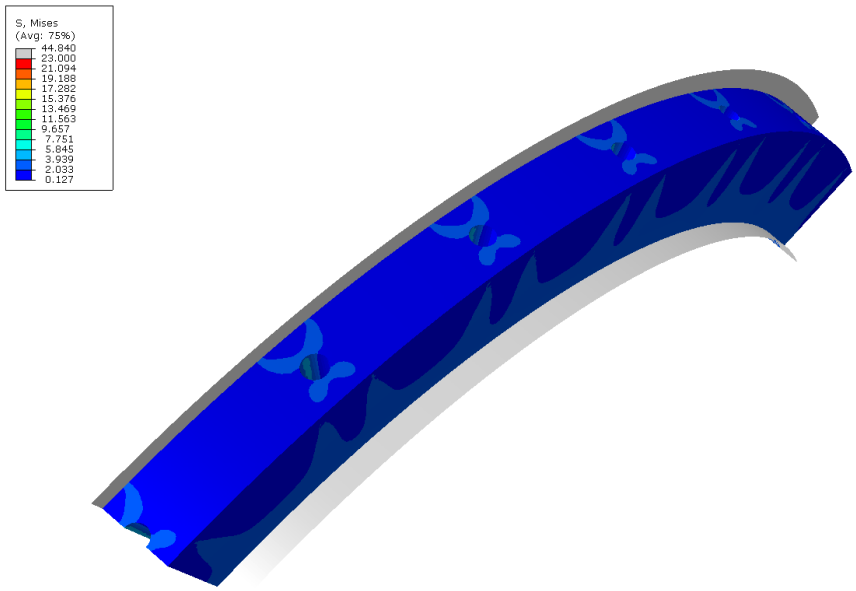

Figure 4.41: Stress field (in MPa) in the near of the balancing bores due to the influence of the pressure balancing bores for linear elastic material behaviour

4.8.2 Influence of the diameter of the pressure balancing bores

In these simulations, the influence of the pressure balancing bore diameter on the displacement is investigated. The simulations are carried out for viscoelastic material behaviour without accounting for viscoplastic creep effects in order to reduce the computation time. However, this is not an incorrect simplification, as the intention of this study is to obtain qualitative information about the influence of the pressure balancing bores. The results in Figure 4.42 show the influence of the diameters of the pressure balancing bores on the maximum displacement into the pressure gap. As the bore diameter increases, the displacement increases sharply compared to the reference packing ring without pressure balancing bores. This is due to the local reduction in structural stiffness as a result of the bores.

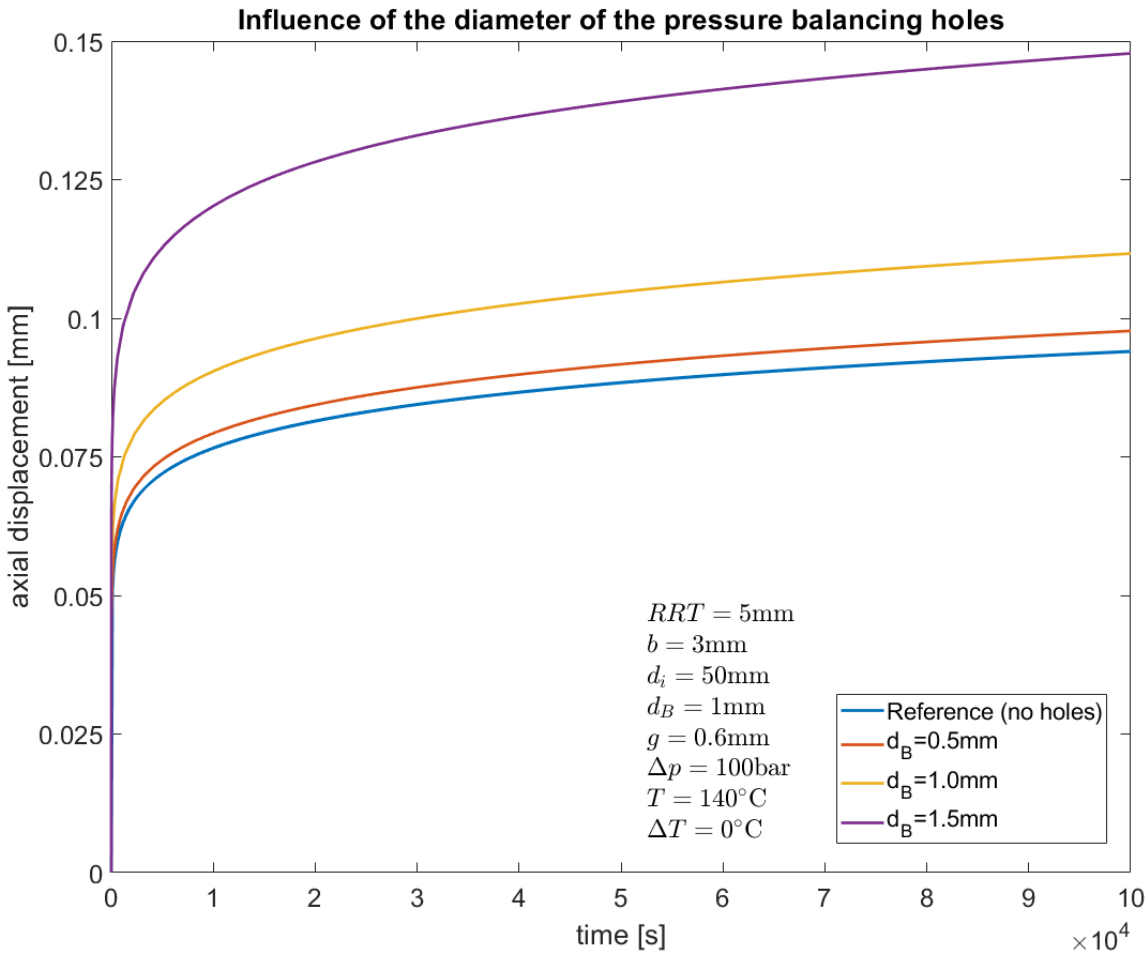

Figure 4.42: Influence of the diameter of the pressure balancing bores on the maximum displacement into the pressure gap

The local reduction in stiffness results not only in locally higher displacements but also in an increase in local stresses. This is of particular importance when the yield strength is exceeded, since viscoelastic creep then occurs in addition to viscoelastic creep.

4.8.3 Influence of the position of the pressure balancing bore

Figure 4.43 shows the influence of the position of the pressure balancing bores on the maximum displacement into the pressure gap. This simulation shows that the displacement into the pressure gap increases the closer the pressure balancing bore is positioned to the pressure gap. Figure 4.43 further shows that the displacement fluctuates. In the region of the pressure equalisation bores, larger displacements occur than between the holes. This is due to the locally reduced stiffness of the packing ring. This is evident from the course of the displacement (see figure 4.43.

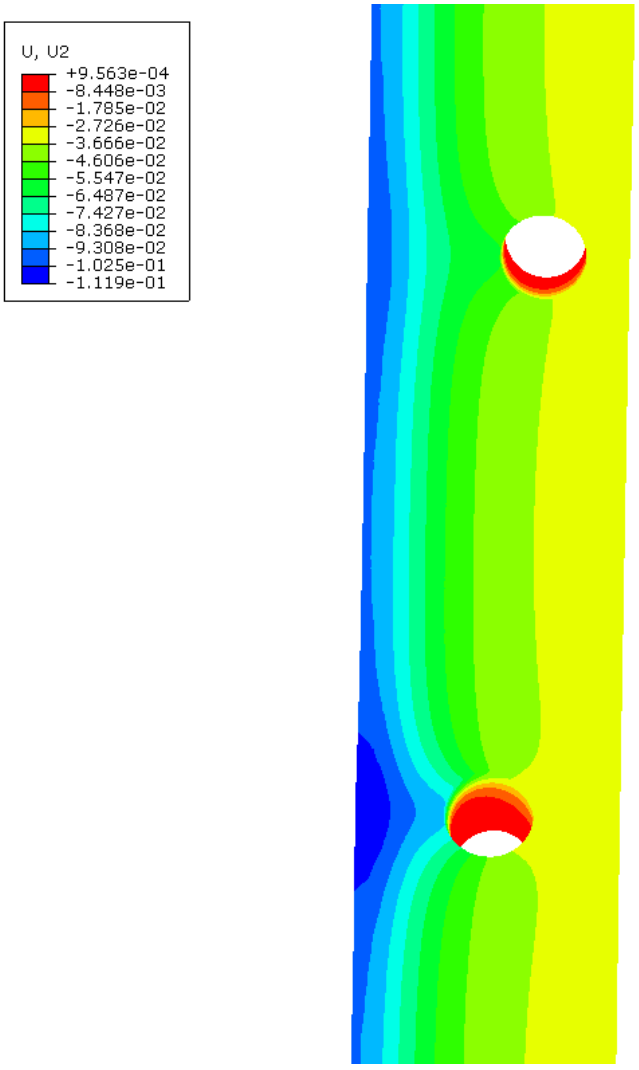

Figure 4.43: Influence of the position of the pressure balancing bores on the axial displacement (in mm) field for assuming viscoelastic material behaviour

Figure 4.44 shows the influence of the position of the pressure balancing bores on the maximum displacements into the pressure gap, assuming a viscoelastic material model. The coordinate system is set in such a way that the eccentricity is related to the centre plane of the packing ring. The eccentricity is positive for displacement in the direction of the free end and negative for displacement in the direction of the housing. The closer the pressure balancing hole is positioned in the area of the pressure gap, the greater the local displacement becomes. The maximum local displacements increase rapidly.

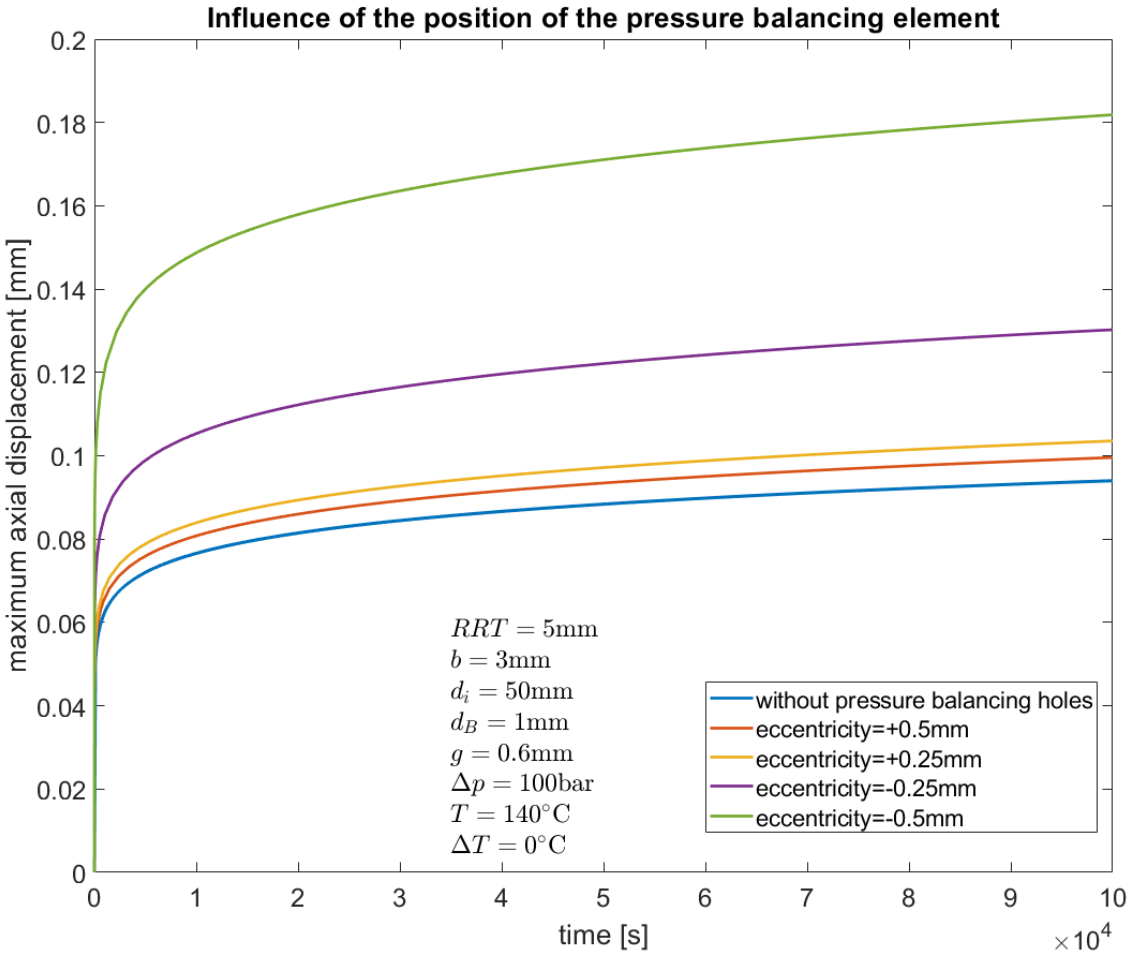

Figure 4.44: Influence of the position of the pressure balancing bores on the maximum displacements in the gap after $\Delta t = 10^5$s using viscoelastic material model

Figure 4.45 shows the course of the displacement into the gap between two pressure compensation bores. If the pressure compensation hole is displaced eccentrically in the direction of the pressure gap, significantly larger displacements occur in the area of the hole. The displacement then drops in the area between the pressure compensation bores. Approximately to the displacement of the packing ring without pressure compensation bores. If the pressure compensation hole is displaced eccentrically in the direction away from the pressure compensation hole, larger displacements still occur in the area of the bores. However, the maximum displacements are then significantly smaller. In the area between the pressure compensation bores, the displacement then drops to the value of the reference ring without pressure balancing elements.

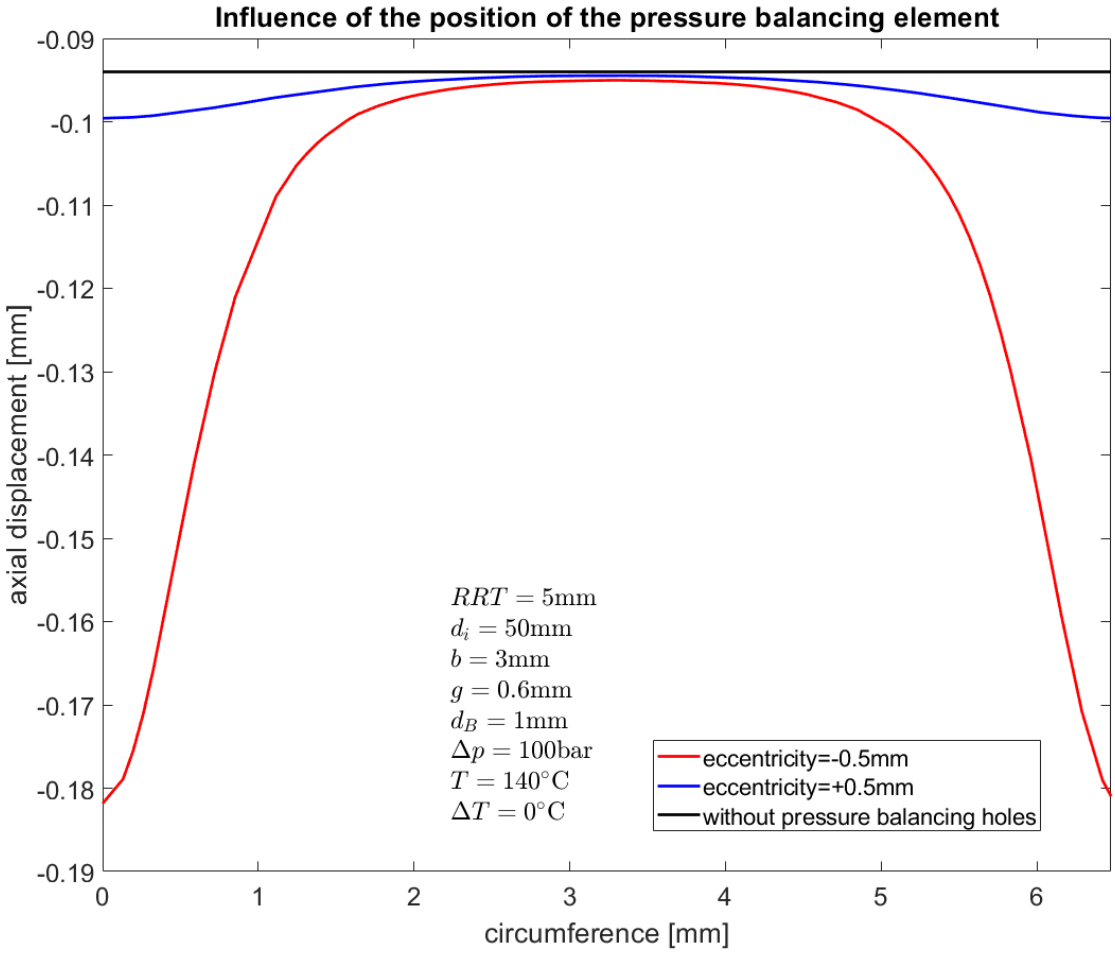

Figure 4.45: Course of the displacement into the pressure gap in the area between two pressure balancing bores after $\Delta t = 10^5$s

4.8.4 Influence of the pressure balancing bores Conclusion

The results of subchapter 4.8 "Influence of the pressure balancing elements" show that the pressure balancing bores do not lead to a reduction of the occurring displacements in the pressure gap. In the area of the pressure balancing bores, the displacements are locally increased to a an extent, that depends on the hole diameter and the position of the bores with respect to off-centre arrangement. In the area between the pressure balancing bores, the occurring displacements drop approximately to the level of the reference packing ring without pressure balancing bores. However, the displacements never fall below the displacements of the reference packing ring. Therefore, the pressure balancing elements are counterproductive with regard to the creep of the packing ring into the pressure gap.

Franz-Josef-Str. 18/III, 8700 Leoben
mechanik@unileoben.ac.at
Chair of Mechanics

4.9 Influence of asymmetry between rod and housing

The aim of this chapter is to determine the influence of the asymmetry between piston rod and packing housing on the displacement of the packing ring into the pressure gap. Due to the assembly process, technical constructions are never mounted exactly centrally.

Franz-Josef-Str. 18/III, 8700 Leoben
mechanik@unileoben.ac.at
Chair of Mechanics

4.10 Discussion

4.10.1 Comparison of simulation results and experimental results

Experimental tests by HOERBIGER Wien GmbH show that the permissible pressure gap widths for typical operating temperatures and maximum pressure difference are in the same range as determined in the context of this master's thesis with the use of numerical simulations. This indicates the validity of the simulation results and the formula obtained from the simulation results to describe the maximum displacement.

4.10.2 Measures to reduce the maximum deformation

There are several ways to reduce the deformations of the ring into the pressure gap. For small packing ring dimensions, the axial thickness can be increased. An increase in the range between 3mm and 10mm is reasonable. An increase above 10mm is, however, not useful because above this value the deformations saturate and can no longer be reduced. The displacement cannot be reduced with pressure compensation elements such as pressure balancing holes. On the contrary, the pressure balancing elements have a negative effect on the occurring displacements. Another way to reduce the displacements that occur is to reduce the temperature of the packing ring. This requires efficient cooling of the packing housing and the piston rod.

4.10.3 Influence of the temperature on the ring design

The temperature has the strongest influence on the creep of the material. As a comparison of Figure 4.34 and Figure 4.37 shows, a temperature increase of $40°$C leads to a reduction of the permissible pressure gap width by a factor of about 5. For the exact dimensioning of the pressure gap, the exact knowledge of the occurring maximum temperatures is indispensable. However, this also requires material data in these temperature ranges. Since no material data is available for temperatures in the range of $180°$C-$200°$C due to the limitations given by the testing device, the critical pressure gap width is determined by extrapolation allowing first reasonable estimates. However, for more reliable results a methodology to measure the missing material data will have to be devised.

4.10.4 Tertiary creep

From the representation of the experimental creep curves (Figure 3.7 to Figure 3.11) it is not obvious whether primary, secondary or tertiary creep is occurring. In primary creep, the creep strain rate slows down, whereas during secondary creep, the creep strain rate $\dot{\varepsilon}$ remains constant. The creep strain ε then increases linearly in the logarithmic diagram. In tertiary creep, the creep strain rate increases as time progresses. The creep strain then also increases non-linearly in the logarithmic representation. More detailed information about the creep behaviour of materials can be found in [2] p279-p283.
Figure 4.46 shows the experimentally determined creep curves of the material for three different temperatures and loads in a logarithmic representation. Here it is straightforward to detect whether primary, secondary or tertiary creep occurs.

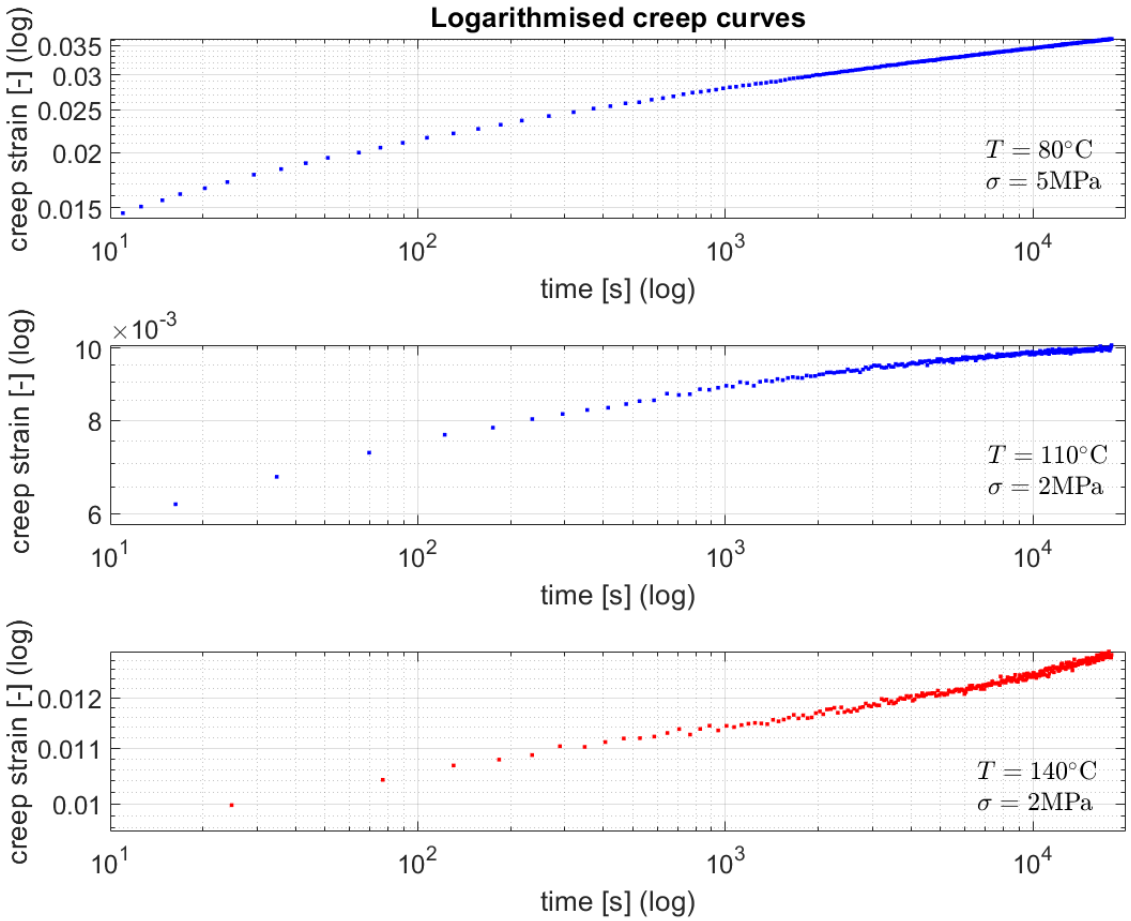

Figure 4.46: Logarithmised experimental creep curves at different temperatures and load levels in the experimental time range. a) Secondary creep for $T = 80°C$ and $\sigma = 5MPa$, b) primary creep for $T = 110°C$ and $\sigma = 2MPa$, c) tertiary creep for $T = 110°C$ and $\sigma = 2MPa$.

Figure 4.46 shows primary, secondary and tertiary creep as they occur at their corrsponding load and temperature levels. Figure 4.46 b) shows that primary creep occurs at a load of 2MPa and a temperature level of 110°. It exhibits a slower increase in creep strain over time. Figure 4.46 c) shows first secondary and then tertiary creep, identifiable by the accelerated increase in creep strain towards the end of the experiment. Thus, in the range of maximum operating temperatures of $T = 180°C$-$200°C$, tertiary creep occurs.

4.10.5 Further deformation mechanisms

In the case of small pressure gaps, other deformation and above all damage mechanisms occur in addition to creep. During the oscillating movement of the piston rod, material is sheared into the narrow gap, which leads to high deformation rates and subsequently to strong heating of the material due to dissipative effects. Over time, this process causes shearing of the material and re-welding of the material, which is visible in a burr-like deformation. Figure 4.47 shows the extrusion of a packing ring.

Figure 4.47: Extrusion of a packing ring [24]

4.10.6 Predictive quality of the material model

In subchapter 3.5 "Material characterisation" it is noticeable that for some temperatures ($T = 140°\text{C}$, $T = 110°\text{C}$, $T = 23°\text{C}$) the material response to the external load is predicted very accurately for all load levels. At other temperature levels ($T = 80°\text{C}$, $T = 55°\text{C}$) there are larger deviations between test data and calibrated material model due to the different creep stages. The creep law used (Norton-Bailey) describes secondary (stationary) creep over time very well but is unsuitable for tertiary creep. Subchapter 4.11.5 explains that the test data are recorded at different creep stages. In the case at $T = 80°\text{C}$, the creep curve is in the secondary creep region at one load level and in the primary creep region at the other two load levels. This means that it is no longer possible for the optimisation algorithm used to match the curves as accurately as the set bounds allow.

Franz-Josef-Str. 18/III, 8700 Leoben
mechanik@unileoben.ac.at
Chair of Mechanics

4.10.7 Comparison with analytical solutions

In this subchapter, the numerical solution is compared with the analytical solution according to Kirchhoff's plate theory. From this, an additional understanding of the mechanical behaviour of the packing rings is gained.

Plate theory describes the deflection of a plate in the form of a partial differential equation. Kirchhoff's plate theory is a generalisation of Bernoulli's beam theory. This theory is subject to a number of limitations.

- small displacements and strains (geometric linearity)
- linear elastic material behaviour (linear material model)
- thickness has to be small compared to the other dimensions
- the cross section of the plate remains flat and normal to the mid-plane of the plate

The governing equation for the deflection w reads

$$\frac{\partial^4 w}{\partial x^4} + \frac{\partial^4 w}{\partial x^2 \partial y^2} + \frac{\partial^4 w}{\partial y^4} = \Delta\Delta w = \frac{p}{K} \tag{4.13}$$

where w is the bending displacement, Δ is the Laplace operator, p is the surface load and K is the plate stiffness.

Mechanical model of the packing ring

Figure 4.48 shows the mechanical model of the packing ring for determining the analytical solution. This is a plate that is partially bedded. Since the packing ring is regarded as a rigid body due to the high Young's modulus, Winkler's bedding coefficient approaches infinity. The pressure on the bedded area also prevents the plate from lifting off. Thus, the bearing at the right end is considered as a fixed constraint. The contact with the piston rod is considered frictionless. Thus, the bearing is modelled as a transverse sliding sleeve.

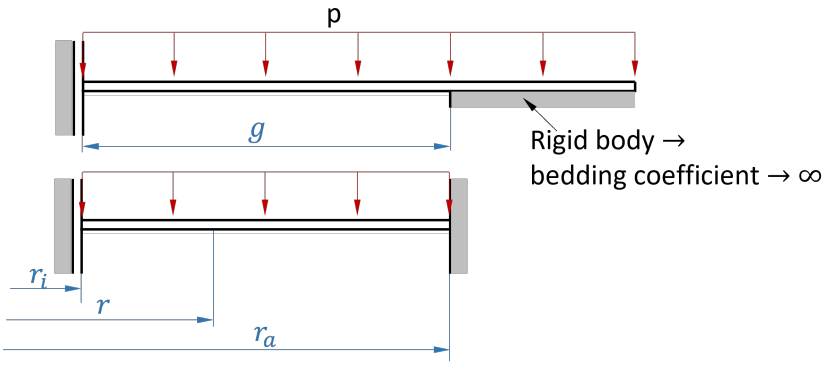

Figure 4.48: Mechanical modelling of the packing ring for the analytical solution

From this model follow the boundary conditions to solve the plate's differential equation. Equation 4.14 to 4.17 lists the boundary conditions

$$w'''(r = r_i) = 0 \tag{4.14}$$

$$w'(r = r_i) = 0 \tag{4.15}$$

$$w(r = r_a) = 0 \tag{4.16}$$

$$w'(r = r_a) = 0 \tag{4.17}$$

Derivation of the analytical solution

The starting point is Kirchhoff's plate differential equation in cylindrical coordinates.

$$\frac{1}{r}\frac{d}{dr}\left[r\frac{d}{dr}\left\{\frac{1}{r}\frac{d}{dr}\left(r\frac{dw}{dr}\right)\right\}\right] = \frac{p}{K} \tag{4.18}$$

After integrating four times, the general solution of the differential equation follows.

$$w(r) = \frac{1}{64}\frac{p}{K}r^4 + \frac{1}{4}C_1 r^2\left(\ln r - 1\right) + \frac{1}{4}C_2 r^2 + C_3 \ln r + C_4 \tag{4.19}$$

The special solution of the differential equation 4.18 follows by substituting the boundary conditions (equation 4.14 to 4.17) into equation 4.19. The special solution of the differential equation 4.18 is given below (equation 4.20), although the expression is long and unmanageable.

$$w(r) = \frac{q_0}{K}[8r^2r_i^2 - 4r^2r_a^2 - 12r_i^4\log r + 12r_i\log r_a + 32r_i^4\log r_a + r^4 + 3r_a^4 - 8r^2r_i^2\log r + 8r^2r_i^2$$
$$\log r_a + 8r_a^2r_i^2\log r - 8r_a^2r_i^2\log r_a - 16r_i^4\log r\log r_a + 16r_i^4\log r\log r_i - 16r_i^4\log r_a\log r_i] \tag{4.20}$$

The shape of the analytical solution for the displacement curve does not agree with the FE solution for the axisymmetric model, see Figure 4.49. The displacement in the FEA drops significantly sharper than in the analytical solution according to Kirchhoff. Even worse, the maximum displacements differ strongly. The reason is that some basic assumptions of Kirchhoff's plate theory are violated. Among other things, the axial thickness of the packing ring is greater than the bending length, whereas Kirchhoff's plate theory is only valid for thin plates. While for thin plates the shear deformations can be neglected (shear stiffness $\rightarrow \infty$) it has to be taken into account for thick plates where the shear deformations are no longer negligible. The large difference in maximum deflections may partly be due to the neglect of shear deformations. Taking them into account requires the plate theory according to Mindlin-Reissner.

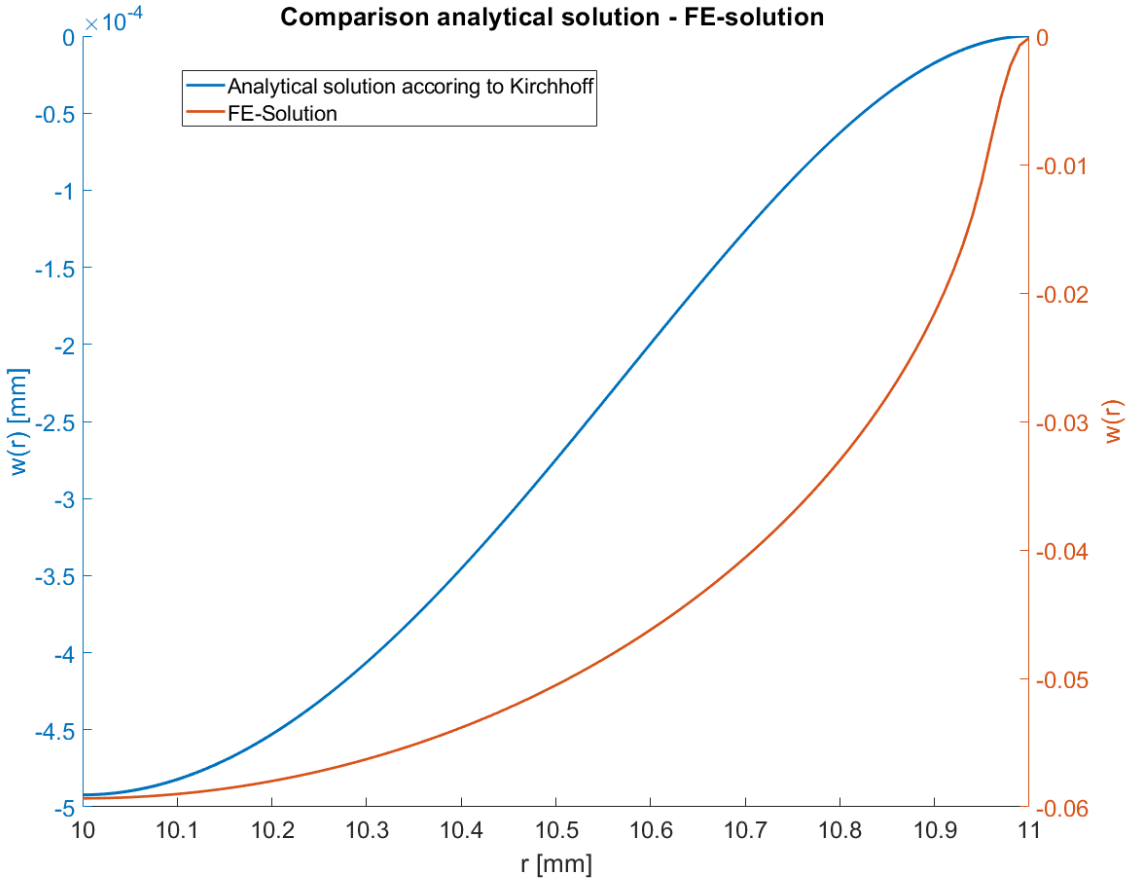

Figure 4.49: Analytical solution according to Kirchhoff's plate theory compared to the FE solution

Figure 4.50 shows the analytical solution according to Mindlin-Reissner and the FE solution. The maximum displacement evaluated with FEM is greater by a factor of 3 than the analytical solution. This is due to the fact that the packing ring does not represent a plate in terms of dimensions and bending length, so treating the ring as a plate is a too rough simplification.

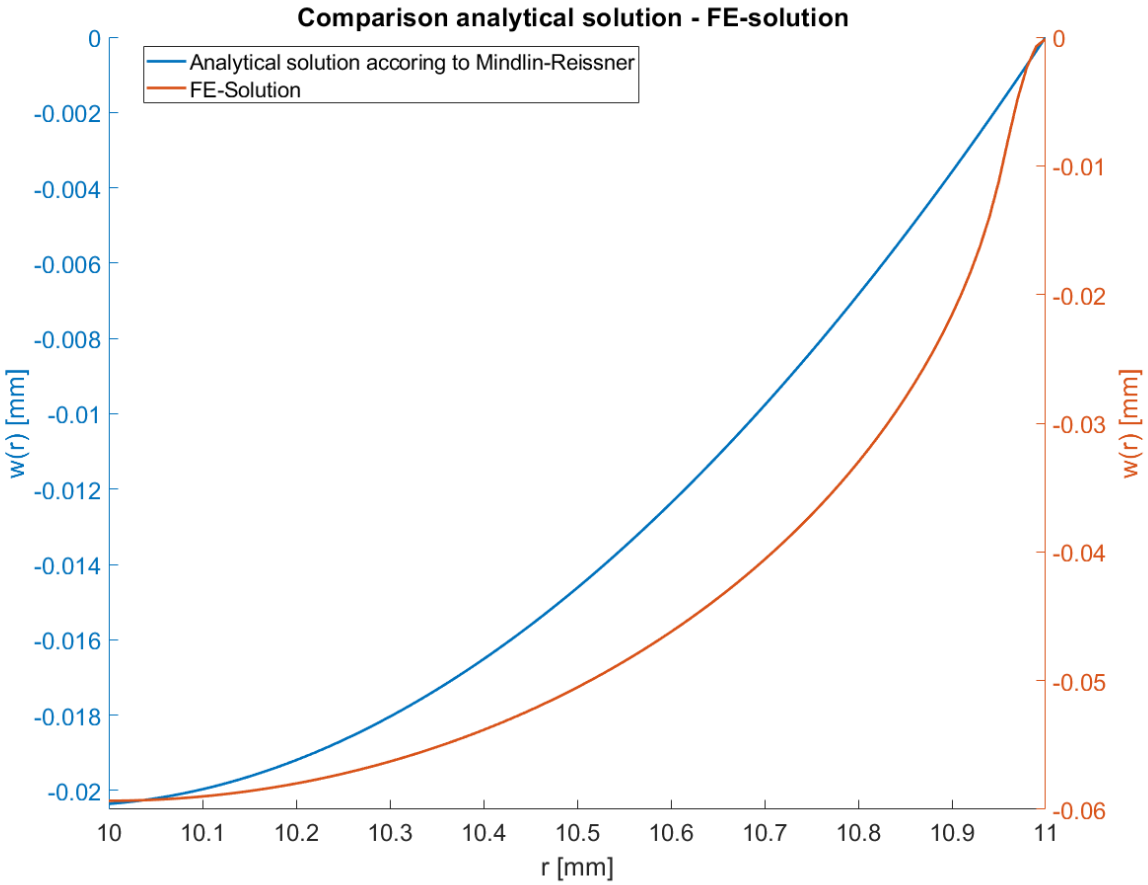

Figure 4.50: Analytical solution according to Mindlin-Reisner plate theory compared to the FE solution

A comparison of the results of figure 4.49 and 4.50 shows that the Mindlin-Reissner plate theory describes both the shape of the displacement and the maximum displacement significantly better than Kirchhoff's plate theory. A comparison of the maximum displacements also shows that the displacements mainly result from the shear and not from bending. When comparing the analytical solution according to Kirchhoff and Mindlin-Reissner it is recognisable that in the solution according to Mindlin-Reisner the slope $\left(\frac{d_w}{d_r}\right)_{r=r_a}$ is not zero. This is not an error but rather is expected due to the shear deformation that is associated with angles changes. The boundary conditions are therefore to be adjusted for Mindlin Reisner so that at the points $r = r_i$ and $r = r_a$ only the slope is zero according to the bending constraint. If the support on the right side is modelled with a fixed support instead of a sliding constraint, the FE solution would be overestimated by a factor of 10.

Chapter 5

Conclusion and Outlook

5.1 Conclusion

The central focus of this master's thesis is to determine the maximum possible pressure gap between the housing and the piston rod. Furthermore, the influence of the different system parameters on the deformation behaviour of the packing ring has to be determined.

Within the scope of this Master's thesis, it is shown that it a static analysis with the rod at standstill yields the same mean displacement of the ring as a cyclic analysis with an oscillating rod. This significantly reduces the computation time.

Furthermore, the results show that the influence of the axial ring thickness has a significant impact on the deformation behaviour of the packing ring. Increasing axial thickness leads to a reduction in creep deformation. However, the results also show that an increase in axial thickness reduces the deformation only up to a value of about $b = 10$mm. Larger dimensions have no influence and are therefore not useful. The radial ring thickness and the inner ring diameter have only a minimal influence on the deformation behaviour of the packing ring. The pressure and the pressure gap width have a large, non-linear influence on the deformation behaviour of the packing ring. Temperature has a significant influence on the creep behaviour of the packing ring material. In the area of viscoelastic-viscoplastic material behaviour, this is due to the temperature dependence of the yield strength and the Young's modulus. An increasing temperature leads to a reduction of the Young's modulus which already results in larger deformations in the elastic range. Higher temperatures also cause a reduction in the yield strength of the material, which means that a larger region of the material plastifies, resulting in stronger viscoplastic creep. For application temperatures in the range of up to $T = 180°$ C the admissible pressure gap is very small and can only be increased for relatively small pressure differences.

The investigation of the influence of the pressure compensation elements shows that the pressure compensation elements lead to a reduction of the deformations. It also shows that the pressure compensation elements should not exceed a certain diameter in order not to reduce the stiffness of the structure too strongly. The diameters of the pressure compensation holes should also not be too small, otherwise the desired effect is not achieved.

5.2 Outlook

5.2.1 Additional damage modes

In further scientific work additional deformation mechanisms such as the shearing and re-welding of the material due to the piston rod movement should be investigated in more detail.

5.2.2 Simulations with tertiary creep law

Furthermore, a tertiary creep law should be used to investigate the behaviour of the packing ring at higher temperatures. It has been shown that already at a temperature of $T = 140°\text{C}$ and a stress of $\sigma = 2\text{MPa}$ tertiary creep occurs after a certain time. Thus, more precise statements about the mechanical behaviour of the packing ring are possible. However, this requires the availability of corresponding material data.

5.2.3 Temperature development due to friction and heat conduction

In addition, the actual temperature development in the packing ring can be investigated in more detail in a future scientific work. In the context of this Master's thesis, piston rod temperatures and housing wall temperatures were specified by HOERBIGER Wien GmbH. Due to the friction between the piston rod and the packing ring, energy is dissipated, which leads to a temperature increase in the ring. Additional energy is dissipated in the material through high strain rates.

Franz-Josef-Str. 18/III, 8700 Leoben
mechanik@unileoben.ac.at
Chair of Mechanics

List of Figures

Bibliography

[1] Abaqus User Manual, Version 6.14

[2] Altenbach H.: Kontinuumsmechanik 4. Auflage, Springer Vieweg, Magdeburg 2018

[3] Amjadi M., Fatemi A.: Creep behavior and modeling of high-density polyethylene (HDPE). POLYMER TESTING, 94, 2021, DOI: 10.1016/j.polymertesting.2020.107031

[4] Babuska T.F., Pitenis A.: Jones M.: Temperature dependent friction behavior of PTFE and MOS_2, Tribology Letters, 63, 2016, DOI: 10.1007/s11249-016-0702-y

[5] Deng M., Latour R.A.: Study of creep behavior of ultra high-molecular-weight polyethylene systems, J. Biomed Mater Res., 40, 1998, p214-23, DOI: 10.1002/(sici)1097-4636(199805)40:2<214::aid-jbm6>3.0.co;2-o

[6] Bergstroem J.: Mechanics of solid polymers, Theory and computational Modeling, 2015, Elsevier Inc.

[7]

[8] HOERBIGER Wien GmbH.

[9] S.R. Holdsworth, Constitutive equations for creep curves and predicting service life, Creep-Resistant Steels, 2008, DOI: 10.1533/9781845694012.2.403

[10] Humpel M.: Evaluation of the influence of material, manufacturing and testing parameters on the leakage of PTFE and PEEK based sealing materials in reciprocating compressors, Master's Thesis, Montanuniversität Leoben, 2019

[11] Kaufmann A.: Wear of dry-running piston rod sealing rings: modelling and experiments, Dissertation, Montanuniversität Leoben, 2019

[12] Kaufmann A., Lindner-Silwester T., Antretter T.: Modeling Dry Wear of Piston Rod Sealing Elements of Reciprocating Compressors Considering Gas Pressure Drop Across the Dynamic Sealing Surface, J. Tribol. 140, 2018, DOI: 10.1115/1.4038863

[13] Lai J., Bakker A.: Analysis of the non-linear creep of high-density polyethylene, Polymer, 36, 1995 p93-99, DOI: 10.1016/0032-3861(95)90680-Z

[14] Lates M. T., Velicu R., Gavrila C. C.: Temperature, Pressure, and Velocity Influence on the Tribological Properties of PA66 and PA46 Polyamides, Materials, 12, 2019, DOI: 10.3390/ma12203452

[15] Mang H .A, Hofstetter G.: Festigkeitslehre, Springer Vieweg, Wien, 2004

[16] Neumann T., Strommel M.: Influence of hydrostatic pressure and volumetric strain on the mechanical long term behavior of polymers, J. of Polymer Engineering, 32, 2012, p327-333, DOI: 10.1515/polyeng-2012-0

[17] Pang D., Wang H., Sun L., Zhu K., Hao X.: Effect of Temperature on Fe-Polytetrafluoroethylene Friction coefficient using Molecular Dynamics Simulation, Tribology Transactions, 65, 2022, DOI: 10.1080/10402004.2022.2077871

[18] Radcliffe C.: Sealing material developments for reciprocating gas compressors, Sealing Technology, 11, 2005, p7-11, DOI: 10.1016/S1350-4789(05)70872-2

[19] Ruetz M.: FE based design from cylinder rings of reciprocating piston compressors, Master's Thesis, Montanuniversität Leoben, 2022

[20] Stommel M., Stojek M., Korte W.: FEM zur Berechnung von Kunststoff- und Elastomerbauteilen, Hanser, 2018

[21] Wriggers P.: Nichtlineare Finite-Elemente Methoden, Springer, 2000

[22] Xiaohan J., Quingqing Z., Jianmei F., Xueyuan P.: Numerical simulation and Experimental Study on Temperature Distribution of Self-Lubricating Packing Rings in Reciprocationg Compressors, Mathematical Problems in Engineering, 2016, 2016, DOI: 10.1155/2016/4029806

[23] Xin D., Feng J., Xu Y., Peng X.: Investigation of Pressure Distriubution and Frictional Heat on Self-Lubricated Piston Rings in Reciprocating Compressors, International Compressor Engineering Conference, 2010

[24] https://www.gallagherseals.com, Accessed on 01.03.2023

Appendix

Here are the relevant Python scripts for building the models.

Python script for axisymmetric FEA model

```
#-----------------------------------------------------------------------
# 2. Masterarbeit-Ruetz
# (c) Dipl.-Ing. Marcel Ruetz
#-----------------------------------------------------------------------

from abaqus import *
from abaqusConstants import*
import regionToolset
import section
import regionToolset
import displayGroupMdbToolset as dgm
import displayGroupOdbToolset as dgo

#-----------------------------------------------------------------------
# Importieren der Messdatensaetze
#-----------------------------------------------------------------------

# Importieren von Pythonmodul numpy
import numpy as np

# Festlegen der Work Directory
import os

os.chdir(r"D:\2. Masterarbeit Ruetz\Python Skripte")

#-----------------------------------------------------------------------
# Erstellen des Modells
#-----------------------------------------------------------------------

Model = mdb.models['Model-1']

#-----------------------------------------------------------------------
# Erstellen der Komponenten
#-----------------------------------------------------------------------

# Importieren des Zeichenmoduls und des Stueckmoduls
import sketch
import part
```


Franz-Josef-Str. 18/III, 8700 Leoben
mechanik@unileoben.ac.at
Chair of Mechanics

```
#-------------------------------------------------------------------------------
# Parameterisierung des Modells
#-------------------------------------------------------------------------------

# Hier werden die zu parameterisierenden Groessen definiert, die
# restlichen (abhaengigen) Groessen werden ausgehend von diesen
# Groessen berechnet

# Radiale Ringdicke
RRT = 5 # mm
# Innendurchmesser des Packungsrings
di = 20 # mm
# Axiale Ringdicke
b = 3.0 #mm
# Spaltdicke
g = 0.2 # mm
# Druckdifferenz
dp = 6 # MPa
# Temperatur
T_Celsius = 140.0 # Celsius
#T_rod = 200.0 #
#T_Cup = 7.0 #
# Vernetzungsgroesse
Meshsize = 0.002 # mm
#Meshsize = 0.0075 # mm
Meshsize = 0.015# mm
# Elementtypen
Elementtype1 = CAX4 # 4-knotiges axialsymmetrische Kontinuumselemente
Elementtype2 = CAX3 # 3-knotiges axialsymmetrische Kontinuumselemente
# Reibungskoeffizient
mu = 0.0
# Simulationsbezeichnung
# Simulationsname_therm = 'Simulation_dT_80_20'
Simulationsname_mech = 'Test_T=110_g=02'
# Berechnete Groessen
T_Kelvin = 273.15 # K
T_Start = T_Kelvin + 60.0  # Celsius
T_Kelvin = T_Kelvin + T_Celsius # K
T_Start = T_Kelvin
p_Umgebung = 0.1 # MPa
p_Zylinder = dp+p_Umgebung # MPa
da = di+2.0*RRT # mm
b_finermesh = -4.0+g-0.5  #mm
# Fertigungsradius des Gaps
r = 0.10 # mm
#g = g - r
dg = di/2.0+g # mm
```

```
#-------------------------------------------------------------------------------
# Definition der Geometrie des Models
#-------------------------------------------------------------------------------


s1 = Model.ConstrainedSketch(name='Packungsring-Skizze',
        sheetSize=200.0)
g, v, d, c = s1.geometry, s1.vertices, s1.dimensions, s1.constraints
s1.sketchOptions.setValues(viewStyle=AXISYM)
s1.setPrimaryObject(option=STANDALONE)
s1.ConstructionLine(point1=(0.0, -100.0), point2=(0.0, 100.0))
s1.FixedConstraint(entity=g[2])

# Erstellen des axialsymmetrischen Models ohne Entlastungsnut
s1.rectangle(point1=(di/2.0, 0.0), point2=(da/2.0, b))
p = Model.Part(name='Packungsring', dimensionality=AXISYMMETRIC,
        type=DEFORMABLE_BODY)
p = Model.parts['Packungsring']
p.BaseShell(sketch=s1)
s1.unsetPrimaryObject()
del Model.sketches['Packungsring-Skizze']

p = Model.parts['Packungsring']
f = p.faces
pickedRegions = f.getSequenceFromMask(mask=('[#1 ]', ), )
#p.deleteMesh(regions=pickedRegions)
f1, e, d1 = p.faces, p.edges, p.datums

# Anpassung der radialen Dicke
if di == 20.0:
    x = 15.
    y = 2.5
if di == 30.0:
    x = 20.
    y = 2.5
if di == 40.0:
    x = 25.
    y = 2.5
if di == 50.0:
    x = 30.
    y = 2.5
if di == 60.0:
    x = 35.
    y = 2.5
if di == 70.0:
    x = 40.
    y = 2.5
```

```
if di == 80.0:
    x = 45.
    y = 2.5
if di == 90.0:
    x = 50.
    y = 2.5
if di == 100.0:
    x = 55.
    y = 2.5
if di == 110.0:
    x = 60.
    y = 2.5
if di == 120.0:
    x = 65.
    y = 2.5
if di == 130.0:
    x = 70.
    y = 2.5
if di == 140.0:

t = p.MakeSketchTransform(sketchPlane=f1[0], sketchPlaneSide=SIDE1,
    origin=(x, y, 0.0))
s1 = Model.ConstrainedSketch(name='__profile__',
        sheetSize=41.23, gridSpacing=1.03, transform=t)
g, v, d, c = s1.geometry, s1.vertices, s1.dimensions, s1.constraints
s1.setPrimaryObject(option=SUPERIMPOSE)
p.projectReferencesOntoSketch(sketch=s1, filter=COPLANAR_EDGES)
s1.rectangle(point1=(-5.0, -2.5), point2=(b_finermesh, -1.6))
p = Model.parts['Packungsring']
f = p.faces
pickedFaces = f.getSequenceFromMask(mask=('[#1]', ), )
e1, d2 = p.edges, p.datums
p.PartitionFaceBySketch(faces=pickedFaces, sketch=s1)
s1.unsetPrimaryObject()
del Model.sketches['__profile__']

# Definition der Flaechen fuer Kontakt mit Rod und Cup
p = Model.parts['Packungsring']
s = p.edges
side1Edges = s.getSequenceFromMask(mask=('[#84]', ), )
p.Surface(side1Edges=side1Edges, name='Kontakt_Rod')
side1Edges = s.getSequenceFromMask(mask=('[#18␣]', ), )
p.Surface(side1Edges=side1Edges, name='Kontakt_Cup')

# Erstellen der Rod als starren Koerper
s = Model.ConstrainedSketch(name='Rod_Sketch',
        sheetSize=200.0)
```

```
g, v, d, c = s.geometry, s.vertices, s.dimensions, s.constraints
s.sketchOptions.setValues(viewStyle=AXISYM)
s.setPrimaryObject(option=STANDALONE)
s.ConstructionLine(point1=(0.0, -100.0), point2=(0.0, 100.0))
s.FixedConstraint(entity=g[2])
s.Line(point1=(di/2.0, -5.0), point2=(di/2.0, b+5.0))
s.VerticalConstraint(entity=g[3], addUndoState=False)
p = Model.Part(name='Rod', dimensionality=AXISYMMETRIC,
        type=DISCRETE_RIGID_SURFACE)
p = Model.parts['Rod']
p.AnalyticRigidSurf2DPlanar(sketch=s)
s.unsetPrimaryObject()
p = Model.parts['Rod']
del Model.sketches['Rod_Sketch']

# Definition des Referenzpunkts an Rod
p = mdb.models['Model-1'].parts['Rod']
v1, e, d1, n = p.vertices, p.edges, p.datums, p.nodes
p.ReferencePoint(point=v1[1])

# Erstellen des Cup als starren Koerper
s = Model.ConstrainedSketch(name='Cup_Sketch',
        sheetSize=200.0)
g, v, d, c = s.geometry, s.vertices, s.dimensions, s.constraints
s.sketchOptions.setValues(viewStyle=AXISYM)
s.setPrimaryObject(option=STANDALONE)
s.ConstructionLine(point1=(0.0, -100.0), point2=(0.0, 100.0))
s.FixedConstraint(entity=g[2])
s.Line(point1=(da/2.0+5.0, 0.0), point2=(dg, 0.0))
s.HorizontalConstraint(entity=g[3], addUndoState=False)
s.Line(point1=(dg, 0.0), point2=(dg, -5.0))
s.VerticalConstraint(entity=g[4], addUndoState=False)
s.PerpendicularConstraint(entity1=g[3], entity2=g[4],
        addUndoState=False)
s.FilletByRadius(radius=r, curve1=g[3], nearPoint1=(dg+0.1,
        0), curve2=g[4], nearPoint2=(dg,
        -0.1))
p = Model.Part(name='Cup', dimensionality=AXISYMMETRIC,
        type=DISCRETE_RIGID_SURFACE)
Model.parts['Cup']
p.AnalyticRigidSurf2DPlanar(sketch=s)
s.unsetPrimaryObject()
del Model.sketches['Cup_Sketch']
```

```
# Definition des Referenzpunktes am Cup
p = Model.parts['Cup']
v2, e1, d2, n1 = p.vertices, p.edges, p.datums, p.nodes
p.ReferencePoint(point=v2[2])

# Definition der Kontaktflaechen am Cup
p = Model.parts['Cup']
s = p.edges
side2Edges = s.getSequenceFromMask(mask=('[#7 ]', ), )
p.Surface(side2Edges=side2Edges, name='Mastersurface_Cup')

#-----------------------------------------------------------------------
# Definition des Materialmodells
#-----------------------------------------------------------------------

# Import des Moduls Material
import material
# Definition des Materials
Model.Material(name='Materialmodell')

# Definition der thermischen Materialeigenschaften
Model.materials['Materialmodell'].Expansion(type=ORTHOTROPIC,
        table=((8e-05, 0.00014, 8e-05), ))
Model.materials['Materialmodell'].Density(table=((1.32e-09, ), ))
Model.materials['Materialmodell'].Conductivity(table=((0.25, ), ))
Model.materials['Materialmodell'].SpecificHeat(table=((
        2160000000.0, ), ))


# Definition der mechanischen Eigenschaften des Materials HY54
Model.materials['Materialmodell'].Elastic(temperatureDependency=ON,
            table=()
# Definition des zeitabhaengigen Verhaltens der Moduli
Model.materials['Materialmodell'].elastic.setValues(
                moduli=INSTANTANEOUS)
# Definition des Plastizit\"atsgesetz
Model.materials['Materialmodell'].Plastic(temperatureDependency=ON,
        table=()
# Creep parameter
Model.materials['Materialmodell'].Creep(table=((0.000133053, 1.38857,
        -0.95954), ))
Model.materials['Materialmodell'].creep.setValues(
        temperatureDependency=ON, table=()
p = Model.parts['Packungsring']
```

```
# Festlegung der Section
Model.HomogeneousSolidSection(name='Section',
        material='Materialmodell', thickness=None)
f = p.faces
faces = f.getSequenceFromMask(mask=('[#3␣]', ), )
region = p.Set(faces=faces, name='Set-6')
# Festlegung des Assingment
p.SectionAssignment(region=region, sectionName='Section', offset=0.0,
        offsetType=MIDDLE_SURFACE, offsetField='',
        thicknessAssignment=FROM_SECTION)
# Definition der Materialorientierung
p = Model.parts['Packungsring']
f = p.faces
faces = f.getSequenceFromMask(mask=('[#3␣]', ), )
region = regionToolset.Region(faces=faces)
orientation=None
Model.parts['Packungsring'].MaterialOrientation(region=region,
        orientationType=SYSTEM, axis=AXIS_3, localCsys=orientation,
        fieldName='', additionalRotationType=ROTATION_NONE, angle=0.0,
        additionalRotationField='', stackDirection=STACK_3)

#-------------------------------------------------------------------------
# Definition des Assembly
#-------------------------------------------------------------------------

# Import des Moduls Assembly
import assembly

a = Model.rootAssembly
a.DatumCsysByThreePoints(coordSysType=CYLINDRICAL, origin=
        (0.0, 0.0, 0.0), point1=(1.0, 0.0, 0.0),
        point2=(0.0, 0.0, -1.0))
p = Model.parts['Cup']
a.Instance(name='Cup-1', part=p, dependent=ON)
p = Model.parts['Packungsring']
a.Instance(name='Packungsring-1', part=p, dependent=ON)
p = Model.parts['Rod']
a.Instance(name='Rod-1', part=p, dependent=ON)
```

```
#-----------------------------------------------------------------------
# Definition der Analyse
#-----------------------------------------------------------------------

# Importieren des Moduls Step
import step

# Definition des Lastaufbringungsstep
Model.StaticStep(name='Lastaufbringung', previous='Initial',
        timePeriod=0.1, initialInc=0.1, minInc=1e-06, maxInc=0.1,
        nlgeom=ON)#, cetol=0.1)

# Definition der Stabilisierung der Gleichgewichtsiteration
Model.steps['Lastaufbringung'].setValues(
        stabilizationMagnitude=0.02,
        stabilizationMethod=DISSIPATED_ENERGY_FRACTION,
        continueDampingFactors=False, adaptiveDampingRatio=0.5)

# Definition des Kriechen Steps
Model.ViscoStep(name='Kriechen', previous='Lastaufbringung',
        timePeriod=350000.0, maxNumInc=1000000, initialInc=0.5,
        minInc=0.000001, maxInc=5000.0, nlgeom=ON, cetol=0.1)

# Definition der Stabilisierung der Gleichgewichtsiteration
Model.steps['Kriechen'].setValues(
        stabilizationMagnitude=0.0002,
        stabilizationMethod=DISSIPATED_ENERGY_FRACTION,
        continueDampingFactors=False, adaptiveDampingRatio=0.05)

# Definition der Ausgabegroessen
Model.FieldOutputRequest(name='Ausgabevariablen',
        createStepName='Lastaufbringung', variables=('S', 'U'))
Model.fieldOutputRequests['Ausgabevariablen'].setValues(
        frequency=1)
Model.fieldOutputRequests['Ausgabevariablen'].setValuesInStep(
        stepName='Kriechen', variables=('S', 'PEEQ', 'CEEQ', 'U'))
```

```
#-----------------------------------------------------------------------
# Definition der Interaction
#-----------------------------------------------------------------------

# Import des Moduls Interaction
import interaction

# Definiton der Kontakteigenschaften
Model.ContactProperty('Kontakt')
Model.interactionProperties['Kontakt'].NormalBehavior(
        pressureOverclosure=HARD, allowSeparation=ON,
        constraintEnforcementMethod=DEFAULT)

# Erstellen des reibungsbehafteten Kontakts
Model.interactionProperties['Kontakt'].TangentialBehavior(
        formulation=PENALTY, directionality=ISOTROPIC,
        slipRateDependency=OFF, pressureDependency=OFF,
        temperatureDependency=OFF, dependencies=0,
        table=((mu, ), ), shearStressLimit=None,
        maximumElasticSlip=FRACTION, fraction=0.005,
        elasticSlipStiffness=None)

# Erstellen des Kontaktes zwischen Packungsring- und Rod
a = Model.rootAssembly
s1 = a.instances['Rod-1'].edges
side2Edges1 = s1.getSequenceFromMask(mask=('[#1 ]', ), )
region1=a.Surface(side2Edges=side2Edges1, name='m_Surf-2')
region2=a.instances['Packungsring-1'].surfaces['Kontakt_Rod']
Model.SurfaceToSurfaceContactStd(name='Int-1',
        createStepName='Initial', master=region1, slave=region2,
        sliding=FINITE, thickness=ON, interactionProperty='Kontakt',
        adjustMethod=NONE, initialClearance=OMIT, datumAxis=None,
        clearanceRegion=None)

# Erstellen des Kontaktes zwischen Packungsring- und Rod
region1=a.instances['Cup-1'].surfaces['Mastersurface_Cup']
region2=a.instances['Packungsring-1'].surfaces['Kontakt_Cup']
Model.SurfaceToSurfaceContactStd(name='Int-2',
        createStepName='Initial', master=region1, slave=region2,
        sliding=FINITE, thickness=ON, interactionProperty='Kontakt',
        adjustMethod=NONE, initialClearance=OMIT, datumAxis=None,
        clearanceRegion=None)
```

```
#-----------------------------------------------------------------------
# Definition der Last und Randbedingungen
#-----------------------------------------------------------------------

# Importieren des Lastmoduls
import load

# Definition des Zylinderdruckes
s1 = a.instances['Packungsring-1'].edges
side1Edges1 = s1.getSequenceFromMask(mask=('[#60 ]', ), )
region = a.Surface(side1Edges=side1Edges1, name='Surf-4')
Model.Pressure(name='Zylinderdruck',
        createStepName='Lastaufbringung', region=region,
        distributionType=UNIFORM, field='', magnitude= dp,
        amplitude=UNSET)

# Definition der Lagerung der Rod
r1 = a.instances['Rod-1'].referencePoints
refPoints1=(r1[2], )
region = a.Set(referencePoints=refPoints1, name='Set-1')
Model.EncastreBC(name='Lagerung_Rod', createStepName='Initial',
        region=region, localCsys=None)

# Definition der Lagerung der Cup
r1 = a.instances['Cup-1'].referencePoints
refPoints1=(r1[2], )
region = a.Set(referencePoints=refPoints1, name='Set-2')
Model.EncastreBC(name='Randbedingung_Cup',
        createStepName='Initial', region=region, localCsys=None)

# Ergaenzen des Temperaturfeldes im Packungsring am Anfang
f1 = a.instances['Packungsring-1'].faces
faces1 = f1.getSequenceFromMask(mask=('[#3 ]', ), )
region = a.Set(faces=faces1, name='Set-3')
Model.Temperature(name='Temperatur_Anfang',
        createStepName='Initial', region=region, distributionType=
        UNIFORM, crossSectionDistribution=CONSTANT_THROUGH_THICKNESS,
        magnitudes=(T_Start,))

# Ergaenzen des Temperaturfeldes im Packungsring stationaer
f1 = a.instances['Packungsring-1'].faces
faces1 = f1.getSequenceFromMask(mask=('[#3 ]', ), )
region = a.Set(faces=faces1, name='Set-3')
Model.Temperature(name='Temperatur_Ende',
        createStepName='Lastaufbringung', region=region,
        distributionType=UNIFORM, crossSectionDistribution=
        CONSTANT_THROUGH_THICKNESS, magnitudes=(T_Kelvin,))
```

```
#-----------------------------------------------------------------------
# Vernetzen des Modells
#-----------------------------------------------------------------------

# Importieren des Vernetzungsmoduls
import mesh

# Vernetzen des Packungsringes
p = Model.parts['Packungsring']
p.seedPart(size=0.1, deviationFactor=0.1, minSizeFactor=0.1)
e = p.edges
pickedEdges = e.getSequenceFromMask(mask=('[#f␣]', ), )
p.seedEdgeBySize(edges=pickedEdges, size=Meshsize, deviationFactor=0.1,
        minSizeFactor=0.1, constraint=FINER)
p.generateMesh()
elemType1 = mesh.ElemType(elemCode=Elementtype1, elemLibrary=STANDARD)
elemType2 = mesh.ElemType(elemCode=Elementtype2, elemLibrary=STANDARD)
f = p.faces
faces = f.getSequenceFromMask(mask=('[#3␣]', ), )
pickedRegions =(faces, )
p.setElementType(regions=pickedRegions, elemTypes=(elemType1, elemType2))

# Vernetzen der Cup
p = Model.parts['Cup']
p.seedPart(size=0.001, deviationFactor=0.1, minSizeFactor=0.1)
p.generateMesh()

# Vernetzen der Rod
p = Model.parts['Rod']
p.seedPart(size=0.1, deviationFactor=0.1, minSizeFactor=0.1)
p.generateMesh()
```

```
#-------------------------------------------------------------------------------
# Definition der durchzufuehrenden Jobs
#-------------------------------------------------------------------------------

# Importieren des Jobmoduls
import job

# Definition des Jobs
mdb.Job(name=Simulationsname_mech, model='Model-1',
        description='Analyse des Kriechverhaltens, Long_Time',
        type=ANALYSIS, atTime=None, waitMinutes=0, waitHours=0,
        queue=None, memory=90, memoryUnits=PERCENTAGE,
        getMemoryFromAnalysis=True, explicitPrecision=SINGLE,
        nodalOutputPrecision=SINGLE, echoPrint=OFF, modelPrint=OFF,
        contactPrint=OFF, historyPrint=OFF, userSubroutine='',
        scratch='', resultsFormat=ODB, multiprocessingMode=DEFAULT,
        numCpus=1, numGPUs=0)

# Starten des Jobs
mdb.jobs[Simulationsname_mech].submit(consistencyChecking=OFF)
```

Changes for the model with moving piston rod

Only a few changes need to be made in the preceding Python script so that the simulation can be carried out with a moving piston rod.

When defining the step, EXPLICIT_ONLY must be set for the integration method. The reason for this is that very small time increments must be selected in order to be able to resolve the displacement process over time.

```
Model.steps['Kriechen'].setValues(cetol=0.1,
        integration=EXPLICIT_ONLY)
```

When defining the boundary conditions, the boundary condition of the piston rod must be changed. Movement in the axial direction has to be possible, but at the same time displacement in the radial direction must be blocked.

```
Model.XsymmBC(name='BC-2', createStepName='Initial',
        region=region, localCsys=None)
```

Furthermore, the movement of the piston rod needs to be defined.

```
Model.PeriodicAmplitude(name='Movement', timeSpan=STEP,
        frequency=freq, start=0.0, a_0=0.0, data=((0.0, 1.0), ))
a = Model.rootAssembly
r1 = a.instances['Rod-1'].referencePoints
refPoints1=(r1[2], )
region = a.Set(referencePoints=refPoints1, name='Set-8')
Model.DisplacementBC(name='Bewegung_der_Kolbenstange',
        createStepName='Kriechen', region=region, u1=UNSET,
        u2=u, ur3=UNSET, amplitude='Movement', fixed=OFF,
        distributionType=UNIFORM, fieldName='', localCsys=None)
```

Changes in the model to account for the inhomogeneous temperature field

Since no mechanical hysteresis losses occur during creep of the packing ring, in contrast to cyclic loading, the thermal and mechanical problems can be treated separately. In this case, the mechanical model is copied and the boundary conditions are changed from mechanical to thermal boundary conditions.

```
#-----------------------------------------------------------------------
# Erstellen des thermischen Modells
#-----------------------------------------------------------------------

# Kopieren des mechanischen Models
mdb.Model(name='Model-1-temperature', objectToCopy=Model)

# Umbenennen des thermischen Models
Model_therm = mdb.models['Model-1-temperature']

# Loeschen der nicht benoetigten Komponenten
del Model_therm.parts['Cup']
del Model_therm.parts['Rod']

# Loeschen der nicht benoetigten Steps
del Model_therm.steps['Lastaufbringung']
del Model_therm.steps['Kriechen']

# Erstellen des Steps fuer stationares Temperaturfeld
Model_therm.HeatTransferStep(name='temperaturefield',
        previous='Initial', response=STEADY_STATE, amplitude=RAMP)

# Definition des Field Outputs
Model_therm.FieldOutputRequest(name='F-Output-1',
        createStepName='temperaturefield', variables=('NT', ))

# Loeschen der Interaktionen
del Model_therm.interactions['Int-1']
del Model_therm.interactions['Int-2']

# Loeschen der Randbedingungen des mechanischen Modells
del Model_therm.boundaryConditions['Lagerung_Rod']
del Model_therm.boundaryConditions['Randbedingung_Cup']

# Definition der Temperaturen am Rand
a = Model_therm.rootAssembly
e1 = a.instances['Packungsring-1'].edges
edges1 = e1.getSequenceFromMask(mask=('[#84 ]', ), )
region = a.Set(edges=edges1, name='Set-4')
```

```
Model_therm.TemperatureBC(name='BC-1',
        createStepName='temperaturefield', region=region, fixed=OFF,
        distributionType=UNIFORM, fieldName='', magnitude=T_rod,
        amplitude=UNSET)

edges1 = e1.getSequenceFromMask(mask=('[#10 ]', ), )
region = a.Set(edges=edges1, name='Set-5')
Model_therm.TemperatureBC(name='BC-2',
        createStepName='temperaturefield', region=region, fixed=OFF,
        distributionType=UNIFORM, fieldName='', magnitude=T_Cup,
        amplitude=UNSET)

# Definition der Vernetzungsparameter
p = Model_therm.parts['Packungsring']
p.deleteMesh()
p.seedPart(size=0.05, deviationFactor=0.1, minSizeFactor=0.1)
p.generateMesh()

elemType1 = mesh.ElemType(elemCode=DCAX4, elemLibrary=STANDARD)
elemType2 = mesh.ElemType(elemCode=DCAX3, elemLibrary=STANDARD)
f = p.faces

faces = f.getSequenceFromMask(mask=('[#3 ]', ), )
pickedRegions =(faces, )
p.setElementType(regions=pickedRegions, elemTypes=(elemType1,
        elemType2))

# Definition des thermischen Jobs
mdb.Job(name=Simulationsname_therm, model='Model-1-temperature',
        description='Long_Time', type=ANALYSIS, atTime=None,
        waitMinutes=0, waitHours=0, queue=None, memory=90,
        memoryUnits=PERCENTAGE, getMemoryFromAnalysis=True,
        explicitPrecision=SINGLE, nodalOutputPrecision=SINGLE,
        echoPrint=OFF, modelPrint=OFF, contactPrint=OFF,
        historyPrint=OFF, userSubroutine='', scratch='',
        resultsFormat=ODB, multiprocessingMode=DEFAULT,
        numCpus=1, numGPUs=0)

# Starten des Jobs
 mdb.jobs[Simulationsname_therm].submit(consistencyChecking=OFF)
```

The output file (.odb) of the calculated stationary temperature field can then be read into the mechanical model. So in the mechanical model, add:

```
# Aufruf des tatsaechlichen Temperaturfeldes
Model.predefinedFields['Temperatur_Ende'].setValues(
        distributionType=FROM_FILE,
        fileName='D:\\2. Masterarbeit Ruetz\\Python Skripte\\temp.odb')
```

Python script for the 3D FEA model

```
#-----------------------------------------------------------------------
# 2. Masterarbeit-Ruetz
# (c) Dipl.-Ing. Marcel Ruetz
#-----------------------------------------------------------------------

from abaqus import *
from abaqusConstants import*
import regionToolset
import section
import regionToolset
import displayGroupMdbToolset as dgm
import displayGroupOdbToolset as dgo

#-----------------------------------------------------------------------
# Importieren der Messdatensaetze
#-----------------------------------------------------------------------

# Importieren von Pythonmodul numpy
import numpy as np

#-----------------------------------------------------------------------
# Erstellen des Modells
#-----------------------------------------------------------------------

Model = mdb.models['Model-1']

#-----------------------------------------------------------------------
# Erstellen der Komponenten
#-----------------------------------------------------------------------

# Importieren des Zeichenmoduls und des Stueckmoduls
import sketch
import part

#-----------------------------------------------------------------------
# Parameterisierung des Modells
#-----------------------------------------------------------------------

# Hier werden die zu parameterisierenden Groessen definiert, die
# restlichen (abhaengigen) Groessen werden ausgehend von diesen
# Groessen berechnet
```

```
# Radiale Ringdicke
RRT = 5.0 # mm
# Innendurchmesser des Packungsrings
di = 50 # mm
# Axiale Ringdicke
b = 3.0 #mm
# Spaltdicke
g = 0.6 # mm
# Durchmesser der Druckausgleichsbohrung
dB = 1.0 #mm
# Position der Druckausgleichsbohrung
pos = 1.5#mm
# Druckdifferenz
dp = 10.0 # MPa
# Temperatur
T_Celsius = 140.0 # Celsius
T_rod = 200.0 #
T_Cup = 7.0 #
# Vernetzungsgroesse
Meshsize = 0.002 # mm
Meshsize = 0.01 # mm
# Elementtypen
Elementtype1 = CAX4 # 4-knotiges axialsymmetrische Kontinuumselemente
Elementtype2 = CAX3 # 3-knotiges axialsymmetrische Kontinuumselemente
# Reibungskoeffizient
mu = 0.0
# Simulationsbezeichnung
Simulationsname_therm = 'Simulation_dT_80_20'
Simulationsname_mech = 'Var_dB_d=1mm'
# Berechnete Groessen
T_Kelvin = 273.15 # K
T_Start = T_Kelvin + 60.0  # Celsius
T_Kelvin = T_Kelvin + T_Celsius # K
T_Start = T_Kelvin
p_Umgebung = 0.1 # MPa
p_Zylinder = dp+p_Umgebung # MPa
da = di+2.0*RRT # mm
ra = da/2.0
ri = di/2.0
dg = di/2.0+g # mm
b_finermesh = -4.0+g-0.5  #mm
# Fertigungsradius des Gaps
r = 0.1 # mm
g = g - r
```

```
#--------------------------------------------------------------------------
# Definition der Geometrie des Models
#--------------------------------------------------------------------------
# Erstellen des Basis-Modells
s = Model.ConstrainedSketch(name='__profile__',
        sheetSize=100.0)
g, v, d, c = s.geometry, s.vertices, s.dimensions, s.constraints
s.setPrimaryObject(option=STANDALONE)
s.ConstructionLine(point1=(0.0, -50.0), point2=(0.0, 50.0))
s.FixedConstraint(entity=g[2])
s.rectangle(point1=(25.0, -1.5), point2=(30.0, 1.5))
p = Model.Part(name='Packungsring', dimensionality=THREE_D,
        type=DEFORMABLE_BODY)
p = Model.parts['Packungsring']
p.BaseSolidRevolve(sketch=s, angle=90.0, flipRevolveDirection=OFF)
s.unsetPrimaryObject()
session.viewports['Viewport: 1'].setValues(displayedObject=p)
del mdb.models['Model-1'].sketches['__profile__']

# Definition der Ausgleichsbohrungen

p = Model.parts['Packungsring']
# Erzeugung eines Datum Punktes im Ursprung
p.DatumPointByCoordinate(coords=(0.0, 0.0, 0.0))
e = p.edges
# Erzeugung einer Hilfslinie
p.DatumAxisByTwoPoint(point1=p.InterestingPoint(edge=e[5], rule=MIDDLE),
        point2=p.InterestingPoint(edge=e[8], rule=MIDDLE))
# Erzeugung der radialen Hilfsebene
e1, d1 = p.edges, p.datums
p.DatumPlaneByThreePoints(point1=d1[2], point2=p.InterestingPoint(
        edge=e1[5], rule=MIDDLE), point3=p.InterestingPoint(edge=e1[8],
        rule=MIDDLE))
# Erzeugung der tangentialen Hilfsebene
d2 = p.datums
p.DatumPlaneByRotation(plane=d2[4], axis=d2[3], angle=90.0)
# Erzeugung der Bohrung 1
e, d1 = p.edges, p.datums
p.HoleThruAllFromEdges(plane=d1[5], edge1=e[6], edge2=e[9],
        planeSide=SIDE1,
        diameter=dB, distance1=b/2.0, distance2=
        ra*cos(2.0*pi*45.0/360.0))

# Erzeugung von Hilfsdatumspunkten
p.DatumPointByCoordinate(coords=(ra*cos(2*pi*30/360), -b/2,
        ra*sin(2*pi*30/360)+0.1))
p.DatumPointByCoordinate(coords=(ra*cos(2*pi*30/360), 0,
```

```
        ra*sin(2*pi*30/360)+0.1))
p.DatumPointByCoordinate(coords=(ra*cos(2*pi*30/360), b/2,
        ra*sin(2*pi*30/360)+0.1))
# Erzeugung der Hilslinie
d2 = p.datums
p.DatumAxisByTwoPoint(point1=d2[9], point2=d2[7])
# Erzeugung der radialen Hilfsebene
d1 = p.datums
p.DatumPlaneByThreePoints(point1=d1[2], point2=d1[9], point3=d1[7])
# Erzeugung der tangentialen Hilfseben
d2 = p.datums
p.DatumPlaneByRotation(plane=d2[11], axis=d2[10], angle=90.0)
# Erzeugung der Bohrung
e1, d1 = p.edges, p.datums
p.HoleThruAllFromEdges(plane=d1[12], edge1=e1[14], edge2=e1[11],
        planeSide=SIDE1, diameter=dB, distance1=pos, distance2=
        ra*cos(2*pi*30/360))

# Definition der Hilfsdatumspunkte
p.DatumPointByCoordinate(coords=(ra*cos(2*pi*60/360), -b/2,
        ra*sin(2*pi*60/360)+0.1))
p.DatumPointByCoordinate(coords=(ra*cos(2*pi*60/360), b/2,
        ra*sin(2*pi*60/360)+0.1))
# Erzeugung der Hilfslinie
d2 = p.datums
p.DatumAxisByTwoPoint(point1=d2[15], point2=d2[14])
# Erzeugung der radialen Hilfsebene
d1 = p.datums
p.DatumPlaneByThreePoints(point1=d1[15], point2=d1[14], point3=d1[2])
# Erzeugung der tangentialen Hilfsebene
d2 = p.datums
p.DatumPlaneByRotation(plane=d2[17], axis=d2[16], angle=90.0)
# Erzeugung der Bohrung
e, d1 = p.edges, p.datums
p.HoleThruAllFromEdges(plane=d1[18], edge1=e[16], edge2=e[13],
        planeSide=SIDE1, diameter=dB, distance1=pos,
        distance2=ra*cos(2*pi*60/360))

# Erzeugung der Hilfsdatumspunkte
p.DatumPointByCoordinate(coords=(ra*cos(2*pi*15/360), -b/2,
        ra*sin(2*pi*15/360)+0.1))
p.DatumPointByCoordinate(coords=(ra*cos(2*pi*15/360), b/2,
        ra*sin(2*pi*15/360)+0.1))
# Erzeugung der Hilfslinie
d2 = p.datums
p.DatumAxisByTwoPoint(point1=d2[21], point2=d2[20])
# Erzeugung der radialen Hilfsebene
```

```
d1 = p.datums
p.DatumPlaneByThreePoints(point1=d1[2], point2=d1[21], point3=d1[20])
# Erzeugung der tangentialen Hilfsebene
d2 = p.datums
p.DatumPlaneByRotation(plane=d2[23], axis=d2[22], angle=90.0)
# Erzeugung der Bohrung
e1, d1 = p.edges, p.datums
p.HoleThruAllFromEdges(plane=d1[24], edge1=e1[18], edge2=e1[15],
        planeSide=SIDE1, diameter=dB, distance1=pos,
        distance2=ra*cos(2*pi*15/360))

# Erzeugung der Hilfsdatumspunkten
v1 = p.vertices
p.DatumAxisByTwoPoint(point1=v1[17], point2=v1[15])
# Definition der radialen Hilfsebene
v2, d2 = p.vertices, p.datums
p.DatumPlaneByThreePoints(point1=d2[2], point2=v2[17], point3=v2[15])
# Definition der tangentialen Hilfsebene
d1 = p.datums
p.DatumPlaneByRotation(plane=d1[27], axis=d1[26], angle=90.0)
# Erzeugung der Bohrung
e, d2 = p.edges, p.datums
p.HoleThruAllFromEdges(plane=d2[28], edge1=e[20], edge2=e[17],
        planeSide=SIDE1, diameter=dB, distance1=pos,
        distance2=ra*cos(2*pi*0/360))

# Erzeugung der Hilfsdatumspunkte
p.DatumPointByCoordinate(coords=(ra*cos(2*pi*75/360), -b/2,
        ra*sin(2*pi*75/360)+0.1))
p.DatumPointByCoordinate(coords=(ra*cos(2*pi*75/360), b/2,
        ra*sin(2*pi*75/360)+0.1))
# Erzeugung der Hilfslinie
d1 = p.datums
p.DatumAxisByTwoPoint(point1=d1[30], point2=d1[31])
# Erzeugung der radialen Hilfsebene
d2 = p.datums
p.DatumPlaneByThreePoints(point1=d2[2], point2=d2[30], point3=d2[31])
p = Model.parts['Packungsring']
# Erzeugung der tangentialen Hilfsebene
d1 = p.datums
p.DatumPlaneByRotation(plane=d1[33], axis=d1[32], angle=90.0)
# Erzeugung der Bohrung
e, d1 = p.edges, p.datums
p.HoleThruAllFromEdges(plane=d1[34], edge1=e[27], edge2=e[25],
        planeSide=SIDE1, diameter=dB, distance1=pos,
        distance2=ra*cos(2*pi*75/360))
```


Franz-Josef-Str. 18/III, 8700 Leoben
mechanik@unileoben.ac.at
Chair of Mechanics

```
# Erzeugung der Hilfslinie
v1 = p.vertices
p.DatumAxisByTwoPoint(point1=v1[23], point2=v1[21])
# Erzeugung der radialen Hilfsebene
v2, d2 = p.vertices, p.datums
p.DatumPlaneByThreePoints(point1=d2[2], point2=v2[23], point3=v2[21])
# Erzeugung der tangentialen Hilfsebene
d1 = p.datums
p.DatumPlaneByRotation(plane=d1[37], axis=d1[36], angle=90.0)
# Erzeugung der Bohrung
e1, d2 = p.edges, p.datums
p.HoleThruAllFromEdges(plane=d2[38], edge1=e1[16], edge2=e1[15],
        planeSide=SIDE1, diameter=dB, distance1=pos, distance2=30.0)

# Erstellen der Rod
s1 = Model.ConstrainedSketch(name='__profile__',
        sheetSize=200.0)
g, v, d, c = s1.geometry, s1.vertices, s1.dimensions, s1.constraints
s1.setPrimaryObject(option=STANDALONE)
s1.ConstructionLine(point1=(0.0, -100.0), point2=(0.0, 100.0))
s1.FixedConstraint(entity=g[2])
s1.Line(point1=(ri, -b/2-1), point2=(ri, b/2+1))
s1.VerticalConstraint(entity=g[3], addUndoState=False)
p = Model.Part(name='Rod', dimensionality=THREE_D,
        type=DISCRETE_RIGID_SURFACE)
p = Model.parts['Rod']
p.BaseShellRevolve(sketch=s1, angle=90.0, flipRevolveDirection=OFF)
s1.unsetPrimaryObject()
session.viewports['Viewport: 1'].setValues(displayedObject=p)
del mdb.models['Model-1'].sketches['__profile__']

# Erzeugung des Cups
s = Model.ConstrainedSketch(name='__profile__',
        sheetSize=200.0)
g, v, d, c = s.geometry, s.vertices, s.dimensions, s.constraints
s.setPrimaryObject(option=STANDALONE)
s.ConstructionLine(point1=(0.0, -100.0), point2=(0.0, 100.0))
s.FixedConstraint(entity=g[2])
s.Line(point1=(dg, -2), point2=(dg, -b/2))
s.VerticalConstraint(entity=g[3], addUndoState=False)
s.Line(point1=(dg, -b/2), point2=(da/2+1, -b/2))
s.HorizontalConstraint(entity=g[4], addUndoState=False)
s.PerpendicularConstraint(entity1=g[3], entity2=g[4], addUndoState=False)
s.FilletByRadius(radius=0.1, curve1=g[3], nearPoint1=(dg,
        -b/2.0-0.2), curve2=g[4], nearPoint2=(dg+1, -b/2.0))
p = Model.Part(name='Cup', dimensionality=THREE_D,
        type=DISCRETE_RIGID_SURFACE)
```

```
p = Model.parts['Cup']
p.BaseShellRevolve(sketch=s, angle=90.0, flipRevolveDirection=OFF)
s.unsetPrimaryObject()
session.viewports['Viewport:␣1'].setValues(displayedObject=p)
del mdb.models['Model-1'].sketches['__profile__']

# Definition der Kontaktflaechen am Packungsring
p = Model.parts['Packungsring']
s = p.faces
side1Faces = s.getSequenceFromMask(mask=('[#2␣]', ), )
p.Surface(side1Faces=side1Faces, name='Kontakt_Ring_Rod')
side1Faces = s.getSequenceFromMask(mask=('[#1000␣]', ), )
p.Surface(side1Faces=side1Faces, name='Kontakt_Ring_Cup')

# Definition der Surface am Cup
p = Model.parts['Cup']
s = p.faces
side2Faces = s.getSequenceFromMask(mask=('[#7␣]', ), )
p.Surface(side2Faces=side2Faces, name='Rod_Flaeche')


# Definition der Referenzpunkte der starren Koerper
p = Model.parts['Cup']
v1, e, d2, n1 = p.vertices, p.edges, p.datums, p.nodes
p.ReferencePoint(point=v1[0])
p = Model.parts['Rod']
v2, e1, d3, n = p.vertices, p.edges, p.datums, p.nodes
p.ReferencePoint(point=v2[0])
```

```
#-----------------------------------------------------------------------
# Definition des Materialmodells
#-----------------------------------------------------------------------

# Import des Moduls Material
import material
# Definition des Materials
Model.Material(name='Materialmodell')

# Definition der thermischen Materialeigenschaften
#Model.materials['Materialmodell'].Expansion(type=ORTHOTROPIC,
#       table=((8e-05, 0.00014, 8e-05), ))
Model.materials['Materialmodell'].Density(table=((1.32e-09, ), ))
Model.materials['Materialmodell'].Conductivity(table=((0.25, ), ))
Model.materials['Materialmodell'].SpecificHeat(table=((
       2160000000.0, ), ))


# Definition der mechanischen Eigenschaften des Materials HY54
Model.materials['Materialmodell'].Elastic(temperatureDependency=ON,
            table=())

# Definition des zeitabhaengigen Verhaltens der Moduli
Model.materials['Materialmodell'].elastic.setValues(
                moduli=INSTANTANEOUS)

Model.materials['Materialmodell'].Plastic(table=())
Model.materials['Materialmodell'].plastic.setValues(
        temperatureDependency=ON, table=()
Model.materials['Materialmodell'].Creep(table=())

# Definition der Section
Model.HomogeneousSolidSection(name='Section␣Ring',
        material='Materialmodell', thickness=None)
p = Model.parts['Packungsring']
c = p.cells
cells = c.getSequenceFromMask(mask=('[#1␣]', ), )
region = p.Set(cells=cells, name='Set-1')
p.SectionAssignment(region=region, sectionName='Section␣Ring',
        offset=0.0, offsetType=MIDDLE_SURFACE, offsetField='',
        thicknessAssignment=FROM_SECTION)
```

```
#-----------------------------------------------------------------------
# Definition des Assembly
#-----------------------------------------------------------------------

# Import des Moduls Assembly
import assembly

a = Model.rootAssembly
a.DatumCsysByDefault(CARTESIAN)
p = Model.parts['Cup']
a.Instance(name='Cup-1', part=p, dependent=ON)
p = Model.parts['Packungsring']
a.Instance(name='Packungsring-1', part=p, dependent=ON)
p = Model.parts['Rod']
a.Instance(name='Rod-1', part=p, dependent=ON)

#-----------------------------------------------------------------------
# Definition der Analyse
#-----------------------------------------------------------------------

# Importieren des Moduls Step
import step

# Definition des Lastaufbringungsstep
Model.StaticStep(name='Lastaufbringung', previous='Initial',
        description='Lastaufbringung', maxNumInc=10000, initialInc=0.5,
        minInc=1e-09, maxInc=1.0, nlgeom=ON)#, cetol=0.1)

# Definition des Kriechen Steps
Model.ViscoStep(name='Kriechen', previous='Lastaufbringung',
        timePeriod=100000.0, maxNumInc=100000, initialInc=0.5,
        minInc=0.0000001, maxInc=1.0, nlgeom=ON, cetol=0.1)

# Definition der Stabilisierung der Gleichgewichtsiteration
Model.steps['Kriechen'].setValues(
        stabilizationMagnitude=0.0002,
        stabilizationMethod=DISSIPATED_ENERGY_FRACTION,
        continueDampingFactors=False, adaptiveDampingRatio=0.05)

# Definition der Ausgabegroessen
Model.FieldOutputRequest(name='Ausgabevariablen',
        createStepName='Lastaufbringung', variables=('S', 'U'))
Model.fieldOutputRequests['Ausgabevariablen'].setValues(
        frequency=1)
```

```
#-----------------------------------------------------------------------
# Definition der Interaction
#-----------------------------------------------------------------------

# Import des Moduls Interaction
import interaction

# Definiton der Kontakteigenschaften
Model.ContactProperty('Kontakt')
Model.interactionProperties['Kontakt'].NormalBehavior(
        pressureOverclosure=HARD, allowSeparation=ON,
        constraintEnforcementMethod=DEFAULT)

# Erstellen des reibungsbehafteten Kontakts
Model.interactionProperties['Kontakt'].TangentialBehavior(
        formulation=PENALTY, directionality=ISOTROPIC,
        slipRateDependency=OFF, pressureDependency=OFF,
        temperatureDependency=OFF, dependencies=0, table=((mu, ), ),
        shearStressLimit=None, maximumElasticSlip=FRACTION,
        fraction=0.005, elasticSlipStiffness=None)

# Definition des Kontaktes Ring-Rod
a = Model.rootAssembly
s1 = a.instances['Rod-1'].faces
side1Faces1 = s1.getSequenceFromMask(mask=('[#1 ]', ), )
region1=a.Surface(side1Faces=side1Faces1, name='m_Surf-1')
region2=a.instances['Packungsring-1'].surfaces['Kontakt_Ring_Rod']
Model.SurfaceToSurfaceContactStd(name='Kontakt_Ring_Rod',
        createStepName='Initial', master=region1, slave=region2,
        sliding=FINITE, thickness=ON, interactionProperty='Kontakt',
        adjustMethod=NONE, initialClearance=OMIT, datumAxis=None,
        clearanceRegion=None)

# Definition des Kontaktes Ring-Cup
region1=a.instances['Cup-1'].surfaces['Rod_Flaeche']
a = Model.rootAssembly
region2=a.instances['Packungsring-1'].surfaces['Kontakt_Ring_Cup']
Model.SurfaceToSurfaceContactStd(name='Kontakt_Ring_Cup',
        createStepName='Initial', master=region1, slave=region2,
        sliding=FINITE, thickness=ON, interactionProperty='Kontakt',
        adjustMethod=NONE, initialClearance=OMIT, datumAxis=None,
        clearanceRegion=None)
```

```
#-----------------------------------------------------------------------
# Definition der Last und Randbedingungen
#-----------------------------------------------------------------------

# Importieren des Lastmoduls
import load

# Definition des Kontaktdruckes
a = Model.rootAssembly
s1 = a.instances['Packungsring-1'].faces
side1Faces1 = s1.getSequenceFromMask(mask=('[#fd9 ]', ), )
region = a.Surface(side1Faces=side1Faces1, name='Surf-2')
Model.Pressure(name='Load-1', createStepName='Lastaufbringung',
        region=region, distributionType=UNIFORM, field='',
        magnitude=dp, amplitude=UNSET)

# Definition der Lagerung der Rod
r1 = a.instances['Rod-1'].referencePoints
refPoints1=(r1[2], )
region = a.Set(referencePoints=refPoints1, name='Set-7')
Model.EncastreBC(name='Rod', createStepName='Initial',
        region=region, localCsys=None)

# Definition der Lagerung des Cups
a = Model.rootAssembly
r1 = a.instances['Cup-1'].referencePoints
refPoints1=(r1[3], )
region = a.Set(referencePoints=refPoints1, name='Set-8')
Model.EncastreBC(name='Cup', createStepName='Initial',
        region=region, localCsys=None)

# Definition der geometrischen Randbedingungen
a = Model.rootAssembly
f1 = a.instances['Packungsring-1'].faces
faces1 = f1.getSequenceFromMask(mask=('[#2004 ]', ), )
region = a.Set(faces=faces1, name='Set-5')
Model.XsymmBC(name='Geometrie_1', createStepName='Initial',
        region=region, localCsys=None)

f1 = a.instances['Packungsring-1'].faces
faces1 = f1.getSequenceFromMask(mask=('[#4020 ]', ), )
region = a.Set(faces=faces1, name='Set-6')
Model.ZsymmBC(name='Geometrie_2', createStepName='Initial',
        region=region, localCsys=None)
```

```
#-------------------------------------------------------------------------------
# Vernetzen des Modells
#-------------------------------------------------------------------------------

# Importieren des Vernetzungsmoduls
import mesh

# Verneten des Cups
p = Model.parts['Cup']
p.seedPart(size=0.1, deviationFactor=0.1, minSizeFactor=0.1)
e = p.edges
pickedEdges = e.getSequenceFromMask(mask=('[#50 ]', ), )
p.seedEdgeBySize(edges=pickedEdges, size=0.01, deviationFactor=0.1,
        minSizeFactor=0.1, constraint=FINER)
p.generateMesh()

# Vernetzen des Rods
p = Model.parts['Rod']
p.seedPart(size=0.1, deviationFactor=0.1, minSizeFactor=0.1)
p.generateMesh()

# Vernetzen des Packungsring
p = Model.parts['Packungsring']
p.seedPart(size=0.075, deviationFactor=0.1, minSizeFactor=0.1)
p.generateMesh()


#-------------------------------------------------------------------------------
# Definition der durchzufuehrenden Jobs
#-------------------------------------------------------------------------------

# Importieren des Jobmoduls
import job

mdb.Job(name=Simulationsname_mech, model='Model-1',
        description='Analyse des Kriechverhaltens, Long_Time',
        type=ANALYSIS, atTime=None, waitMinutes=0, waitHours=0,
        queue=None, memory=90, memoryUnits=PERCENTAGE,
        getMemoryFromAnalysis=True, explicitPrecision=SINGLE,
        nodalOutputPrecision=SINGLE, echoPrint=OFF, modelPrint=OFF,
        contactPrint=OFF, historyPrint=OFF, userSubroutine='',
        scratch='', resultsFormat=ODB, multiprocessingMode=DEFAULT,
        numCpus=1, numGPUs=0)

mdb.jobs[Simulationsname_mech].writeInput()
```